Design and Evaluation of a Quasi-Passive Robotic Knee Brace: On the Effects of Parallel Elasticity on Human Running

by

Grant A. Elliott

S.B. Physics
S.B. Electrical Engineering and Computer Science
Massachusetts Institute of Technology (2006)

M.Eng. Electrical Engineering and Computer Science
Massachusetts Institute of Technology (2007)

Submitted to the Department of
Electrical Engineering and Computer Science
in partial fulfillment of the requirements for the degree of

Doctor of Philosophy in Electrical Engineering and Computer Science

at the

MASSACHUSETTS INSTITUTE OF TECHNOLOGY

February 2012

© Massachusetts Institute of Technology 2012. All rights reserved.
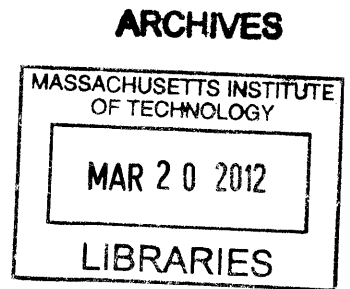
Author . . . .
Department of Electrical Engineering and Computer Science
Jan 13, 2012

Certified by . . . .
Hugh Herr
Associate Professor of Media Arts and Sciences
Thesis Supervisor

Accepted by . . . .
Leslie A. Kolodziejski
Chair of the Committee on Graduate Students

Design and Evaluation of a Quasi-Passive Robotic Knee Brace: On the Effects of Parallel Elasticity on Human Running

by

Grant A. Elliott

Abstract

While the effects of series compliance on running biomechanics are documented, the effects of parallel compliance are known only for the simpler case of hopping. As many practical exoskeleton and orthosis designs act in parallel with the leg, it is desirable to understand the effects of such an intervention. Spring-like forces offer a natural choice of perturbation, as they are both biologically motivated and energetically inexpensive to implement.

To this end, this thesis investigates the hypothesis that the addition of an external elastic element at the knee during the stance phase of running results in a reduction in knee extensor activation so that total joint quasi-stiffness is maintained. To test this, an exoskeleton is presented, consisting of a leaf spring in parallel with the knee joint and a clutch which engages this spring only during stance. The design of a custom interference clutch, made necessary by the need for high holding torque but low mass, is discussed in detail, as are problems of human attachment. The greater applicability of this clutch design to other problems in rehabilitation and augmentation is also addressed.

Motion capture of four subjects is used to investigate the consequences of running with this exoskeleton. Leg stiffness is found to increase with distal mass, but no significant change in leg stiffness or total knee stiffness is observed due to the activation of the clutched parallel knee spring. However, preliminary evidence suggests differing responses between trained marathon runners, who appear to maintain biological knee torque, and recreational runners, who appear to maintain total knee torque. Such a relationship between degree of past training and effective utilization of an external force is suggestive of limitations on the applications of assistive devices.

Thesis Supervisor: Hugh Herr
Title: Associate Professor of Media Arts and Sciences

Acknowledgments

Contents

List of Figures

List of Tables

Chapter 1

Introduction

An exoskeleton which successfully modifies human gait to reduce joint loading, muscle fatigue, or metabolic demand of locomotion has applications in several areas:

- **Biomechanics:** An exoskeleton with proven augmentative capabilities would be an invaluable research tool in studying neuromuscular control strategies as it permits the selective application of external assistive forces.

- **Load Bearing:** Soldiers and firefighters, among others, have occupations which require brisk movement over varying terrain while burdened with significant load. An augmenting exoskeleton could offer a potentially life-saving increase in endurance or capability while potentially also reducing damaging loads on the knee and ankle.

- **Mobility and Recreation:** The prevalence of knee injury poses both health and quality of life problems. A device which permits an active lifestyle by reducing the load on an injured joint could mitigate these. In cases of severe joint damage, such an exoskeleton could also be used as a walking orthosis to permit normal walking in patients with otherwise limited mobility. Moreover, the purely recreational benefits of any device which permits extended activity cannot be overlooked.

Despite this utility, metabolic augmentation of human locomotion has proved an elusive goal. Though a number of exoskeletons have been built (see Section 1.1), none

has demonstrated a significant reduction in the metabolic demand of locomotion.

This thesis considers the problem of building an exoskeleton to accommodate running gait. As discussed in Section 1.2, the knee is known to behave largely elastically. Because of this, an appropriate external assistive force may be applied during stance phase using a low mass passive spring in parallel with the joint. If the neuromuscular system responds to such an external force by reducing activation of the knee extensors, total metabolic demand or loading in the joint may decrease. Unfortunately, the effects of such parallel elasticity are relatively uninvestigated to date.

This thesis addresses the hypothesis that the addition of an external elastic element at the knee during the stance phase of running results in a reduction in knee extensor activation so that total joint quasi-stiffness is maintained. If true, metabolic demand may be reduced if an external stiffness near that of the biological joint is applied. This question is investigated with measurements of joint kinematics and kinetics, electromyography, and total metabolic demand. The results inform the design of future exoskeletons and orthoses.

1.1   Existing Lower Limb Exoskeletons

Exoskeletons may loosely be classified as intended to augment human capabilities, such as load capacity or ambulatory speed, or to increase human endurance, by lowering the metabolic demand of a given activity. While the ultimate intent of the exoskeleton described here is to reduce muscle activation and increase endurance in running, this discussion considers both types of devices as the division is frequently blurred. For instance, a device intended to reduce the metabolic demand of a movement may alternatively permit the execution of that movement at higher speed for a given metabolic demand. Moreover, some orthotic devices, intended to restore lost functionality, may be thought of as exoskeletons.

Additionally exoskeletons are classified as passive, quasi-passive, or active based on their usage of power. Passive exoskeletons require no energy source and generally consist of linkages, springs, and dampers. Active devices, in contrast, add energy to

16

the human gait cycle, usually through motors or hydraulic cylinders. Quasi-passive devices lie between, unable to inject energy into the gait cycle, but nonetheless requiring a power supply, usually to operate electronic control systems, clutches, or variable dampers. Typically, though not necessarily, the power requirement of a quasi-passive device is small.

Finally exoskeletons may be described as primarily acting in series or in parallel with the wearer's limbs.

The history of exoskeleton research (see Herr[23] and Dollar[13] for overviews) can be traced back to a passive parallel spring architecture patented by Yagn in 1890[45] and shown in Figure 1-1a. Though never demonstrated, the device sought to augment running and jumping by transferring loads through external passive springs in parallel with each leg, thereby unburdening the biological joints. This device bears resemblance to that described here, though the mechanism for disengaging the parallel spring during swing phase must be triggered manually. A very similar device to Yagn's, shown in Figure 1-1b, without any mechanism for disengaging the spring has proven effective in augmenting hopping, as described in more detail in Section 1.3.

Alternatively, passive springs may act in series with the natural leg, rather than in parallel. The legitimacy of such an approach is buoyed by the improvement of track athlete performances simply by changing the compliance of the ground[28]. The Springbuck shoe, which incorporates a carbon fiber leaf spring into its sole reduces the metabolic demand of running by 2%. The PowerSkip[5], a much larger series spring, marketed as a recreational device, visibly augments jumping height in promotional videos. Trials of a more intricate series spring architecture marketed as the SpringWalker[12], have shown that it increases metabolic demand by 20%, even when control subjects are burdened by an equivalent mass[23]. All of these devices are shown in Figure 1-1.

Unlike these passive springs, many exoskeletons are active or quasi-passive and are consequently limited by practical power supplies and actuators. Such limitations are obvious as early as General Electric's Hardiman prototype [35], perhaps the first exoskeleton ever constructed. Hardiman, shown in Figure 1-2a was intended to augment

17
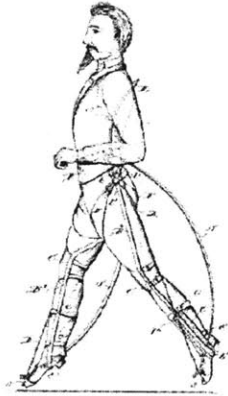
(a) Yagn's parallel elastic running exoskeleton proposal [45]

(b) MIT's parallel elastic hopping exoskeleton [20]
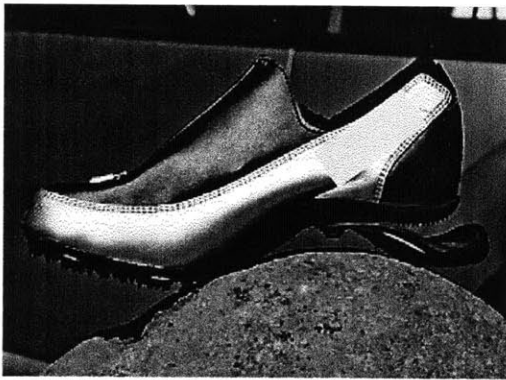
(c) Series elastic SpringBuck shoe [23]
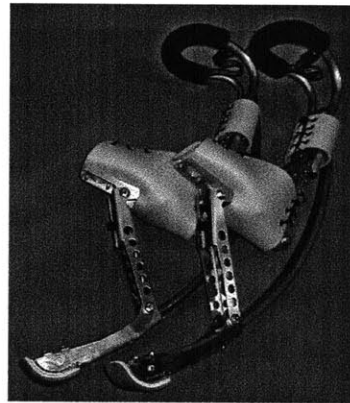
(d) Series elastic PowerSkip [5]

(e) Series elastic SpringWalker [12]

Figure 1-1: Five passive lower limb exoskeletons based on springs.

human strength in both the upper and lower limbs using extremely large hydraulic actuators. Although only the upper limbs enjoyed limited success, Ralph Mosher's observations in proposing the exoskeleton reflect equally on modern designs for lower limbs.

Mosher saw the Hardiman project as a logical progression from Handyman, a telerobotic pair of arms which granted a human user natural spacial controls over remote actuators. In combining the superior control and planning of a human with the strength and robustness of a robot, Mosher identified problems in power supplies, mechanical interface to the wearer, and mechanical interface to the outside world. Mosher recognized the necessity of kinesthetic sense to prevent unbounded mechanical interactions, such as crushing a manipulated object or losing balance, and proposed entrusting the human with this control by using force feedback and leveraging natural human control strategies. Modern robotic devices attempt to account for some such issues with electronic control strategies. Others, such as the contact instability problem[26], which manifests when an actuator transitions into contact with an outside object, are frequently dealt with through the use of mechanical compliance[38]. Nonetheless, feedback issues continues to plague exoskeleton designs where force feedback may be lost at the interface to the wearer (as a result of rigid surfaces beneath the feet, for instance). Worse still, user discomfort and fatigue brought about due to the mechanical interface, another problem raised by Mosher, are cited as problems for nearly all exoskeletons to date.

More recently, the vision of Hardiman's lower limb system has come to pass, in the form of several load bearing exoskeletons, intended to augment human load capacity during walking by transferring force directly to the ground through structures in parallel to the legs. The Berkeley Lower Extremity Exoskeleton (BLEEX) and the Human Universal Load Carrier (HULC) which evolved from it, are effectively bipedal robots which accommodate a user. The BLEEX is even capable of independent balance and locomotion. The architecture is active, with 8 of its 14 degrees of freedom actuated by hydraulic cylinders (and in later prototypes by electric motors with hydraulic transmissions). The BLEEX requires 1.3kW of hydraulic power

(a) Active hydraulic driven Hardiman, the legs of which were never used [35]

(b) Active Sarcos exoskeleton, hydraulic with an offboard compressor (not shown) [40]

(c) Active Berkeley Lower Extremity Exoskeleton (BLEEX), driven by electric motors with hydraulic transmission [46]

(d) Active Human Universal Load Carrier (HULC), a descendant of BLEEX [24]
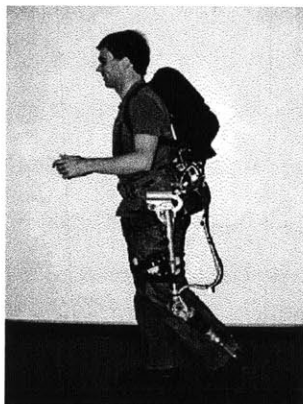
(e) Quasi-passive MIT exoskeleton [43]
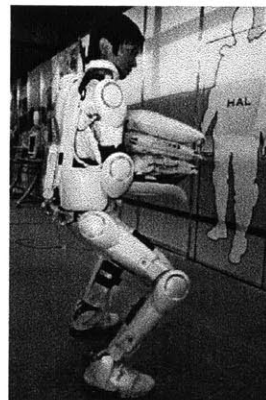
(f) Active Hybrid Assisstive Limb (HAL), driven by electric motors [21]

Figure 1-2: Six active and quasi-passive lower limb exoskeletons, all acting in parallel.

to walk at 1.3m/s, 224W to operate valves, and an additional 540W of hydraulic power for maneuvers which require the adduction-abduction actuators[46]. Unlike Mosher's Hardiman proposal, BLEEX walks with a minimum of sensory input from the user, relying instead on internal sensing to generate stable gait and using the human user only for a directing force[27]. Unfortunately, no published results to date have demonstrated a reduction in metabolic demand while walking in BLEEX or HULC. Moreover, BLEEX is limited to a fairly slow maximum speed of 1.3m/s and, because it requires a very substantial power supply, has limiting range.

In contrast, the MIT load bearing exoskeleton utilizes a quasipassive architecture, with springs at the ankle and hip and a magnetorheological damper at the knee[42]. (A short-lived revision made this exoskeleton active through the addition of a hip flexion-extension motor[43].) Since the quasipassive architecture cannot walk on its own, a controller like that used in BLEEX is not possible. Instead, control is derived entirely from user dynamics; a state machine determines phases of gait based on on-board kinematic sensors and varies the damping of the exoskeletal knee joints so that each leg is effectively rigid during stance and free-swinging during swing[43]. In this way, the exoskeleton is able to transmit load from its backpack frame directly to the ground, unburdening the human user. The device did not demonstrate a reduction in metabolic demand in subjects carrying a 75kg payload, though the operational exoskeleton outperformed the exoskeleton configured as dead weight, indicating both the value of the elastic and magnetorheological systems and the importance of minimizing weight and constraints placed on the user. The MIT exoskeleton can operate at higher speeds than BLEEX, up to 2m/s.

Finally, several exoskeletons do not load directly to the ground, but instead augment torque at specific joints. Using lightweight pneumatic muscles to assist ankle plantar flexion and a control strategy based on electromyography (EMG) sensing of muscle innervation, the University of Michigan's ankle-foot orthosis has demonstrated a reduction in metabolic demand both in level ground and incline walking[41]. Unfortunately, this device relies on an external (and very heavy) pneumatic compressor and is not portable as the wearer must remain tethered. The Hybrid Assistive Limb
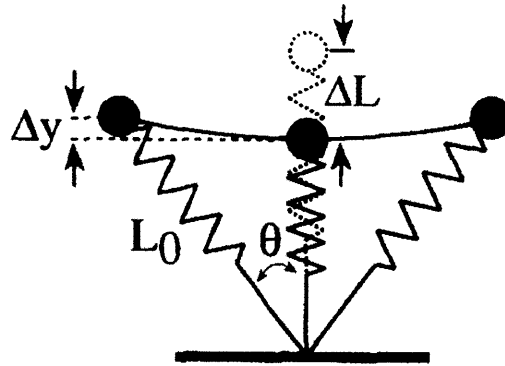
Figure 1-3: Stance phase of running modeled as a mass rebounding off a leg spring. Figure from [15].

(HAL) similarly uses electric motors to augment torque at the hip, knee, shoulder, and elbow. Using a control strategy based on kinematic sensing and EMG, HAL has demonstrated increased capacity in lifts and presses and reduction of muscle activation during locomotion[25], but no quantitative results have been published regarding metabolic augmentation.

1.2 Kinetics and Kinematics of Running

While walking resembles, and is most simply modeled as, an inverted pendulum with center of mass gravitational and kinetic energy oscillating out of phase, running most resembles a mass bouncing on a linear spring[33],[14][37]. Gravitational and kinetic energy remain primarily in phase in running while elastic energy stored in tendons contributes an out of phase component. In fact, the ground reaction force during stance phase varies approximately linearly with compression of effective leg length. Consequently, significant predictive power may be obtained from a simple spring-mass model which treats the body as a point mass bounding on a constant stiffness spring[33].

Following convention, the gait cycle (depicted in Figure 4-3) begins at foot strike. During early stance phase, the leg's effective length (the distance from the center of mass to the ground) decreases as the knee flexes and the ankle dorsiflexes. During
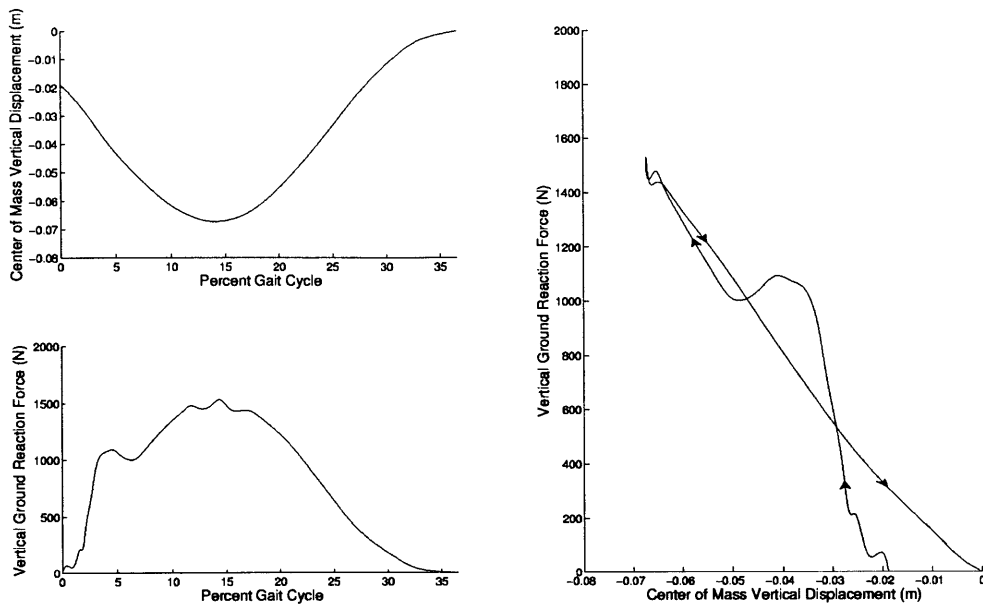
Figure 1-4: Spring-like behavior of the leg in the vertical axis during running's stance phase, showing predominantly spring-like behavior. Effective leg length is measured from center of mass to ground during stance. The initial peak in vertical ground reaction forces is associated with impact effects. Data adapted from [15].
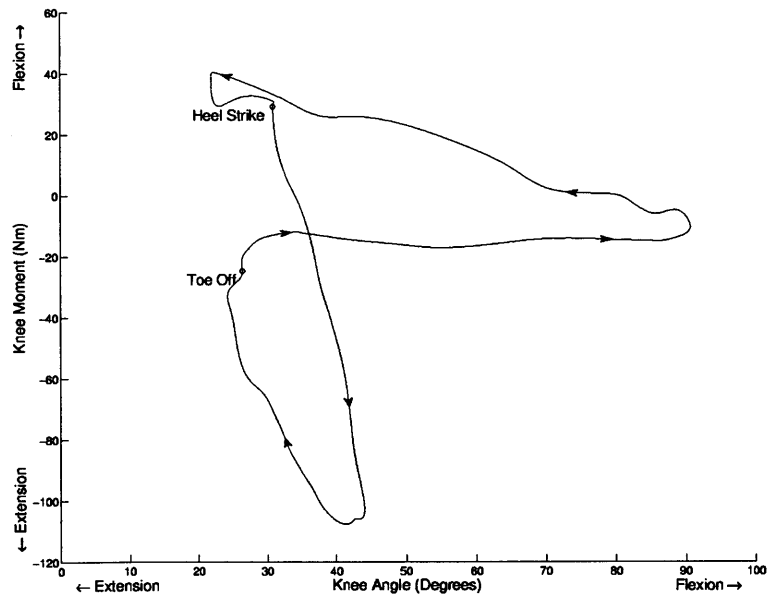
Figure 1-5: Torque and angle of the knee during running. The knee behaves approximately as a clutched spring, exerting little torque during swing (from toe off to heel strike), but acting as a stiff spring during stance (from heel strike to toe off). Data adapted from [37].

23

this time, the ground reaction force steadily increases[29][37] to three times body weight in distance running[36]. After midstance, when the body's center of mass is directly above the point of contact, this trend reverses; the leg extends while the ground reaction force decreases until the moment of toe off when swing phase begins.

Swing phase, during which the leg is not in contact with the ground but is moving forward and preparing to support the body in a subsequent stance phase, follows toe-off and accounts for more than 60% of the gait cycle[37]. As swing phase typically occupies more than half of the gait cycle, an aerial phase exists during which both legs are in swing. In order to accelerate the leg forward as quickly as possible, a hip flexor moment approaching 200Nm[3] is applied while the leg's moment of inertia is simultaneously reduced by a large knee flexion. In terminal swing, the knee must again extend prior to foot strike.

As a result of its opposing roles in stance and swing, the leg can be thought of as a two stiffness system - nearly zero in swing and very stiff in stance. This may be observed directly in the torque-angle trajectory of the knee (Figure 1-5) and ankle, which resemble those of a clutched spring.

Following McMahon and Cheng[33], the elastic behavior of the full leg in stance phase may be modeled as a mass bounding on a so-called leg-spring, which connects the center of mass to the foot, as shown in Figure 1-3. First, consider the one dimensional problem of vertical displacement of center of mass. As shown in Figure 1-4 this displacement varies linearly with vertical ground reaction force, if a vertical spring supported the center of mass throughout stance. This effective spring is characterized by k_{vert}, given by

$$k_{vert} = \frac{F_{z,peak}}{\Delta y} \tag{1.1}$$

where $F_{z,peak}$ is the maximum vertical component of the ground reaction force and Δy is the vertical displacement of the center of mass.

Due to the angle subtended, however, the effective leg spring in Figure 1-3, characterized by k_{leg}, is compressed from its rest length L_0 by ΔL much larger than Δy,

24
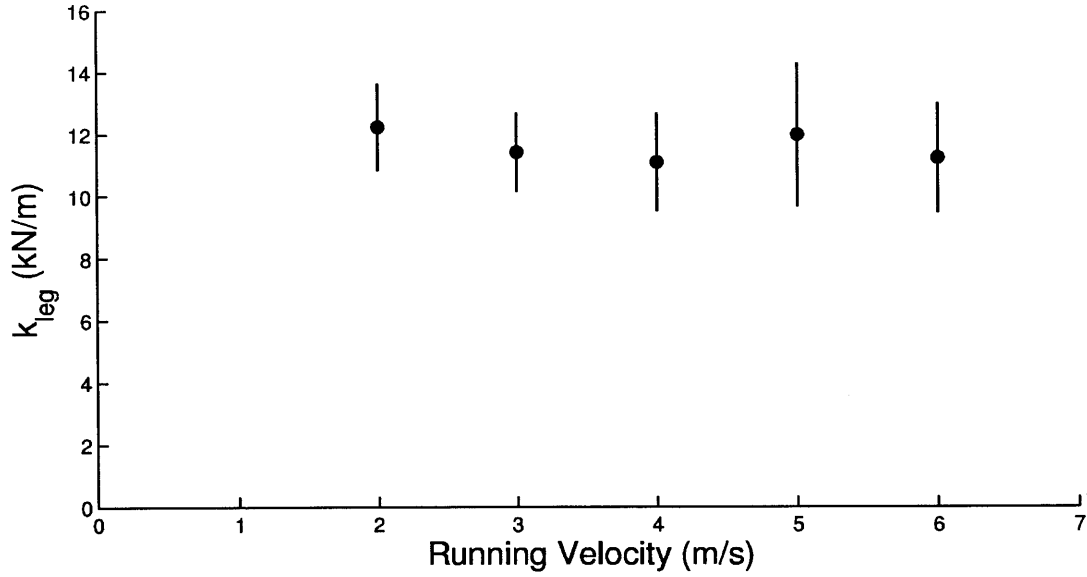
Figure 1-6: The effective leg stiffness k_{leg} depends weakly on running speed. Adapted from [14].

so that

$$k_{leg} = \frac{F_{z,peak}}{\Delta L} \tag{1.2}$$

Assuming symmetry of absorptive and generative stance with θ representing half the total subtended angle, it may be shown geometrically that ΔL is given by

$$\Delta L = \delta y + L_0 \left(1 - \cos\theta\right) \tag{1.3}$$

Moreover, it can be shown [33] that the effective θ is a function of forward velocity u and ground contact time t_c:

$$\theta = \sin^{-1}\left(\frac{ut_c}{2L_0}\right) \tag{1.4}$$

k_{leg} is used to characterize running gaits and must, by definition, be smaller than k_{vert}. For typical running speeds (3-5 m/s), the effective k_{leg} is on the order of 10kN/m and varies relatively little with speed[33][14] as shown in Figure 1-6. Even with body weight supported in simulation of low gravity, leg stiffness does not change[22]. However, leg stiffness is not invariant; it does increase for instance if stride frequency
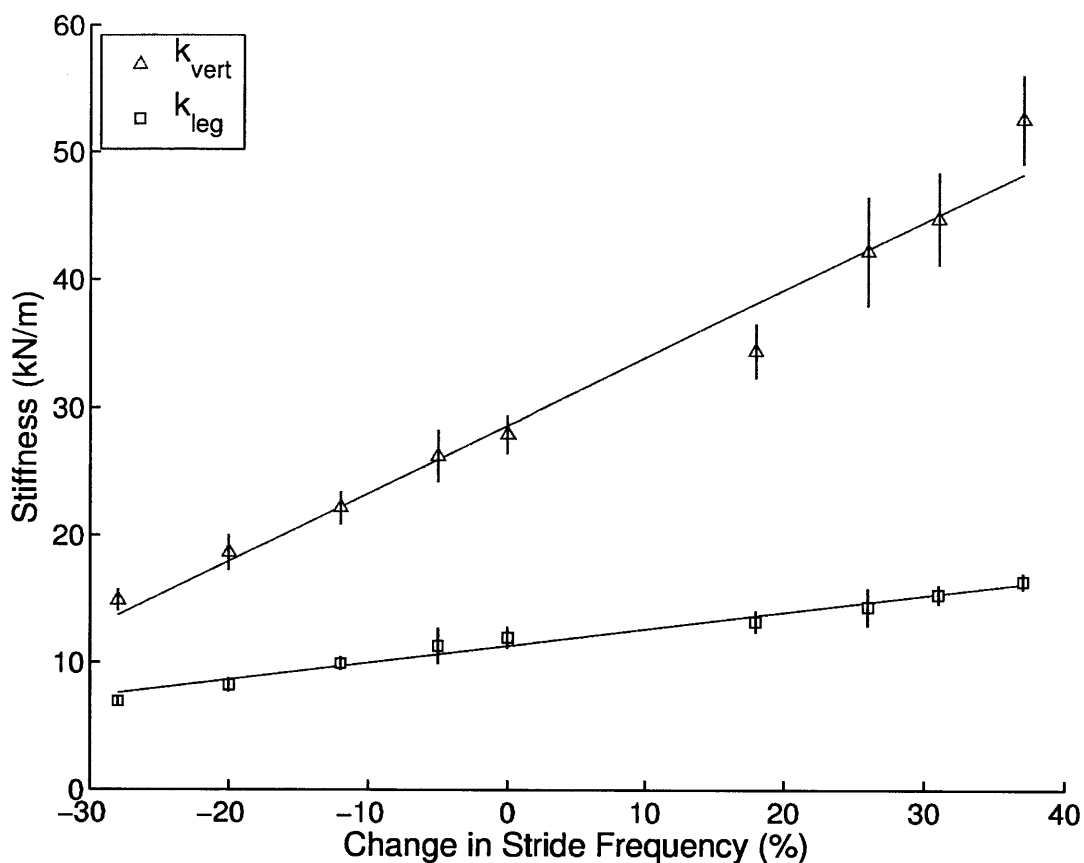
Figure 1-7: The effective leg stiffnesses k_{leg} and k_{vert} increase with stride frequency. Adapted from [15].

is deliberately increased[15], as shown in Figure 1-7.

This spring-like dynamic of leg joints likely derives from passive energy storage, accounting for the efficiency of human running. Tendons and ligaments have been implicated in the energy transfer and storage observed during running stance phase[4][1][8], though it is important to note that even ideal energy storage of this kind is not without cost as the series muscle must exert an opposing force to enable tendon stretch. Even a nearly isometric contraction, yielding little or no net mechanical work incurs a significant metabolic cost[32][1].

(a) Unlocked and flexed, offering minimal resistance in swing phase

(b) Locked and extended, preparing for impact in terminal swing phase

(c) Locked and compressed, storing energy in stance phase
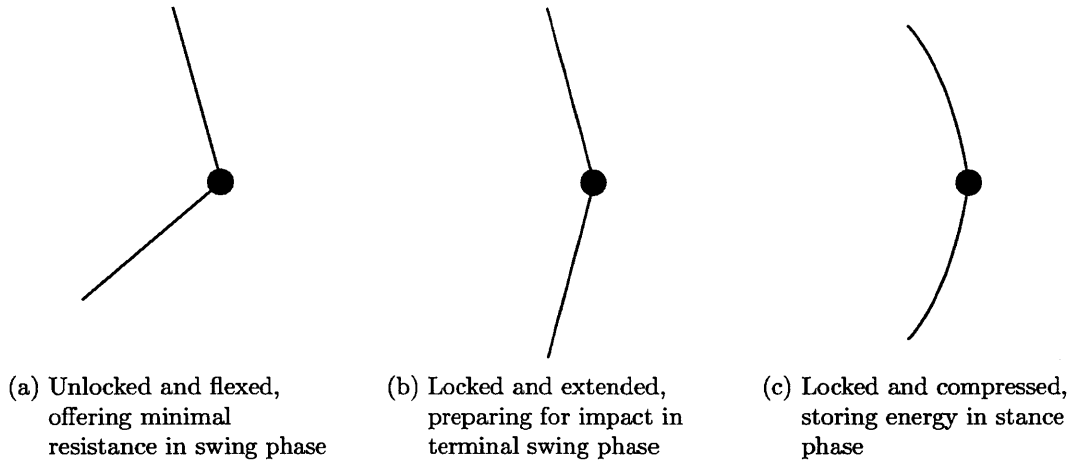
Figure 1-8: Conceptual behavior of a collapsable bow spring with exoskeletal knee joint, as used to augment running.

1.3 Augmentation of Hopping and Running

One may hypothesize that if the role of tendon could be fulfilled externally, series muscle activation could be reduced or eliminated while total kinetics, including the exoskeletal contribution, are preserved. In fact, there is evidence that total leg stiffness, including external contributions, is maintained in bounding gaits. If a series elasticity, namely a compliant ground surface, is introduced, total k_{vert} including the series compliant surface is maintained[18][28], even when doing so requires increasing biological leg stiffness by up to 68%. This adaptation is extremely fast, occurring within the very first step after transition to the compliant surface[19]. In hopping, the presence of a parallel spring has been shown to reduce biological leg stiffness in order to achieve the necessary k_{vert}, even when the external spring is non-linear[20]. An observed decrease in metabolic cost is hypothesized to be due to a decrease in activation of the ankle plantar flexors and knee extensors. Finally, if a passive spring is placed only across the ankle joint during hopping, total leg stiffness, k_{leg}, and total ankle quasi-stiffness, including the exoskeletal contribution, are both similarly conserved[17]

This thesis investigates a modification to the hopping exoskeleton in which the bow spring may collapse at an exoskeletal knee joint during swing phase but subsequently

lock rigidly prior to stance, as shown conceptually in Figure 1-8. Such a device permits a normal swing phase while augmenting stance phase as the hopping exoskeleton does. In light of the limitations of past exoskeletons described in Section 1.1, the design of this exoskeleton focuses heavily on minimizing power consumption, mass, and the influence of the device on natural sensing and dynamics. Moreover, this architecture is robust in that it may be repurposed to span one or several joints of the leg.

This device is used to study the effects of parallel stiffness at the knee on human running. Specifically, the influences of such an external spring on total leg stiffness and individual joint stiffnesses are investigated using motion capture and inverse dynamics with healthy recreational runners.

The design of such a quasipassive running exoskeleton is described in this document in three parts:

- **Human Attachment (Chapter 2):** Attachment to the human body poses both the functional question of which joints should be spanned by the parallel elastic element and the pragmetic question of how an elastic element may be fixed to the body in order to safely and comfortably transfer load.

- **Mechanical Design (Chapter 3):** Commercially available clutches capable of locking the spring and withstanding load during stance phase are far too heavy to be comfortably attached to the leg during running, necessitating the development of a custom high-torque clutch.

- **Control (Chapter 4):** Locking and unlocking the parallel spring requires precise timing and high reliability and ideally is performed using only intrinsic sensing at the exoskeletal knee.

Subsequently, in **Clinical Testing and Results (Chapter 5)**, the results of an experiment investigating the kinematic effects of parallel stiffness applied to the human knee in running are presented. Finally, **Discussion (Chapter 6)** considers the consequences of this work, both to biomechanics and to the future of mechanical interventions.

28

Chapter 2

Human Attachment

Load-bearing attachment to the human body poses several problems. First, there is a question of which joints the exoskeleton's springs should span. Subsequently, the problem of attachment itself is made particularly daunting by the compressibility of soft tissue and the ability of skin to translate relative to the underlying skeleton during motion.

2.1   Joint Geometry

The device described in this thesis constitutes a platform by which parallel elasticity may be applied to one or several joints of the leg, depending on the choice of harness. In principle, a harness needs simply to connect the body's center of mass to the ground through the passive compliance offered by the exoskeleton, but any number of geometries may accomplish this goal. Since all devices of this type span the knee, energy is stored during early stance knee flexion and returned during late stance extension. Energy storage due to motion in other joints depends on our choice of architecture and, in particular, whether the proximal attachment of the spring spans the hip and whether the distal attachment spans the ankle. Figure 2-1 schematically depicts the several exoskeleton geometries.

Though the experiment presented in Chapter 5 uses configuration (a), spanning only the knee, it is worthy of mention that configurations (b), (c), and (e) have been
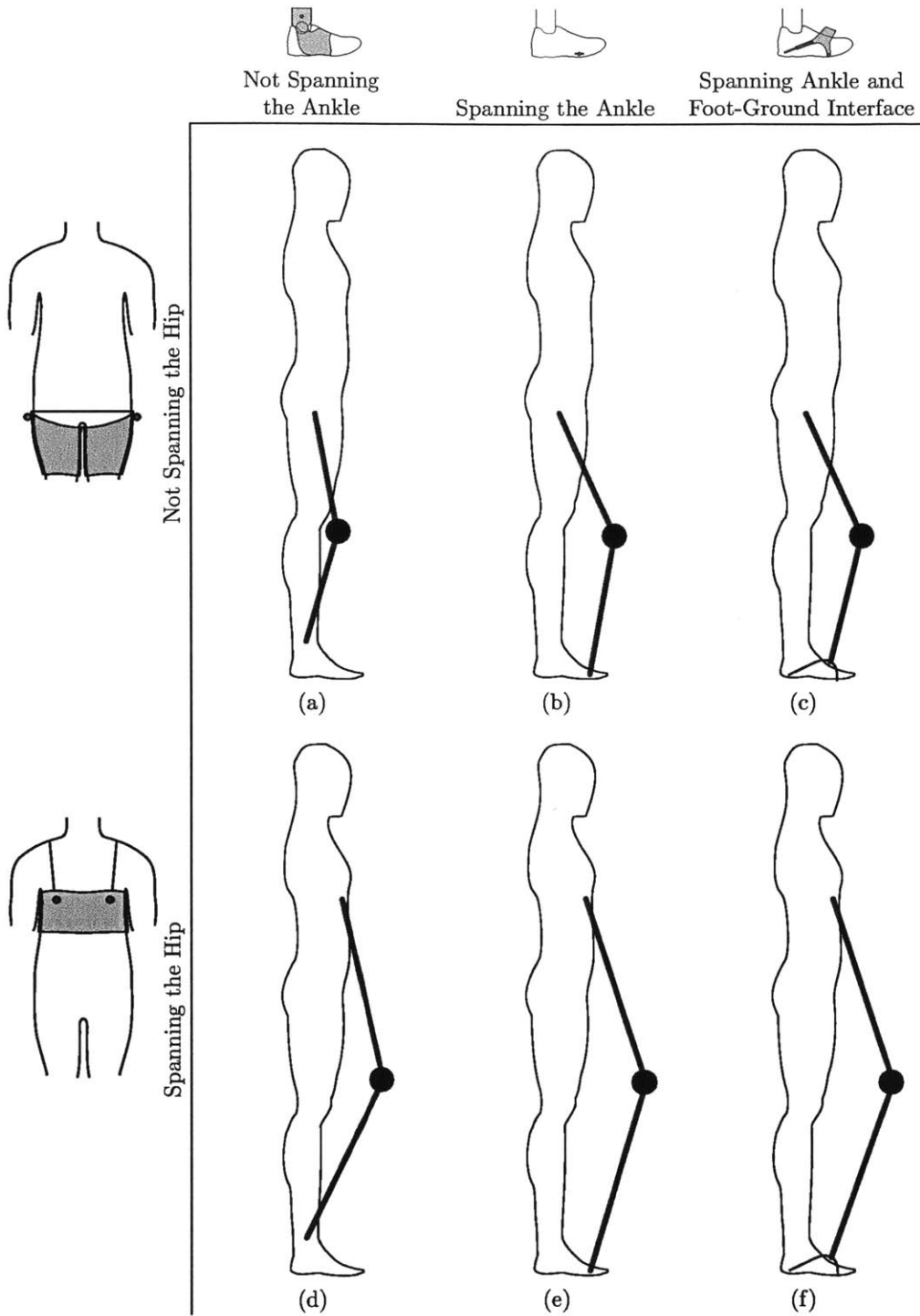
Figure 2-1: Possible configurations of the clutched parallel elastic exoskeleton by combination of exemplary proximal and distal attachments from Figures 2-2 and 2-3. Though shown with anterior spring orientation, posterior orientation is also possible. Configuration (a) is ultimately investigated here.

built and tested to varying degrees. Configuration (b), which spans the ankle and knee, corresponds to the hopping exoskeleton from which this works evolved (though the original harness may in practice permit very small moment arms about the hip). Unfortunately, the rigid toe attachment is better suited to hopping than to running, as it requires forefoot striking, thereby dramatically changing gait, and the mass of the device must be borne by the ankle during swing, thereby significantly increasing metabolic demand. Configuration (c) introduces a center of pressure tracking foot attachment to address the former problem and permit heel or midfoot striking, but this attachment point is complicated and prone to failure. Finally, configurations such as (e), with significant moment arms about the hip require a chest harness, which has proven significantly less comfortable than a cuff around the thigh in extended use.

If the spring spans the hip, a harness may be designed so that energy is stored during hip flexion and returned during hip extension. Because the torso remains nearly upright, an attachment around the pelvis (Figure 2-2c) like the rigid harness used in earlier hopping experiments or to the chest (Figure 2-2d) may be used to provide small or large moment arms about the hip. Alternatively, a pelvic harness aligned with the center of hip rotation (Figure 2-2b) minimizes this moment arm and attaching distal to the hip, as by compressive cuffs around the thigh (Figure 2-2a), eliminates hip involvement.

The ankle joint is more complicated. The conceptually simplest distal attachments are those in which attachment occurs above the ankle, as in Figure 2-3a. In these designs, rotation of the ankle does not affect spring compression. However, loads cannot be transferred directly into the ground; they must be transferred through the human skeleton. Even in the absence of ankle involvement, a single degree of freedom is still necessary at the attachment of the spring to accommodate rotation of the spring end due to bowing. A simple plain bearing permitting rotation in the sagittal plane suffices. Construction of these designs proves difficult due to migration and the inability to compress the calf without affecting the gastrocnemius and soleus. As with the pelvic compression harness, it is possible to approximate an above the ankle design by loading to the ground through an offset point nearly concentric with the

31

ankle as in Figure 2-3b, but in practice it is difficult to build such a structure into a shoe with sufficient rigidity. It is simpler to attach to knee or ankle braces, also shown in Figure 2-3a, to prevent migration.

If ankle involvement is desired, an attachment point may be placed near the ball of the foot, as in Figure 2-3c so that ankle dorsiflexion causes compression of the spring during early stance. A single degree of freedom is still sufficient, as it permits both ankle motion and bowing of the spring. For practical construction, this joint may be rigidly attached to the the toe cleat of a biking shoe, as it was in hopping exoskeleton. Ankle spanning of this sort assumes that the user toe runs, striking and leaving the ground on the ball of the foot. Unfortunately, as most runners do not naturally toe-strike as prominently as this design requires, ankle plantar flexors tend to fatigue quickly while wearing this harness. Additionally, the rigid sole and metal plate at the cleat proves uncomfortable for some users. Ideally, an attachment to the foot which spans the ankle should account for natural heel or mid-foot strikes followed by anterior motion of the center of pressure leading up to toe off on the ball of the foot. Such an attachment point may be thought of as spanning both the ankle and the foot-ground interface. One way of constructing such a device is depicted schematically in Figure 2-3d.

2.2   Harness Evolution

The harness used for the exoskeleton has evolved significantly over its development, originally spanning the knee and ankle and eventually only spanning the knee.

The original harness, shown in Figure 2-4a, is nearly identical to the harness developed for a hopping exoskeleton. A rigid proximal frame is attached to the waist and groin using a standard climbing harness while the structure is compressed against the pelvis, as in Figure 2-2b. A three degree-of-freedom joint concentric to the hip offers full range of motion of the exoskeletal spring, which attaches distally to a one degree-of-freedom joint lateral to the toe of a shoe, as in Figure 2-3c. Unfortunately, this design assumes the symmetrical loading found in hopping and tends to rotate in
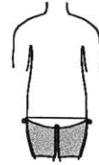
(a) Molded cuffs compress the thighs, likely elastically supported by the opposing hips and potentially part of a full knee brace. Care is taken to avoid compressing the hamstrings. Attachment is typically lateral (shown); anterior and posterior attachments are possible but uncomfortable and unwieldy.
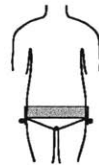
(b) A rigid frame compresses the pelvis and is anchored by a climbing harness around the legs. Attachment is lateral and approximately aligned with the greater trochanter. As such, it is approximately concentric to the hip and may be considered as not spanning the joint. This harness was used with in the hopping exoskeleton.

(c) The pelvis compressing frame in (b) is used with attachment points located significantly above the hip. Attachment is typically lateral (shown) or posterior; anterior attachment is possible but unwieldy.

(d) A molded cuff compresses the chest with shoulder straps to minimize migration. Load may also be shared with thigh cuffs (right). Attachment is anterior or posterior.

Figure 2-2: Three possible attachments for the proximal end of the bow spring. Some designs allow the spring to span the hip joint, while others eliminate hip involvement. A single sagittal plane rotation joint indicated by a dark circle permits flexion of the bow spring in all cases.

Not Spanning the Ankle
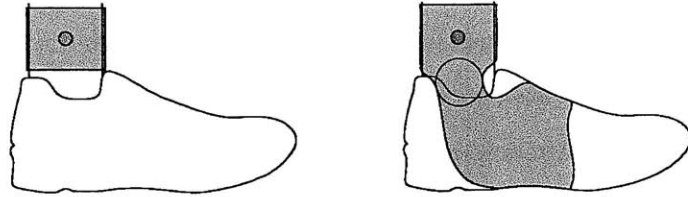
(a) Molded cuff compresses the calf, likely integrated into a full knee or ankle brace (shown, right) to reduce migration.
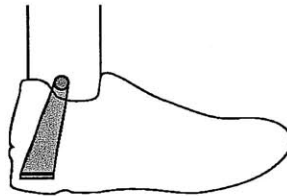
(b) Rigid attachment to the heel, offset to be approximately concentric to the ankle.

Spanning the Ankle
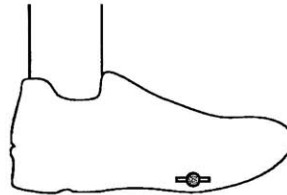
(c) Rigid attachment at the toe. Forces toe running. This attachment was used in the hopping exoskeleton.

Spanning Ankle and Foot-Ground Interface
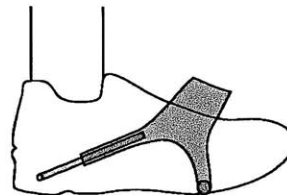
(d) An additional two degrees of freedom (one rotational, one linear) permit direct ground contact independently of foot position, allowing normal heel strike and toe off while loading directly into the ground.

Figure 2-3: Four possible attachments for the distal end of the bow spring. Some designs allow the spring to span the ankle joint, while others eliminate ankle involvement. A single sagittal plane rotation joint indicated by a dark circle permits flexion of the bow spring in all cases. Attachments are shown configured for lateral attachment, but may also be used for anterior or posterior attachment.

(a) Pelvic harness with toe attachment

(b) Thigh cuff harness with toe attachment
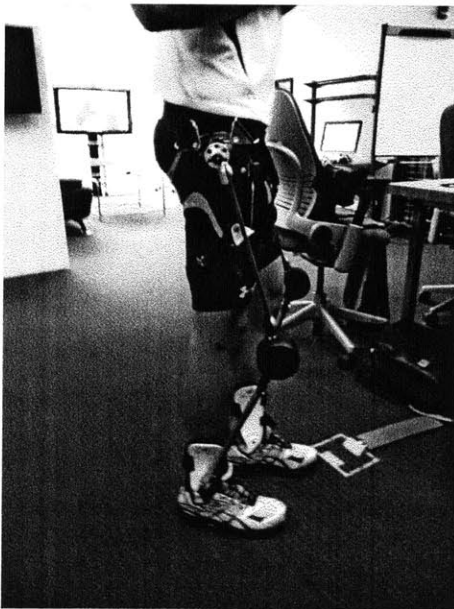
(c) Thigh cuff harness with shank attachment
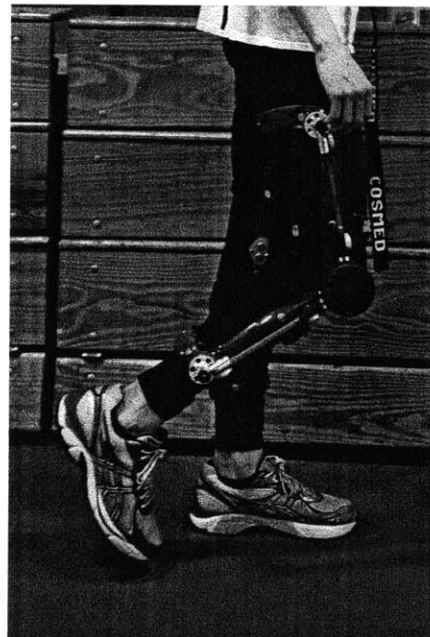
(d) Knee brace harness

Figure 2-4: Selected harness designs

35

the coronal plane when loaded unilaterally, making it poor at loading the exoskeletal spring. This harness is also heavy and somewhat uncomfortable to wear and the mass of the exoskeleton must be borne through the ankle in swing, making it very costly metabolically.

An alternate proximal harness, shown in Figure 2-4b, loads through molded thigh cuffs as in Figure 2-2a. This design offers greater hip mobility, less discomfort, and a significantly reduced mass. Most importantly, the proximal attachment point is far less able to move up the leg under load, improving energy storage in the spring.

Loading the spring propertly using a distal attachment rigidly connected to the toe requires a plantar flexed toe-striking gait which is not natural for most runners. One solution to this problem, shown in Figure 2-5, is an articulated distal attachment which allows the spring to load through the ground even as the foot moves around it. At heel strike, the spring contacts the ground below the toe. As the foot rolls forward, the linear and rotary joints allow the spring contact point to remain stationary until toe off, after which return springs reset the device. This design requires manual tuning of two degrees of freedom to match the wearer's foot size and foot angle at heel-strike. It also increases leg length slightly, potentially causing ground interference in late swing. Ultimately, without full integration into a shoe, this attachment proved too complex and fragile for practical use.

Alternatively, the problem of ankle articulation can be avoided by not spanning the ankle. An alternative distal harness, shown in Figure 2-4c, attaches the exoskeleton to the shank, loading to the ground through a stirrip, as in Figure 2-3a. This additionally solves the problem of supporting the exoskeletal mass through the ankle during swing. Unfortunately, a satisfactory ankle joint was never achieved. Those which were attempted either proved uncomfortably heavy or failed under load.

This knee-spanning architecture can be achieved using a harness similar to a traditional polycentric knee brace with elements borrowed from prosthetic socket technology, shown in Figure 2-4d. On either side of the knee, the exoskeleton attaches to the leg using rubber-lined carbon fiber cuffs molded to one wearer. Care has been taken to remove material from the cuffs in areas where muscle bellies may protrude,
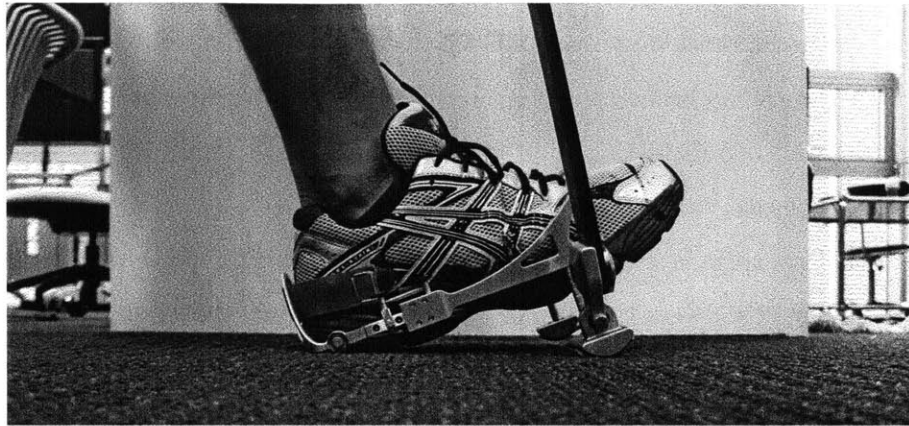
(a) Heel Strike

(b) Midstance
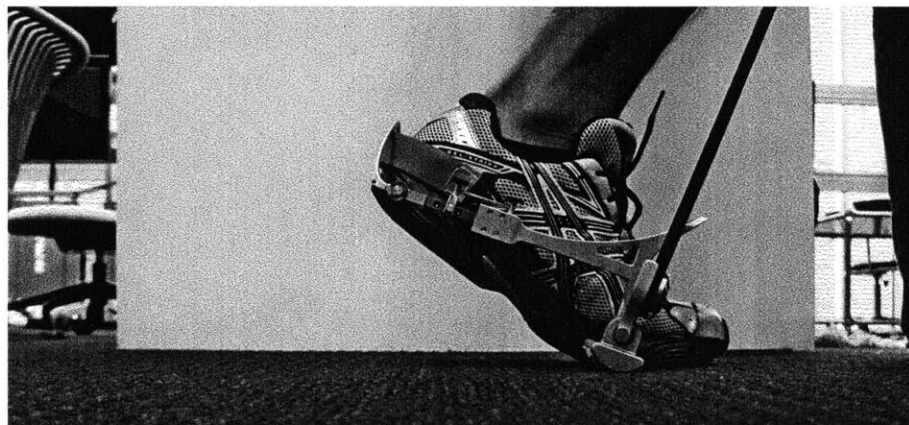
(c) Toeoff

Figure 2-5: An articulated distal attachment which spans both the ankle and the foot-ground interface.

most notably around the hamstrings and gastrocnemius. Rigid carbon fiber strips back the brace at its most proximal and distal extents and independently adjustable velcro straps secure the brace to the leg both anterior and posterior at four heights (two proximal and two distal). The brace may be padded to improve fit when worn by other than the cast subject.

The exoskeletal springs are attached laterally to the thigh cuffs. Lateral mounting has the advantage of allowing the springs to follow the form of the leg relatively closely, but the disadvantage that it widens the wearer and produces a larger than normal torque about the center of mass during stance. For these reasons, efforts have been made to reduce the lateral displacement of the exoskeleton as much as possible.

The experiment presented in Chapter 5 considers this knee brace harness, corresponding to configuration (a) in Figure 2-1. For this purpose, spanning only the knee is adventageous in that it facilitates biomechanical analysis of the exoskeleton's effects on a single joint. Pragmatically, this configuration also holds particular promise as a practical orthosis. One may hypothesize that, during running, a robotic knee brace built in this way could reduce load and therefore pain for sufferers of chronic knee pain. Such a device could even permit recreational running in patients currently forced to avoid high impact activities.

Chapter 3

Mechanical Design

An exoskeletal knee joint that permits running is difficult to build. The human knee experiences torques which may reach 200Nm during stance phase of running. Assuming that the exoskeleton geometry is similar to that of the natural leg, the proposed exoskeletal knee joint should be rated to loads of at least this in order to permit any of the various attachment configurations described in Chapter 2. In practice, the natural leg will still bear some fraction of this load, rendering this rating conservative. The exoskeletal knee must lock precisely at peak knee extension, immediately before the swing phase retraction which precedes foot strike, to ensure that the spring begins deforming immediately at foot strike and maximum energy is stored. Consequently, the device must offer a high resolution of potential locking angles (or ideally a continuum) and must be capable of engaging quickly. Latency compensation (see Section 4.2.2) proves reliable at accurately predicting peak extension up to 50ms in advance, so the device must be capable of locking within that window. Finally, due to the high metabolic demand of forward swing and the corresponding necessity for a low moment of inertia about the hip, the joint must permit large knee flexion up to 135° and contribute as little distal mass to the leg as possible. These design specifications are enumerated in Table 3-1.

Due to the large number of components and relative complexity of this design, notation can become troublesome. The following convention is used. If it is necessary to disambiguate the component or subassembly being discussed, a single letter

Symbol	Description	Goal	Achieved
T	Holding Torque	200 Nm	190 Nm
F_r	Radial Load	3,000 N	4,780 N
F_a	Axial Load	1,000 N	4,050 N
Δt_{eng}	Engagement Time	50 ms	26 ms
	Resolution	2 ^{o}	1.8 ^{o}
	Range of Motion	135 ^{o}	130 ^{o}
	Mass	1,000 g	710 g
	Diameter	100 mm	85 mm
	Thickness	50 mm	49 mm

Table 3-1: Design specifications for the exoskeletal knee clutch. As the clutch has not been driven to failure, its maximum load capacities are estimated.

Component	Subscript
Clutch Subassembly	c
Transmission Subassembly	t
Ring Gear	r
Planet Gear	p
Sun Gear	s
Sun Gear Rim	h
Clutch Plate	p
Linear Bearing	l
Elastic Element	e
Brace	b

Table 3-2: Subscripts used to disambiguate the component or subassembly being referenced, listed in order of appearance.

subscript is used. If the symbol in question were to normally contain a subscript, the component subscript will follow it, with a comma separating the two. The subscripts used are summarized in Table 3-2. A similar convention is used for materials, as shown in Table 3-6. Modifiers such as *min* and *max* will follow all other subscripts, again preceded by a comma.

3.1   Exoskeletal Knee

No commercially available clutch or brake is suitable for these specifications. Consider the available technologies:

- **Particle brakes** use an electromagnet to bind together a ferrous powder, impeding the motion of a brake rotor through it. Particle brakes permit very accurate control of torque, which varies almost linearly with applied voltage.

- **Friction clutches** force two surfaces against each other, using the friction between them to prevent slippage. A sufficient normal force must be applied in order for the clutch to remain locked. This force may be provided by air pressure, springs, or permanent or electro-magnets. The wrap spring clutch is a unique friction clutch in which positive feedback exists between applied torque and the frictional force engaging the clutch.

- **Toothed clutches** are similar to friction clutches, but use disks with interlocking tooth structures instead of relying purely on friction. Toothed clutches may withstand significant torque, but at the cost of discretizing the possible engagement angles. In some cases a synchronizer is necessary to ensure that the toothed disks do not begin to engage at other than an allowed engagement angle.

Of these options, toothed clutches offer by far the highest holding torque for a given volume, as load is shared over all teeth, producing a large shear area of resistance. Unfortunately, as shown in Figure 3-1, even the lightest commercially available device offering sufficient holding torque for our application has an unacceptably high mass of 1.6kg. Equally troubling, toothed clutches offer only discretized engagement angles with poor resolution (5° is typical). As a result, it proved necessary to design a custom toothed clutch with an integrated planetary gearbox which decreases load on the clutch plates and increases effective resolution. The complete device, depicted schematically in Figure 3-2, is constructed so that the distal bow spring attachment serves as input to the ring of a planetary system whose planet carrier is fixed to the proximal assembly. The output of the planetary system (the sun) is coupled through a toothed clutch to the proximal assembly, effectively locking the joint when the clutch is engaged by activation of the solenoid.
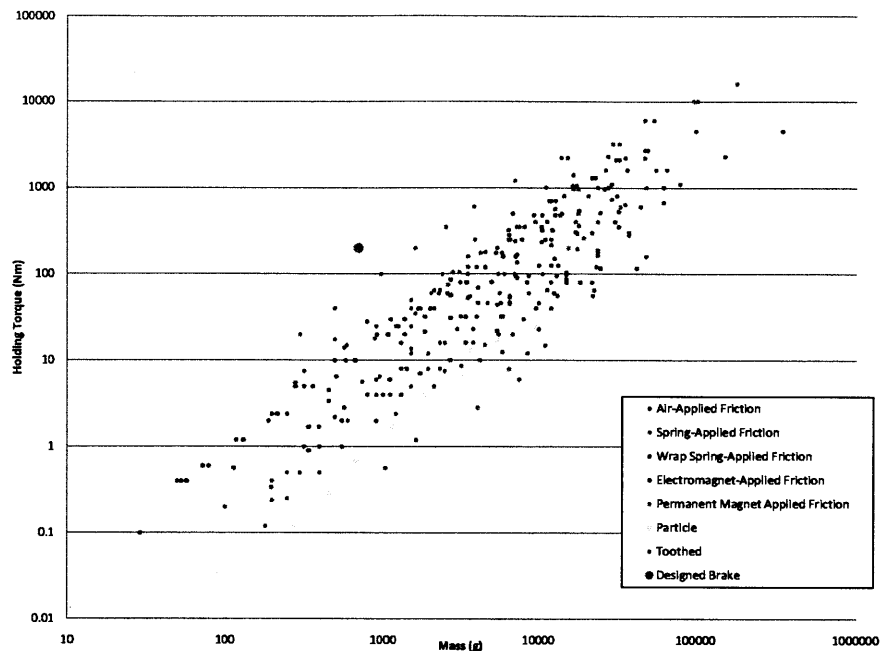
Figure 3-1: Maximum holding torque versus mass plotted on log-log axes for several hundred commercially available clutches and brakes. For comparison, the exoskeletal knee described here is also shown, plotted with a mass which additionally includes electronics, instrumentation, and mounting.

The complete exoskeletal knee is intended to be as light as possible in a package comparable in size to the human knee with no medial protrusions. As inertia in the distal portion is detrimental to rapid knee flexion, the majority of mass should be located in the proximal subassembly. To reduce and facilitate maintenance, efforts should be made to minimize internal wiring. Finally, to simplify manufacturing and encourage the production of spare parts, as many parts as possible should be achiral. The self-contained electromechanical system, shown in Figures 3-3 and 3-4, includes mounting, power supply, and electronics and withstands a 200Nm load while fitting in an 85mm diameter by 49mm thick package with a mass of only 710g.

3.1.1 Clutch

At the heart of the mechanism is the toothed clutch, which selectively couples the output of the planetary gearbox rigidly to the proximal assembly. One clutch plate therefore rotates with the planetary sun and is coupled by gearing to the distal attach-
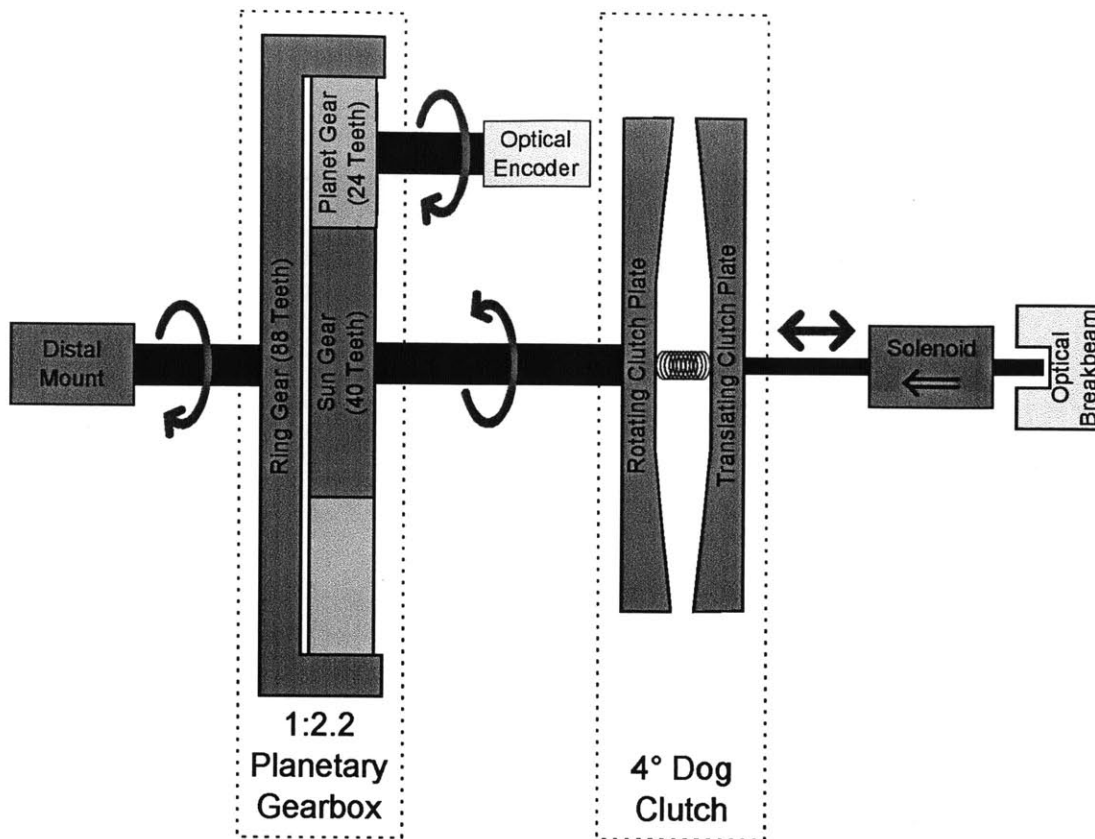
Figure 3-2: Schematic depiction of the designed clutch, showing the dog clutch, integrated planetary gearbox, and instrumentation. The system, including the orbit of the planetary gearbox, is depicted as mechanically grounded to the proximal assembly. Note that though the actual device is functionally equivalent to this depiction, its construction varies significantly.

Symbol	Description	Value
N_c	Clutch Plate Tooth Count	90
h_c	Clutch Plate Tooth Height	2.0 mm
w_c	Clutch Plate Tooth Width	1.5 mm
d_c	Clutch Plate Tooth Depth	6.5 mm
$r_{i,c}$	Clutch Plate Tooth Inner Radius	22.5 mm
$r_{o,c}$	Clutch Plate Tooth Outer Radius	29.0 mm
$r_{b,c}$	Clutch Plate Coupling Boss Radius	16.0 mm
t_c	Clutch Plate Thickness	1.5 mm

Table 3-3: Constants related to mechanical design of the clutch plates.
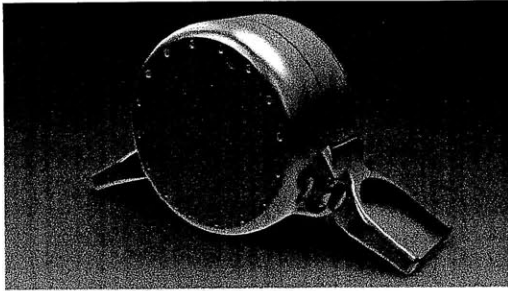
(a) Fully assembled
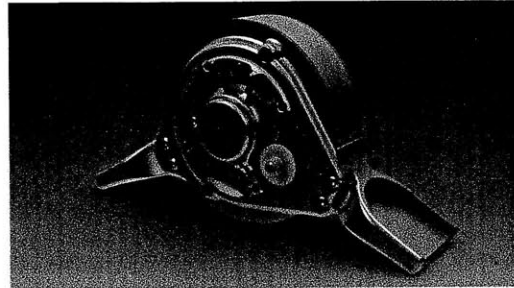
(b) Latteral assembly removed to show encoder disk, solenoid, and solenoid mount
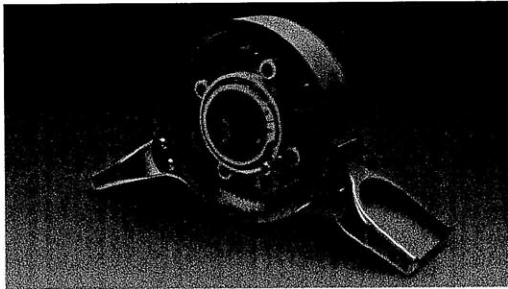
(c) Lateral planet carrier removed to show planetary gearbox
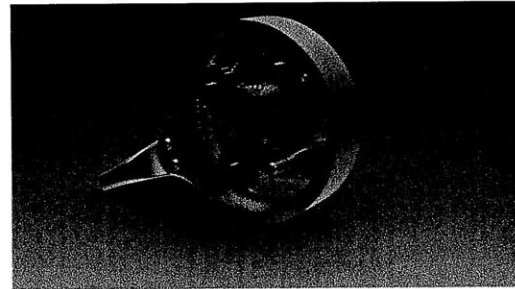
(d) Medial planet carrier and translating clutch plate removed to show rotating clutch plate
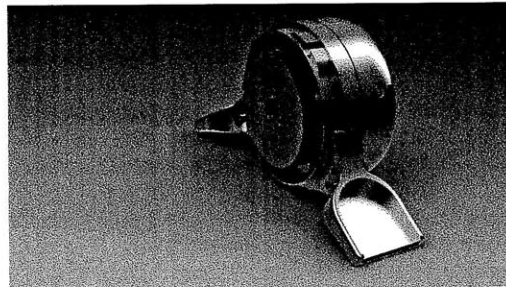
(e) Reverse angle with medial components removed to show both clutch plates in the disengaged state

Figure 3-3: Renders of the right exoskeletal knee joint.
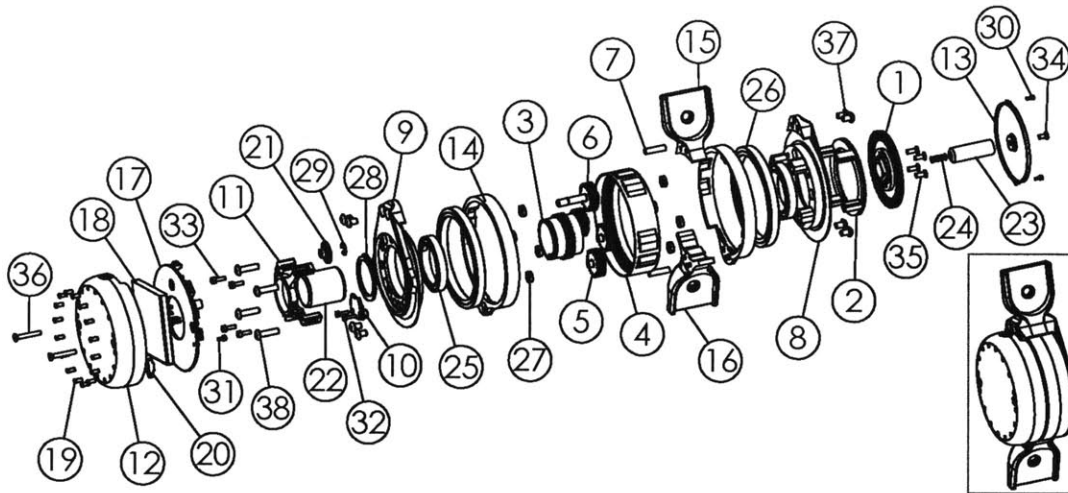
No.	Name	Material	Mass (g)	Quantity
1	Rotating Clutch Plate (Right)	Titanium Grade 2	28.6	1
2	Translating Clutch Plate (Right)	Titanium Grade 5	18.7	1
3	Sun Gear	Titanium Grade 5	22.5	1
4	Ring Gear	Titanium Grade 5	48.9	1
5	Planet Gear	Titanium Grade 2	8.3	3
6	Long Planet Gear	Titanium Grade 2	9.9	1
7	Pin	Titanium Grade 2	0.9	2
8	Medial Planet Carrier	Aluminum 6061	49.5	1
9	Lateral Planet Carrier	Aluminum 6061	57.8	1
10	Hard Stop	Aluminum 6061	2.2	1
11	Solenoid Mount	Aluminum 6061	8.6	1
12	Lateral Cap	Aluminum 6061	38.1	1
13	Medial Cap	Aluminum 6061	6.5	1
14	Distal Ear	Aluminum 6061	20.3	2
15	Proximal Mount	Aluminum 6061	32.6	1
16	Distal Mount	Aluminum 6061	36.6	1
17	Circuit Board	(Multiple)	25.0	1
18	Lithium Polymer Battery	(Multiple)	16.8	1
19	Light Pipe	Acrylic	0.0	16
20	Right Angle Light Pipe	Acrylic	0.2	1
21	EP4 Optical Encoder Disk	Aluminum 6061	3.0	1
22	LT8x9 Solenoid	Brass and Copper	55.0	1
23	Solenoid Plunger	Ductile Iron	22.6	1
24	Solenoid Return Spring	Steel	0.2	1
25	Sun Bearing	Steel AISI304	20.0	2
26	Ring Bearing	Steel AISI304	56.8	2
27	Planet Bearing	Bronze SAE841	0.5	8
28	Retaining Ring	Cast Carbon Steel	3.7	1
29	E-Clip	Cast Carbon Steel	0.2	1
30	M1.6x0.35x4 Cap Screw	Steel	0.5	2
31	M2x0.4x4 Cap Screw	Steel	0.3	2
32	M2x0.4x8 Cap Screw	Steel	0.4	2
33	M2.5x.45x8 Cap Screw	Steel	0.7	4
34	M3x0.5x6 Flat Head Screw	Steel	0.5	1
35	M3x0.5x8 Flat Head Screw	Steel	0.6	4
36	M3x0.5x20 Flat Head Screw	Steel	1.4	2
37	M4x0.7x6 Cap Screw	Steel	1.2	8
38	M4x0.7x16 Cap Screw	Steel	2.3	4

Figure 3-4: The right knee clutch at 1:5 scale shown assembled and exploded with its bill of materials. The first 17 entries in the bill of materials are custom made; the remainder are available off the shelf. The device is oriented as one would face a wearer, so that the lateral direction is to the left of the drawing. The clutch plates (Section 3.1.1) are to the far right and the planetary gearbox (Section 3.1.2) is in the center. The left knee clutch varies only in the orientation of the proximal and distal mounts, the initial orientation of the sun gear relative to the hard stop, and the use of left-handed dog clutch plates.
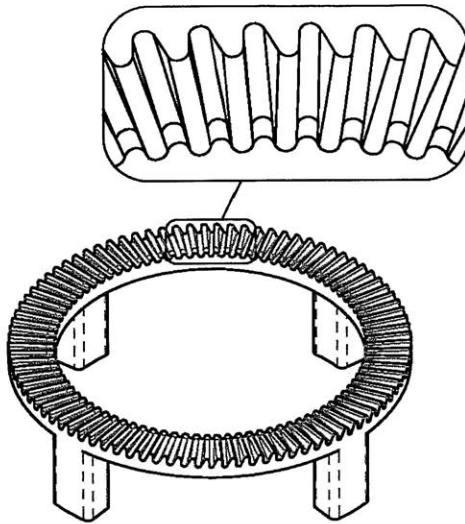
Figure 3-5: The translating clutch plate shown actual size with a detail 4:1 view of the sawtooth geometry.

ment while the other is constrained only to translate axially relative to the proximal assembly and is driven by a solenoid to engage the rotating plate.

To avoid the need for a synchronizer, the sawtooth dog clutch (Figure 3-5), is preferred to the square tooth castle clutch. The dog topology ensures that during partial engagement an energy gradient exists which tends to align and fully engage the clutch. To minimize wear, the sharp roots and tips of the teeth are filleted. Unfortunately, this also introduces an unengaged unstable equilibrium, but in practice any movement of the device remedies this potential problem.

The choice of a dog clutch also permits a ratcheting effect; when engaged, the joint cannot be flexed, but extension remains possible. Consequently, control strategies may err in favor of early engagement before the knee has reached peak extension. Deliberately doing so is not a reasonable strategy, however. Extension of the joint during clutch engagement is somewhat impeded and presumably contributes a non-negligible metabolic cost.

The clutch plates are produced in titanium to minimize weight and two different alloys (grades 2 and 5) are used to reduce galling. The geometry of the clutch plates is heavily constrained by tight integration with the planetary gearbox (see Sec-

46

Symbol	Description	Value
R_t	Planetary Transmission Ratio	2.2
P_t	Number of Planets	4
m_t	Planetary Spur Gear Module	0.8 mm
ϕ_t	Planetary Spur Gear Pressure Angle	20 ^{o}
f_t	Planetary Spur Gear Face Width	6.0 mm

(a) Constants related to the gross transmission

Description	Ring	Planet	Sun
Number of Teeth	$N_r = 88$	$N_p = 24$	$N_s = 40$
Number of Bearings	$B_r = 2$	$B_p = 2$	$B_s = 2$
Pitch Radius	$r_{p,r} = 35.2$ mm	$r_{p,p} = 9.6$ mm	$r_{p,s} = 16.0$ mm
Base Radius	$r_{b,r} = 33.0$ mm	$r_{b,p} = 9.0$ mm	$r_{b,s} = 15.0$ mm
Addendum Radius	$r_{a,r} = 34.4$ mm	$r_{a,p} = 10.4$ mm	$r_{a,s} = 16.8$ mm
Root Radius	$r_{r,r} = 36.2$ mm	$r_{r,p} = 8.6$ mm	$r_{r,s} = 15.0$ mm
Rim Inner Radius			$r_{i,s} = 13.3$ mm

(b) Constants parameterizing gears of the transmission

Table 3-4: Constants related to mechanical design of the transmission. Note that not all listed constants are independent.

tion 3.1.2) to an inner diameter of 45mm and outer diameter of 58mm. These parts are manufactured by contour milling, enforcing a minimum base fillet at the inner radius of 1/64" and thereby limiting the resolution to 4° (90 teeth). Because they must ratchet in opposite directions, the clutch plates for the right and left assemblies use reversed sawteeth, making these plates the only chiral components in the design.

3.1.2 Planetary Gearbox

A planetary gearbox is incorporated primarily to compensate for the discretized resolution offered by the dog clutch. This gearing additionally reduces the torque applied to the dog clutch which in turn reduces frictional binding of the plates, increasing the maximum torque under which disengagement can occur.

The gearbox is constructed with the planet carrier fixed to the proximal assembly, the ring connected to the distal attachment as input, and the sun connected to the dog clutch as output. The thickness of the complete device is limited by the solenoid's length; to not increase this further, the sun gear is hollow and passes around
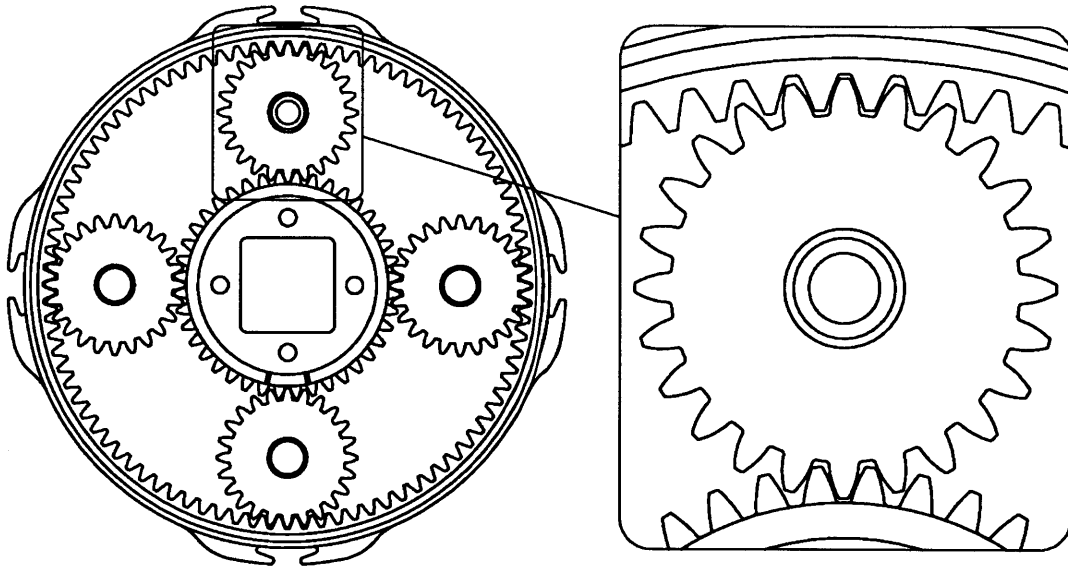
Figure 3-6: Planetary gearbox, shown full scale, with detail 3:1 view showing the involute gear interfaces associated with a single planet.

the solenoid (which does not rotate relative to the proximal assembly). This sets a minimum diameter for the sun and limits the achievable gear ratio, set by the ratio of the ring pitch diameter to the sun pitch diameter. Minimizing the total package diameter, after taking into account available bearings, yields ring, planet, and sun tooth counts of 88, 24, and 40 with a 0.8mm tooth module chosen to ensure multiple tooth engagement at all times. This corresponds to a ratio of 2.2:1 and a final effective clutching resolution of 1.8°. Accommodating bearings leaves a gear width, w, of 6mm.

As in the clutch, titanium is used to minimize weight and two different alloys are used to minimize galling. Grade 2 titanium is insufficient to achieve the desired maximum torque without plastic deformation (see Section 3.3.2), so the planet gears are specified as the less common grade 4 titanium[1]. The ring and sun gears are specified as grade 5. Tooth profiles are cut by wire EDM to 0.5mil tolerance.

The planetary gearbox is also used to limit the range of motion of the clutch to

---

[1]In practice, the more readily available grade 2 titanium was used for the planet gears, derating the exoskeletal knee joint to 110Nm. It was determined that for the lifetime expected of the prototype exoskeletal knee clutch, the increased wear and potential slight plastic deformation were acceptable, given the paucity of tests which would expose the exoskeleton to torques in excess of this.

prevent hyperextension or collision of the attachment points. The usable range of motion is approximately 130° which, after gearing, corresponds to 286° of rotation of the sun relative to the proximal assembly. A hard stop is attached to the planet carrier and may be engaged on either side by a tab protruding from the sun gear, permitting precisely the desired 286° of motion. This subassembly is achiral, though the sides of the hard stop corresponding to full flexion and full extension reverse between the left and right assembled joints.

3.2 Elastic Element

The elastic element of the exoskeleton consists of thin strips of semi-rigid unidirectional "E" fiberglass laminate located proximal and distal to the lockable exoskeletal knee joint, as shown in Figure 1-8. The net system constitutes a compression spring, characterized by the geometry of these elastic elements. While varying elastic modulus and cross-section allows for variation of spring stiffness, the form of the force-distance relationship depends on spring and attachment geometry. Simulation of the spring deformation therefore allows for the design of nearly-linear or highly nonlinear springs in the various geometries described in Section 2.1. As the deformations experienced exceed those typically considered in small angle approximations, it is necessary to perform a finite element analysis to characterize the net spring.

First, consider a single strut compressed axially with hinges at each end, having elastic modulus E, 2nd moment of area I, and length L. Divide this strut into N elements, each of which deflects some angle α_i with constant bending radius and fixed arc length L. The slopes of these N elements must always match where two elements meet. This division into elements is shown in Figure 3-7.

The constitutive law of bending gives moment by

$$M = -EI\frac{d^2w}{dx^2} \tag{3.1}$$

where x denotes axial distance and w denotes off-axis deformation[10]. This may be

49
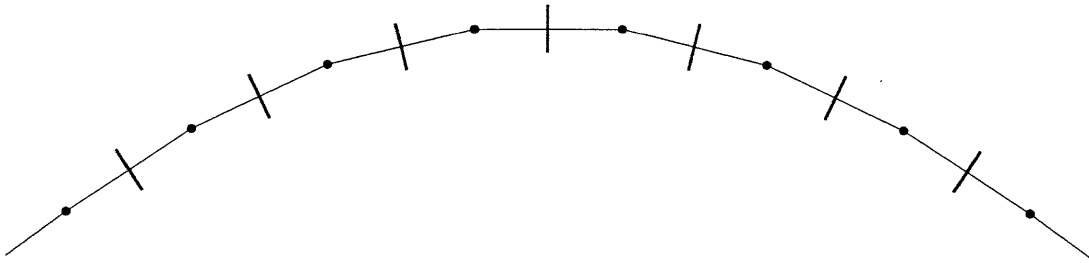
Figure 3-7: Finite element division of an elastic strut. Meetings between elements are denoted by red lines and the ability of each element to deflect is denoted by a hinge joint, though in actuality the model treats each segment as bending with constant radius.

rewritten in terms of the radius of curvature R_i or, equivalantly, the subtended angle α_i for an element of length L/N:

$$M_i = -EI\frac{1}{R_i} \tag{3.2}$$

$$= -EI\frac{N}{L}\alpha_i \tag{3.3}$$

The energy stored in order to achieve this configuration may be found by integrating:

$$U_i = \int_0^{\alpha_i} EI\left(\frac{N}{L}\right)\alpha\,d\alpha \tag{3.4}$$

$$= \frac{1}{2}EI\left(\frac{N}{L}\right)\alpha_i^2 \tag{3.5}$$

Therefore the total energy stored in a strut composed of elements each subtending α_i is

$$U = \frac{1}{2}EI\left(\frac{N}{L}\right)\sum_{i=1}^{N}\alpha_i^2 \tag{3.6}$$

As the physical spring will choose its lowest energy configuration, it suffices to minimize equation Equation 3.7 over the space of α_i subject to external boundary conditions. In this case, because the endpoints are hinged, the only boundary condition is the distance between the endpoints (that is, the amount of compression on the spring). This final length l may be calculated by straightforward, if algebraically complicated, geometry (which may be normalized by the arc length L) and the error
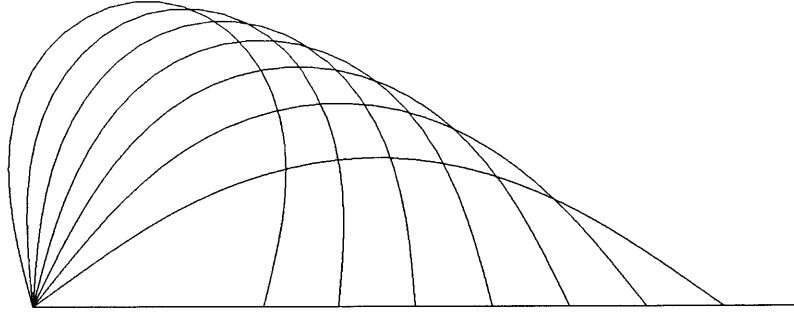
Figure 3-8: Example large angle deflection of an initially straight spring strut with constant EI product. Curves show deflections associated with compression of 0% to 70% of length in increments of 10%. Note that these deflected shapes are independent of rest length L, 2nd moment of area I, and modulus E.

in compression distance added to the cost function. The configuration of the spring may be found by minimizing a cost function of the form

$$C = \sum_{i=1}^{N} \alpha_i^2 + \lambda(l_{config}(\vec{\alpha}) - l_{goal})^2 \tag{3.7}$$

where λ is large so that the length error tends to zero. Though more computationally efficient approaches surely exist, Nelder-Mead Simplex, as implemented in MATLab's *fminsearch*, is sufficient to perform this optimization if performed using small steps in compression and using the previous result to seed each subsequent optimization. Spring force (which due to the hinged attachment must be purely along the line connecting the endpoints) is then given by

$$F = \frac{dU}{dx} \tag{3.8}$$

This model predicts equivalant configurations following large angle deformation for all choices of E and I after normalizing for L. Example deformations of a single strut are shown in Figure 3-8. These deformed shapes were verified using available elastic materials.

The clutch architecture introduces complexity in the geometric analysis due to
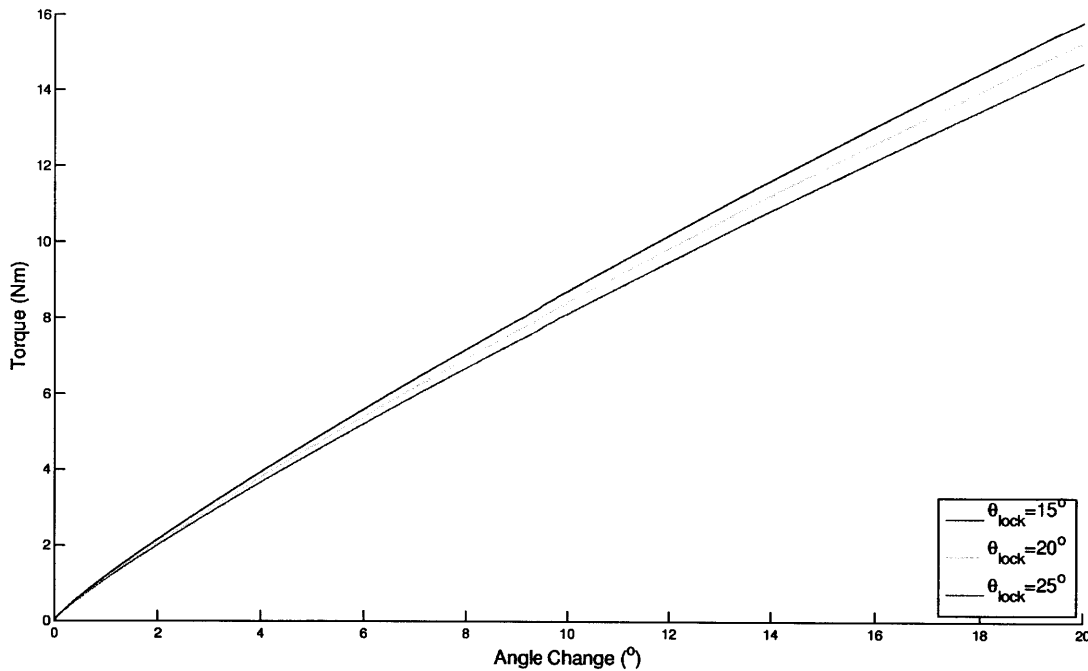
Figure 3-9: Exoskeleton torque as a function of change in knee brace angle. The spring is slightly sub-linear. Note also the weak dependence on brace angle at locking.

the presence of two elements and the introduction of inflexible regions where elastic struts meet the exoskeletal clutch or harness attachments, but the principles and Equation 3.7 still apply. Using the known geometry of the knee brace harness, it is furthur possible to calculate the moment about the knee using

$$M = \frac{dU}{d\theta_{brace}} \tag{3.9}$$

though it is worth noting that the torque profile of the spring depends not only on the final angle of the harness but also on the angle at which the clutch was first locked (though the latter effect is weak).

For structs of rectangular cross section, the 2nd moment of area is given by

$$I = \frac{1}{12}wt^3 \tag{3.10}$$

where w is the width of the strut and t is the thickness. Once lengths of the two

Symbol	Description	Value
$R_{p,b}$	Knee Brace Proximal Length	260 mm
$R_{c,b}$	Knee Brace Joint Length	241 mm
$R_{d,b}$	Knee Brace Distal Length	19 mm
$E_{p,b}$	Proximal End Point Rigid Length	44 mm
$E_{d,b}$	Proximal End Point Rigid Length	44 mm
$J_{p,b}$	Proximal Joint Rigid Length	89.75 mm
$J_{d,b}$	Proximal Joint Rigid Length	89.75 mm
$L_{p,e}$	Proximal Elastic Element Flexible Length	130 mm
$L_{d,e}$	Distal Elastic Element Flexible Length	130 mm

Table 3-5: Constants related to the elastic element and knee brace.

struts and various harness and clutch related geometries are fixed, the torque profile of the spring may be calculated for unit EI and scaled to facilitate design of various stiffnesses springs.

For ease of manipulation, calculated energy storage was fit to a model given by

$$U = (A + B\theta_{lock}) \left(\theta_{brace} - \theta_{lock}\right)^C \qquad (3.11)$$

so that the moment is given by

$$M = C \left(A + B\theta_{lock}\right) (C) \left(\theta_{brace} - \theta_{lock}\right)^{C-1} \qquad (3.12)$$

The model's predicted calculated torque-angle relationship was verified using a torque sensor for one choice of spring. Subsequent springs were designed by measuring the bending modulus E using small angle beam deflection and calculating second moment of area I geometrically. The EI product was verified experimentally for springs used in human trials.

For the knee brace and elastic element geometry specified in Table 3-5, it was found that the spring is well characterized by

$$M = EI \left(\frac{5.13}{m} + \frac{2.43}{mrad}\theta_{lock}\right) (1.866) \left(\theta_{brace} - \theta_{lock}\right)^{0.866} \qquad (3.13)$$

where harness angle is measured between the proximal and distal segments in radians.

53

Symbol	Description	Value
ρ_{Al}	Density of 6061 Aluminum	2.70 g/cm^3
$\sigma_{y,Al}$	Tensile Yield Strength of 6061 Aluminum	276 MPa
E_{Al}	Elastic Modulus of 6061 Aluminum	68.9 GPa
ρ_{Ti2}	Density of Grade 2 Titanium	4.51 g/cm^3
$\sigma_{y,Ti2}$	Tensile Yield Strength of Grade 2 Titanium	275 MPa
E_{Ti2}	Elastic Modulus of Grade 2 Titanium	105 GPa
ρ_{Ti4}	Density of Grade 4 Titanium	4.51 g/cm^3
$\sigma_{y,Ti4}$	Tensile Yield Strength of Grade 4 Titanium	480 MPa
E_{Ti4}	Elastic Modulus of Grade 4 Titanium	105 GPa
ρ_{Ti5}	Density of Grade 5 Titanium	4.42 g/cm^3
$\sigma_{y,Ti5}$	Tensile Yield Strength of Grade 5 Titanium	880 MPa
E_{Ti5}	Elastic Modulus of Grade 5 Titanium	110 GPa
ρ_{Bz}	Density of SAE 841 Bronze	6.8 g/cm^3
K_{Bz}	Strength Constant of SAE 841 Bronze	180 MPa
ρ_{Fg}	Density of GC-70-ULS Fiberglass	1.94 g/cm^3
$E_{Bend,Fg}$	Elastic Modulus in Bending of GC-70-ULS Fiberglass	24.1 GPa

Table 3-6: Constants related to materials used in the exoskeletal knee clutch. Data for fiberglass determined experimentally; all other data from [31].

The parameter $C = 1.866$ is found to be slightly below 2 for this geometry, indicating that the effective torsional spring is incrementally less stiff as angle increases. Using $EI = 3.41 Nm^2$, the product of the spring used in Chapter 5, Figure Figure 3-9 shows the slightly sub-linear torque-angle relationship for this geometry, as well as its weak dependence of stiffness on engagement angle.

3.3 Failure Analysis

Verifying the maximum achievable torque, radial force, and axial force, specified in Table 3-1, requires careful analysis of the clutch and gear box as well as the bearings and various support components. Here, both analytical techniques and finite element analysis are used to determine conservative ratings of the exoskeletal knee. Material properties used in this analysis are summarized in Table 3-6.

In particular, the maximum holding torque in the exoskeletal knee is potentially

Component	$T_{max,calc}$	$T_{max,fea}$
Clutch Teeth	480 Nm	1,560 Nm
Ring Gear Teeth	650 Nm	
Planet Gear Teeth Against Ring Gear Teeth	300 Nm	
Planet Gear Teeth Against Sun Gear Teeth	190 Nm	190 Nm
Sun Gear Teeth	290 Nm	
Sun Gear Hub	2,000 Nm	2,070 Nm
Clutch Plate	730 Nm	700 Nm
Linear Bearing	1,100 Nm	
Planet Bearing	310 Nm	

Table 3-7: Maximum calculated exoskeletal knee torque as limited by failures in several components. Where performed, results of finite element analysis are also presented

(a) Partially engaged (b) Fully engaged
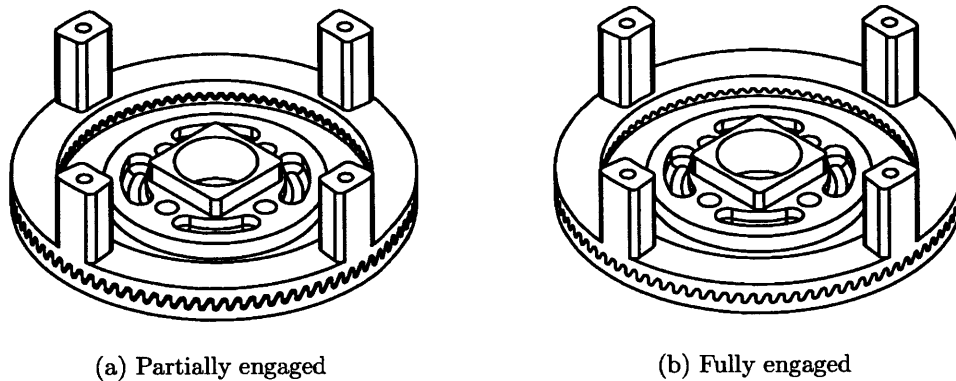
Figure 3-10: The clutch plates, shown actual size, partially and fully engaged

constrained by failures in several components. Such failures due to applied torque are summarized in Table 3-7.

3.3.1 Clutch Tooth Bending

Under ideal conditions, the solenoid is activated while rotating slowly and fully engages (the configuration shown in Figure 3-10b) before any load is applied. Assuming perfect meshing, the stress can be estimated using the shear relation and grade 2

55

titanium's lower yield stress:

$$\sigma = \frac{F_{total}}{A_{total}} \tag{3.14}$$

$$= \frac{T_c/r_{i,c}}{\pi(r_{o,c}^2 - r_{i,c,i}^2)} \tag{3.15}$$

$$\tag{3.16}$$

which yields

$$T_{c,y} = \pi r_{i,c}(r_{o,c}^2 - r_{i,c}^2)\sigma_{y,Ti2} \tag{3.17}$$

$$= 9.3kNm \tag{3.18}$$

$$T_{max} = R_t T_{c,y} \tag{3.19}$$

$$= 20.4kNm \tag{3.20}$$

It is clear that the teeth will not fail in shear mode when exposed to expected torque. Tooth bending during partial engagement is a far more constraining failure mode. Unfortunately, the complex geometry of the clutch plates does not lend itself to analytical techniques. The very conservative approximation presented here is able to establish the sufficiency of the clutch plate geometry, though finite element analysis is the dominant design tool.

Approximate a single tooth of a clutch plate as an isosceles triangular prism (in truth, the tooth is asymmetric to increase holding torque in the desired direction and necessarily tapers into the inner radius) with characteristic dimensions given in Table 3-3. Consider the moment about the base of this tooth when a tangential force is applied by an identical tooth of the mating clutch plate with a level of engagement characterized by η, where $\eta = 1$ represents full engagement and $\eta = 0$ represents only the tips of the teeth making contact. If pressure is constant over the region of

contact, this moment is given by

$$M = \int_{(1-\eta)h_c}^{h_c} \frac{F_t}{\eta h_c} z \, dz \qquad (3.21)$$

$$= \frac{F_t h_c}{\eta} \left(1 - \frac{\eta}{2}\right) \qquad (3.22)$$

This is, of course, equivalent to a point load F applied at a height

$$z_{eff} = \left(1 - \frac{\eta}{2}\right) \qquad (3.23)$$

at the middle of the region of contact. At this height, the width of the tooth is given by

$$w_{eff} = 2\left(1 - \frac{z}{h_c}\right)\left(\frac{w_c}{2}\right) \qquad (3.24)$$

$$= \left(\frac{\eta}{2}\right) w_c \qquad (3.25)$$

Conservatively, now treat the tooth as a rectangle with width w_{eff} and height z_{eff}. It has 2nd moment of area

$$I = \frac{w_{eff}^3 d_c}{12} \qquad (3.26)$$

$$= \frac{\eta^3 3 w_c^3 d_c}{96} \qquad (3.27)$$

Consequently, the tooth experiences a bending stress given by

$$\sigma = \frac{My}{I} \qquad (3.28)$$

$$= 12\left(\frac{2-\eta}{\eta^2}\right)\left(\frac{h_c}{w_c^3 d_c}\right) F_t \qquad (3.29)$$

The tangential force in the worst case occurs at the inner radius and is distributed evenly over all teeth:

$$F_t = \frac{T_c/r_{i,c}}{n_c} \qquad (3.30)$$

57

This yields a limit on torque on the clutch plate

$$T_{c,max} = \frac{1}{12} \left(\frac{\eta^2}{2-\eta} \right) \left(\frac{w_c^2 d_c}{h_c} \right) n_c r_{i,c} \sigma_{y,Ti2} \qquad (3.31)$$

Finally, including the transmission ratio, the holding torque at the output is given by

$$T = R_t T_c \qquad (3.32)$$

It should be noted that the leading term in Equation 3.31 is purely geometrical and arises from the modeling the tooth as a triangle loaded at a point. A less conservative model may be produced by modeling the tooth as trapezoidal with tip width given by αw_c to model the effect of tip and root fillets. Moreover, the point loading approximation need not be used in the trapezoidal model; the stress due to the applied pressure may be found by integrating over the region of contact (This is not possible with the triangular model due to a singularity at the tip). The tooth model used affects the η dependence through a geometric term $\gamma(\eta)$, but not the functional form of this torque limit.

$$T_{c,max} = \frac{1}{\gamma(\eta)} \left(\frac{w_c^2 d_c}{h_c} \right) n_c r_{i,c} \sigma_y \qquad (3.33)$$

Point Loaded Triangle :
$$\gamma(\eta) = 12 \left(\frac{2-\eta}{\eta^2} \right) \qquad (3.34)$$

Point Loaded Trapezoid :
$$\gamma(\eta) = 12 \left(\frac{2-\eta}{(\eta(1-\alpha)+2\alpha)^2} \right) \qquad (3.35)$$

Continuously Loaded Trapezoid :
$$\gamma(\eta) = 6 \left(\frac{1}{\eta(1-\alpha)} \right) \left(\frac{1}{\eta \left(1+\frac{1-\eta}{\eta}\alpha \right)} - \frac{1}{1-\alpha} \ln \left(\frac{1-\alpha}{\alpha}\eta + 1 \right) \right) \qquad (3.36)$$
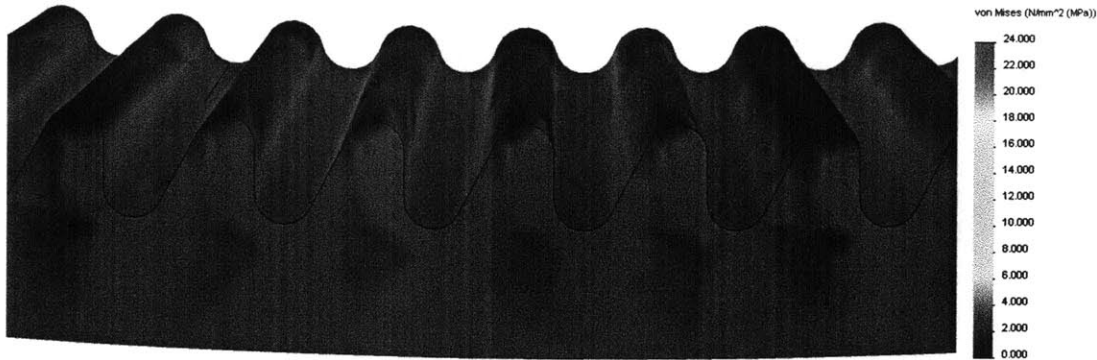
Figure 3-11: Finite element analysis of the clutch teeth.

All three models predict the peak loads in excess of those expected within the bounds of normal operation (η close to 1). Assuming a worst case engagement of $\eta = 0.75$, finite element analysis predicts yield at 710Nm, corresponding to 1560Nm at the output, far exceeding expected load. Finite element analysis of loading during the worst expected case (90Nm on the plate) is shown in Figure 3-11.

These tooth bending approximations assume that load is shared over all teeth. This is true if the plate is machined to sufficient tolerance that bending of a given tooth will bring it into contact with the next tooth. Using the triangular model, the displacement of a tooth when $n_e ng$ teeth are engaged is given by

$$\delta = \left(\frac{M}{EI}\right)\left(\frac{z_{eff}^2}{2}\right) \tag{3.37}$$

$$= \frac{1}{n_{eng}}\left(\frac{1}{E}\right)\left(\frac{T_c}{r_{i,c}}\right)\left(\frac{h_c^3}{w_c^3 d_c}\right)\left(\frac{48}{\eta^3}\right) \tag{3.38}$$

Under the loads expected on the clutch plate, this displacement is on the order of the $0.0005in$ tolerance to which the plates may be manufactured, validating the above calculations.

3.3.2 Spur Gear Tooth Bending

The maximum stress on a single involute spur gear tooth with face width f, module m, and geometry factor Y experiencing a tangential load F_t is given by the Lewis

59
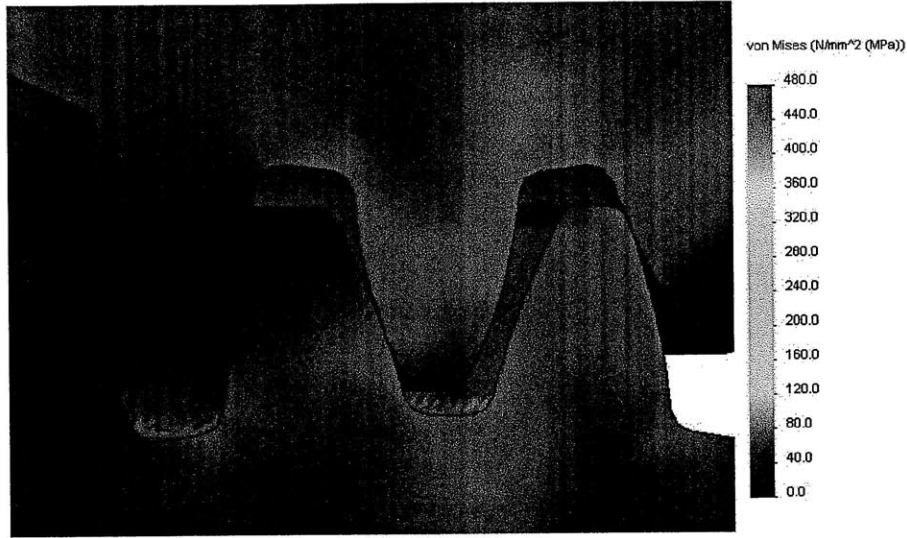
Figure 3-12: Finite element analysis of the interface between a planet gear (top) and the sun gear (bottom).

bending equation[39]:

$$\sigma_y = \frac{F_t}{Yfm} \tag{3.39}$$

The geometry factor is a function of pressure angle, the number of teeth on the gear, and the number of teeth on the mating gear. It is typically determined by table lookup.

To determine the maximum tangential force on a single gear at the interface to a second gear, the contact ratio, a measure of the number of teeth sharing load, must also be considered. For two gears X and Y, the contact ratio is a function of the base and addendum radii, the pressure angle ϕ, and the module m[39]:

$$c_{X-Y} = \frac{\sqrt{r_{a,X}^2 - r_{b,X}^2} + \sqrt{r_{a,Y}^2 - r_{b,Y}^2} - d\sin\phi}{\pi m \cos\phi} \tag{3.40}$$

Finally, an additional derating rim thickness factor K_B, determined by table lookup, accounts for the weakness of a thin rim supporting a hollow gear. The tangential force at the interface of gear X to gear Y is thus limited by bending of the teeth of gear X to

$$F_{t,X-Y} = \frac{\sigma_y Y_{X-Y} c_{X-Y} fm}{K_{B,X}} \tag{3.41}$$

60

Symbol	Description	Ring-Planet	Planet-Ring	Planet-Sun	Sun-Planet
σ_y	Yield Strength	880 MPa	480 MPa	480 MPa	880 MPa
c	Contact Ratio	2.61	2.61	1.70	1.70
Y	Geometry Factor	0.43	0.36	0.35	0.40
K_B	Rim Thickness Factor	1	1	1	1.4
τ_{max}	Knee Torque at Yield	650 Nm	300 Nm	190 Nm	290 Nm

Table 3-8: Summary of tooth bending at the four gear interfaces of the transmission

In the planetary gearbox, the tangential force associated with any of the gear to gear interface is shared over the planets and given by

$$F_t = \frac{T/r_{p,r}}{P_t} \tag{3.42}$$

Therefore, output torque is limited by tooth bending of gears X at the interface to gear Y by

$$T_{max} = (P_t f_t m_t r_{p,r}) \left(\frac{Y_{X-Y} c_{X-Y}}{K_{B,X}} \right) \sigma_y \tag{3.43}$$

where $X - Y$ may be $r - p$, $p - r$, $p - s$, or $s - p$. For all four interfaces, contact ratios calculated from Equation 3.40, geometry factors and rim thickness factors found by table lookup, and resulting maximum output torques calculated from Equation 3.43 are summarized in Table 3-8. Bending of planet gear teeth at the interface to the sun gear proves the most limiting and in fact is the first component of the exoskeletal knee joint to fail, at 190Nm, slightly shy of the stated goal of 200Nm. While this Finite element analysis, shown in Figure 3-12, confirms this result.

This failure, it should be noted, results only in plastic deformation of the planetary teeth. While such deformation would affect device lifetime and may affect the smoothness of the transmission, it would not result in catastrophic failure of the clutch.

3.3.3 Coupling Torsion

The coupling between the transmission and the clutch consists of the thin-walled titanium tube from which the sun gear protrudes and the flat titatium disk which
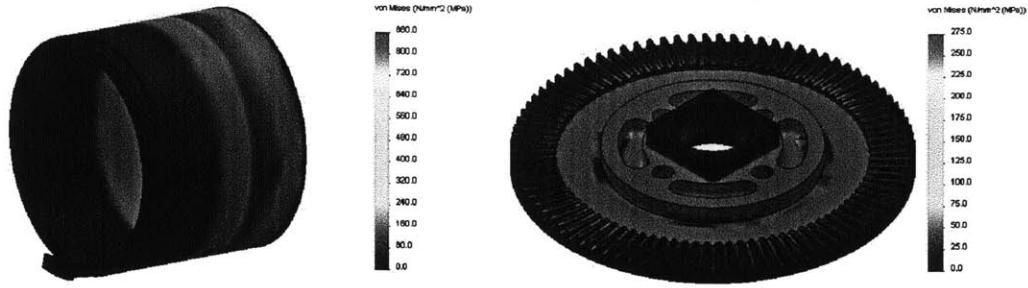
(a) Yield in the sun gear rim is predicted at 943Nm, corresponding to 2,075Nm at the output.

(b) Yield in the rotating clutch plate is predicted at 318Nm, corresponding to 700Nm at the output.

Figure 3-13: Finite element analysis showing torque applied to the elements which couple the planetary gear box to the clutch.

comprises the rotating clutch plate. The connection between these sections includes substantial mating bosses and is unlikely to fail, but either section may fail in shear due to the applied torque.

Consider first the shear on the thin walled tube with inner radius r_i and outer radius r_o subjected to applied torque T about its axis. The maximum shear stress is given by

$$\tau = \frac{T r_o}{J} \tag{3.44}$$

where J is the polar moment of inertia[10], which for a tube is given by

$$J = \frac{\pi}{2} \left(r_o^4 - r_i^4 \right) \tag{3.45}$$

As the torsion produces uniaxial shear at any given point, the shear stress is half the tensile stress and yield is expected at $\tau = \sigma_y/2$. We find then that the torque at yield is given by

$$T_y = \frac{\pi}{2} \left(\frac{\sigma_y}{2} \right) \left(\frac{r_o^4 - r_i^4}{r_o} \right) \tag{3.46}$$

Finally, substituting the dimensional and material properties of the sun gear's rim

62

yields

$$T_{y,h} = \frac{\pi}{2} \left(\frac{\sigma_{y,Ti5}}{2} \right) \left(\frac{r_{b,s}^4 - r_{i,s}^4}{r_{b,s}} \right) \tag{3.47}$$

$$= 910Nm \tag{3.48}$$

$$\tag{3.49}$$

This corresponds well to finite element analysis, which predicts yield of the rim at 940Nm, as shown in Figure 3-13a. Including the transmission ratio, the maximum torque at the output is given by

$$T_{max} = R_t T_{y,h} \tag{3.50}$$

$$= 2000Nm \tag{3.51}$$

This result is a full order of magnitude beyond expected loads.

Similarly, consider the shear on a disk of thickness t fixed at radius r_o with a torque applied at radius r_i. The maximum shear is given by

$$\tau = \frac{T}{r_i A} \tag{3.52}$$

where A is the area about which the shearing force is applied. Here A is the surface of a cylinder of radius r_i and thickness t:

$$A = 2\pi r_i t \tag{3.53}$$

The torque at yield is therefore

$$T_y = \pi \sigma_y r_i^2 t \tag{3.54}$$

$$= \pi \sigma_{y,Ti2} r_{b,c}^2 t_c \tag{3.55}$$

$$= 330Nm \tag{3.56}$$

As shown in Figure 3-13b, finite element analysis performed with a more accurate

model of load transfer from the sun gear's rim predicts failure at an inconsequentially lower torque of 320Nm. After the transmission ratio, the maximum torque at the output is given by

$$T_{max} = R_t T_{y,p} \tag{3.57}$$

$$= 730Nm \tag{3.58}$$

This is similarly well above expected loads.

3.3.4 Linear Bearing Loading

While the clutch is locked, torque is transferred from the translating clutch plate to the planetary gear box through the bosses of the cage which link the translating clutch plate to the solenoid. Therefore, the bearing surface which supports the cage bosses must support a tangential load of at most

$$F_{l,t} = \frac{T}{r_{c,i}} \tag{3.59}$$

distributed over a total surface area approximated as $N_l = 4$ rectangles measuring $w_l = 3.2mm$ wide and $h_l = 6.3mm$ tall

$$A_l = N_l w_l h_l \tag{3.60}$$

The linear bearing will yield when

$$\sigma_y = F_{l,t}/A_l \tag{3.61}$$

This occurs once the torque on the cage reaches

$$T_{y,l} = \sigma_{y,Al} r_{i,c} N_l w_l h_l \tag{3.62}$$

$$= 500Nm \tag{3.63}$$

This estimate is very conservative as it fails to account for the decreasing tangential force as radius increases and neglects load bearing of filleted regions. Nonetheless, the calculated capacity drastically exceeds the expected loads.

$$T_{max} = R_t T_{y,l} \tag{3.64}$$

$$= 1,100 Nm \tag{3.65}$$

3.3.5 Planet Bearing Loading

A pair of oil-impregnated bronze plain bearings support each planet and must withstand a radial load while the clutch is locked and the ring attempts to rotate relative to the sun. This load is shared over $P_t = 4$ planets with $B_p = 2$ bearings each and is thus given by

$$F_{r,p} = \left(\frac{2T}{r_{p,r}} \right) \Big/ (P_t B_p) \tag{3.66}$$

The maximum radial load on a plain bearing of length $L = 2.5mm$, inner radius $r_i = 2.5mm$, and strength constant $K = K_{Bz}$, is given by

$$C_{r,p} = 2r_i L K \tag{3.67}$$

$$= 2250 N \tag{3.68}$$

Substituting, the planet bearings experience this limiting radial load $F_{r,p} = C_{r,p}$ at an output torque given by

$$T_{max} = \frac{P_t B_p r_{p,r} C_{r,p}}{2} \tag{3.69}$$

$$= 310 Nm \tag{3.70}$$

which is above the expected torque.

65

3.3.6 Ring Bearing Loading

The two ring bearings which support the rotating distal end of the exoskeletal knee bear all radial and axial loads placed on the device. As radial load will be shared evenly over the two bearings, the rated radial load of the exoskeletal knee is simply twice the the dynamic radial load capacity of each bearing:

$$F_{r,max} = B_r C_{r,r} \tag{3.71}$$

$$= 4780N \tag{3.72}$$

This exceeds the specified 3,000N radial force expected in running if body weight is loaded exclusively through the clutch.

Although the bearings are X-type, they are singly supported on the inner race in order to avoid over constraint when used in a pair, and as such behave similarly to angular contact bearings. The axial load which may be borne by the exoskeletal knee is therefore given by the dynamic thrust load capacity of the bearing:

$$F_{a,max} = C_{a,r} \tag{3.73}$$

$$= 4050N \tag{3.74}$$

Significant axial loads are not expected under normal circumstances; such loads will at most be a small fraction of the radial load due to off-axis loading. This rating is therefore far more than necessary.

Chapter 4

Control

4.1 Electronics and Instrumentation

To increase reliability and facilitate maintenance, the system is designed with a minimum number of routed wires. To this end, all electronics are packaged together within a cap-shaped subassembly which attaches to the lateral face of the proximal assembly and is easily removed for maintenance. This lateral subassembly contains a 2000mAh lithium polymer battery cell and the circuit board, both fixed to a milled aluminum housing. The circuit board is annular, to accommodate the last 2mm of solenoid travel through the center of the board. All sensors (Table 4-1) are mounted directly to the circuit board and, where necessary, interface optically to appropriate mechanical transducers within the clutch. Only a single pair of wires, connecting the solenoid to the circuit board, links the lateral assembly to the body of the clutch. A floorplan of the circuit board is shown in Figure 4-1.

An AtMega168PA AVR microcontroller operating at 12MHz controls the clutch, using a development framework described in Section 4.2. A set of sixteen LEDs, directed to the face of the lateral subassembly by light pipes, provides visual indication of state. More complete diagnostic logs are available through USB tethering or may be recorded on an onboard MicroSD card for later analysis. The microcontroller may be reprogrammed over USB.

A three degree of freedom inertial unit comprising a dual-axis MEMs accelerometer

Measurement	Part	Technology	Interface	Resolution	Range	Bandwidth
Anterior-Posterior Acceleration Superior-Inferior Acceleration	ADIS16006	MEMS Accelerometer	SPI	$0.038 m/s^2$	$\pm 49 m/s^3$	100Hz
Sagittal Plane Angular Rate	ADIS16100	MEMS Gyroscope	SPI	1.12^o	$\pm 1380^o/s$	185Hz
Exoskeletal Knee Angle	E4P (Disk) AEDR (Reader) LS7336R (Counter)	Reflective Encoder	SPI	0.068^o	$0\text{-}135^o$	
Clutch Engagement Distance	EE-SX1109	Break Beam	Analog	0.1mm	0-2mm	

Table 4-1: Sensors used in the exoskeletal knee.

and a MEMs gyroscope provides acceleration and rotation rate sensing within the sagittal plane. The accelerometers are primarily used to assess heel strike. Because the circuit board is fixed to the proximal assembly, the gyroscope is indicative of hip rotational velocity and is used to assess midswing and midstance. Rotation rate in midswing is particularly informative as an indication of running velocity.

Rotation of the clutch is measured using a reflective optical encoder. The quadrature phase disk is mounted to one of the planets rather than directly to the distal subassembly, both to accommodate the solenoid at the center of the device and to obtain an effective increase in resolution from the higher speed of the planets. It aligns with the PCB-mounted reader when the lateral subassembly is installed.

Solenoid position feedback is obtained from an infrared break beam sensor soldered to the PCB interacting with an aluminum flag machined into the solenoid mount. This flag is dimensioned such that the sensor saturates when the cage is completely disengaged, but provides analog sensing over the final 2mm of engagement, including any partial tooth engagements. This sensor is non-linear and exhibits slight hysteresis. For practical purposes, it offers 0.1mm resolution.

Three power rails are generated from the 3-4.2V battery supply by switching converters. A 3.3V rail, produced by a four switch buck-boost converter, powers all onboard logic and most sensors. A 5V rail, produced by a boost converter, is needed to power the optical encoder and gyroscope, as 3.3V variants are unavailable. Finally, a 24V rail, produced by a boost converter, is used to power the solenoid. A 3V low dropout linear regulator is placed between the 3.3V rail and the accelerometer to eliminate power supply ripple, to which this sensor is particularly sensitive. The battery is charged over USB and is protected in hardware from over-current, over-

	V_{Batt}	3.3V	5V
Battery Management	14 µA		
Microcontroller		5 mA	
Accelerometer		1.5 mA	
Gyroscope			7.1 mA
Encoder Reader		15 mA	2.1 mA
Encoder Counter		200 µA	
Optical Break Beam		8 mA	
Real Time Clock	15 nA	80 µA	
LED Drivers		390 µA	
Total Current	14 µA	30.2 mA	9.2 mA
Total Power	52 µW	100 mW	46 mW

(a) Electronics power on battery, 3.3V, and 5V rails

Closing Duty Cycle	1.00
Closing Power	13 W
Closing Time	28.6 ms
Closing Energy	375 mJ
Holding Duty Cycle	0.24
Holding Power	725 mW
Holding Time (Typ.)	300 ms
Holding Energy (Typ.)	330 mJ
Total Energy (Typ.)	705 mJ
Stride Period (Typ.)	1.3 s
Total Power (Typ.)	540 mW

(b) Typical solenoid power on 24V rail

Rail	P_{load}	Efficiency	$P_{battery}$
V_{Batt}	52 µW	100 %	52 µW
3.3V	100 mW	82 %	122 mW
5V	46 mW	92 %	50 mW
24V	540 mW	79 %	685 mW
			857 mW

(c) Total power drawn from battery

Table 4-2: Typical power consumption of exoskeletal knee clutch. V_{Batt} power and switching converter efficiencies are calculated assuming nominal 3.7V battery.
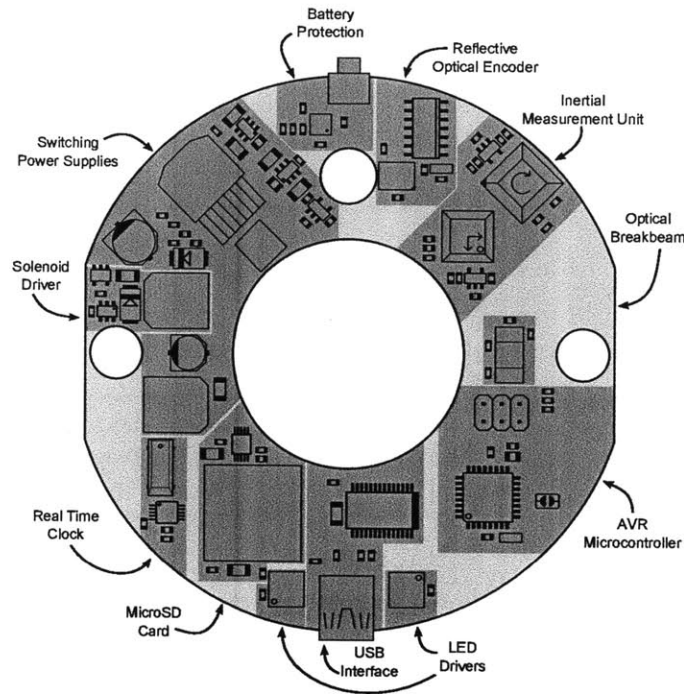
Figure 4-1: Floor plan of the exoskeletal knee clutch's circuit board, actual size.

voltage, and under-voltage. To conserve battery, the system is powered down by software after a period of inactivity on all sensors.

4.2 Firmware

Optimal control of the exoskeletal knee joint produces full engagement at the time of maximum knee extension shortly before heel strike and full disengagement prior to toe off. Ideally, each exoskeletal knee achieves this independently and requires no extrinsic inputs. The controller is implemented within a framework developed with prosthetic and orthotic systems in mind. The control problem itself is divided into two primary components: analyzing the gait cycle using kinematic sensing (Section 4.2.1) and compensating for the electromechanical latency of the clutch (Section 4.2.2). Additionally, a pulse and hold strategy is implemented to reduce power consumption in the solenoid once the clutch is fully engaged (Section 4.2.3).

The control framework, written for the AVR AtMega*8 line of microcontrollers,
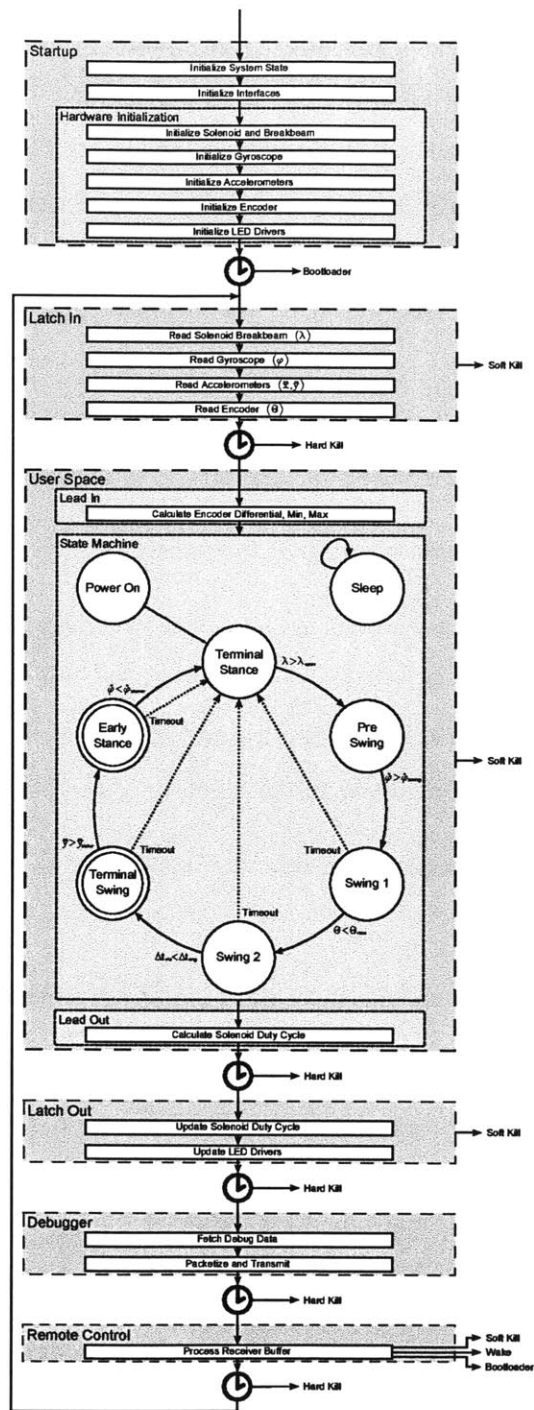
Figure 4-2: Program flow through the framework used to control the exoskeletal knee joint. The solenoid is activated during doubly circled states. Arrows exiting to the right indicate atypical paths, which at least briefly shut down the normal control loop. Not shown here, an interrupt triggered by pressing the kill button causes an immediate soft kill.

71

provides synchronous read-out of all sensors and update of all output devices as well as diagnostic and remote control capabilities. In particular, it is designed so that the space accessible to an end user is both easy to develop in and relatively well sandboxed. As this framework provides all low level functionality, discussion here focuses on the two primary components of the exoskeleton control problem: analyzing the gait cycle using kinematic sensing and compensating for the electromechanical latency of the clutch.

The framework, shown as configured for the exoskeletal knee clutch in Figure 4-2, implements synchronous time division for five phases of operation occurring in a loop:

- **Latch In:** All input devices are read into memory.

- **User Space:** A state machine is updated based on newly updated input data. Lead In and Lead Out subphases are executed immediately before and immediately after the statemachine's update and are suited for filtering inputs and updating closed-loop controllers independently of the current state.

- **Latch Out:** Changes made to output devices during the User Space phase are applied to hardware.

- **Debugger:** A programmable set of data is logged, usually to USB or onboard memory.

- **Remote Control:** A programmable set of memory locations may be updated, usually over USB. The remote control also provides for remote soft kill and wake as well as access to a bootloader so that new system code may be loaded.

Time division is enforced by a timer interrupt and a timeout results in an immediate hard kill, in which all potentially hazardous outputs are turned off and the system is shut down pending a reset from physical input or via the remote control. Program flow is blocked until the completion of a phase's time division if it completes early, guaranteeing synchronization at the start of each phase.

A soft kill, in which program flow continues, but potentially hazardous outputs are turned off and the state machine is forced into sleep, may be entered by pressing a

kill switch, by software request during the Latch In, User Space, or Latch Out phases, or by request over the remote control.

The framework is structured considering three types of user - the framework designer, system builders, and end users - and attempting to minimize development complexity for the latter two. System builders are responsible for setting initial configuration parameters, including appropriate timing settings, and providing libraries for the set of input and output hardware available on a particular system. They are also responsible for providing basic behaviors such as indications of successful startup or system kill. System builders can also provide wrapper functions to tailor hardware libraries to their application and may install a system level Lead In and Lead Out, which are executed in user space, but not configurable by the end user. Macros automatically build code for Hardware Initialization, Latch In, and Latch Out, based on the available hardware libraries.

End users work primarily within the state machine, though some users may need to use the Lead In and Lead Out to configure filters and closed loop controllers. End users can also configure the channels used by the debugger and remote control. It is particularly important to note that end users interact only with system memory and do not read sensors or update output devices directly.

In the context of these three development levels, a soft kill blocks execution of end user level code, while continuing to execute system and framework level code. A hard kill permits execution only of critical framework level code.

The debugger and remote control interface to a user-configurable MATLab program, which provides the user with real time graphs and logs. Debug packets are synchronized at the packet level and include encodings of the variable types being transmitted, so end users need only provide names and, if necessary, conversion factors for each channel.

4.2.1 Gait Analysis

The framework provides a user-friendly environment for implementing a gait analysis state machine. Figure 4-3 depicts a stereotyped running gait, including knee and

73

Symbol	Description	Units
$\ddot{x}$	Anterior-Posterior Acceleration	m/s^2
$\ddot{y}$	Superior-Inferior Acceleration	m/s^2
$\dot{\psi}$	Sagittal Plane Angular Velocity	$^o/s$
θ	Exoskeletal Knee Angle	^{o}
λ	Scaled Optical Break Beam Reading	
Δt_{state}	Time Since Last State Change	ms
Δt_{eta}	Predicted Time to Peak Knee Extension	ms
η	Fractional Clutch Engagement	

Table 4-3: Variables related to exoskeletal knee control, grouped into direct sensor readings and calculated internal state.

Symbol	Description	Value
f	Update Frequency	750 Hz
Δt_{eng}	Clutch Engagement Time	30 ms
λ_{open}	Optical Break Beam Open Threshold	0.20
λ_{closed}	Optical Break Beam Closed Threshold	0.90
W	Latency Compensation Window Size	32
$\dot{\psi}_{swing}$	Sagittal Plane Angular Velocity Swing Threshold	190 $^o/s$
$\dot{\psi}_{stance}$	Sagittal Plane Angular Velocity Stance Threshold	-28 $^o/s$
$\ddot{y}_{strike}$	Superior Acceleration Heel Strike Threshold	17.2 m/s^2
$\Delta\theta_{flexion}$	Hysteresis Width to Detect Peak Knee Flexion	2 ^{o}
$\Delta\theta_{swing}$	Minimum Knee Excursion in Swing	44 ^{o}
D_{open}	Solenoid Duty Cycle While Closing	1.00
D_{closed}	Solenoid Duty Cycle Once Closed	0.24
$\Delta t_{Swing1,max}$	Maximum Time in Swing 1	200 ms
$\Delta t_{Swing2,max}$	Maximum Time in Swing 2	320 ms
$\Delta t_{TerminalSwing,max}$	Maximum Time in Terminal Swing	120 ms
$\Delta t_{EarlyStance,min}$	Minimum Time in Early Stance	40 ms
$\Delta t_{EarlyStance,max}$	Maximum Time in Early Stance	200 ms
$\Delta t_{TerminalStance,min}$	Minimum Time in Terminal Stance	20 ms

Table 4-4: Constants related to exoskeletal knee control, grouped into intrinsic hardware properties, tunable parameters, and tunable state machine time constraints
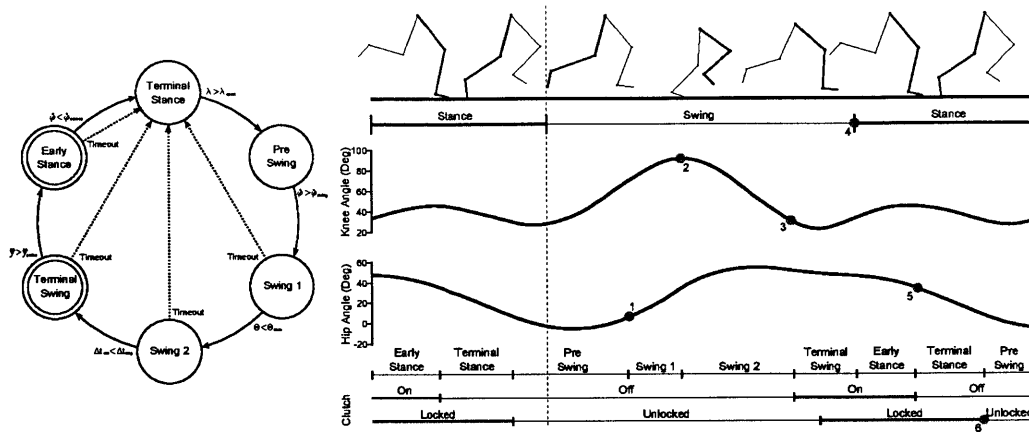
Figure 4-3: Depiction of events used to identify and act on phases of the gait cycle. See Section 4.2.1 for an explanation of state exit conditions. Biological hip and knee angle data is stereotyped. More than one cycle is shown to clarify the periodic nature of this action.

hip angles. Relying exclusively on the onboard sensor measurements introduced in Table 4-1, a simple state machine suffices to interpret the phases of this gait:

1. **Preswing:** Toe-off completes, the knee flexes in order to minimize its moment of inertia for forward swing, and the hip begins to flex accelerating the leg forward. Positive rotation of the gyroscope exceeding $\dot{\psi}_{swing}$ causes transition to Swing 1.

2. **Swing 1:** The knee continues to flex, eventually achieving maximum flexion. Once the exoskeletal knee angle has extended beyond its observed maximum flexion by a hysteresis band $\Delta\theta_{flexion}$, the state machine advances to Swing 2.

3. **Swing 2:** The knee begins to extend in preparation for heel strike. The solenoid latency compensation algorithm is activated. Once the projected time to maximum knee extension Δt_{eta} is less than the known clutch engagement time Δt_{eng} and the exoskeletal knee angle has decreased by at least $\Delta\theta_{swing}$, the solenoid is activated and the state machine progresses to Terminal Swing.

4. **Terminal Swing:** The clutch engages shortly before the foot touches the ground. Vertical acceleration in excess of $\ddot{y}_{strike}$ at impact causes transition

75

to Early Stance.

5. **Early Stance:** The biological knee flexes while the ankle dorsiflexes, resulting in a shortening effective leg length. With the clutch engaged, the exoskeletal knee does not flex and the bow spring bears load, storing energy. The hip flexes, propelling the body forward. The resulting negative rotation of the gyroscope in excess of $\dot{\psi}_{stance}$ causes deactivation of the solenoid and transition to Terminal Stance.

6. **Terminal Stance:** The center of mass reaches its lowest point, after which the biological knee and ankle reverse direction, resulting in a lengthening effective leg length. Although the solenoid is off, the clutch is bound by the large applied torque. As toe off nears, the effective leg length approaches and eventually exceeds that when the clutch was engaged, allowing it to relax to its disengaged state. The detection of this disengagement by the Break beam sensor causes transition to Preswing.

The solenoid is activated, using a pulse and hold strategy to reduce power consumption, while in the Terminal Swing and Early Stance states. Were the clutch able to engage infinitely quickly, the Swing 2 state could simply monitor for a minimum in the knee encoder and engage the clutch immediately as it transitions to Terminal Swing. In practice, it is necessary to activate the solenoid slightly prior to the true encoder minimum. This prediction is carried out by the latency compensation algorithm.

4.2.2 Latency Compensation

A significant latency is associated with the electromechanical system comprising the solenoid, return spring, and translating clutch plate. Experimentally, the delay from application of 24V to the solenoid to full engagement of the clutch is approximately 30ms. As this time is comparable to the duration of late swing, it is necessary to compensate for the electromechanical latency, firing the solenoid early to ensure that
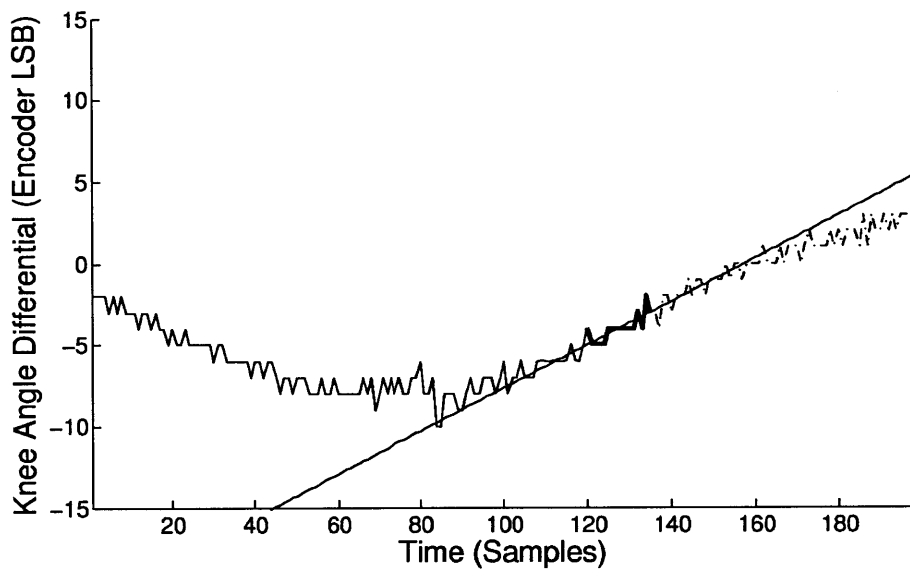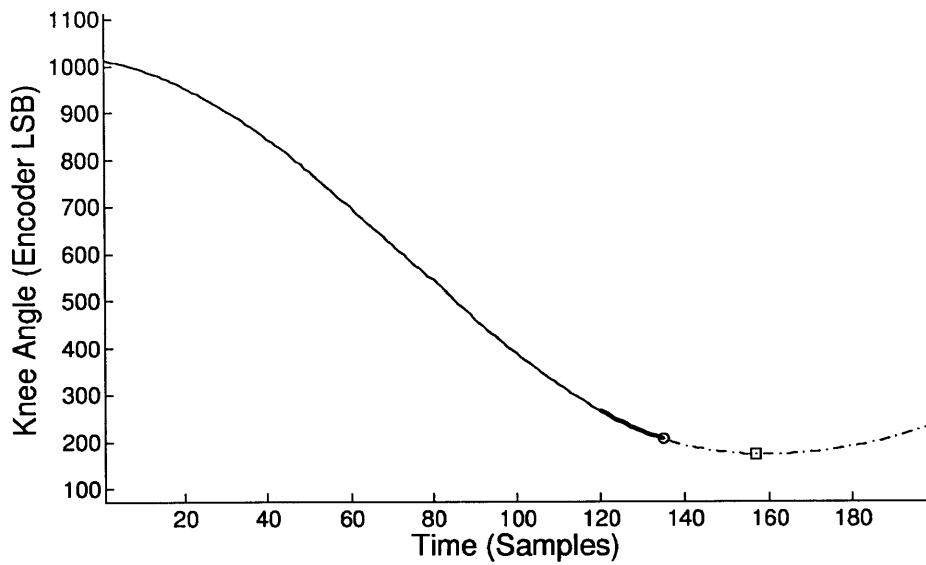
Figure 4-4: Simulation of solenoid latency compensation predicting peak knee extension as described in Section 4.2.2. Actual exoskeletal knee data recorded at 800 samples per second is used. The bold region represents the window of data used in the final iteration before firing the solenoid. The firing time is denoted by a circle while the predicted extremum is denoted by a square. Data from time after the solenoid firing is dotted. Note the correspondence between the predicted and actual times of peak knee extension.

77

the clutch is fully engaged at the time of maximum knee extension. The latency compensation algorithm in use during the Swing 2 phase accomplishes this.

We consider only late swing phase between peak knee flexion and heel strike (isolated by the technique presented in Section 4.2.1). During this phase, knee angle is approximately parabolic so we may fit the observed encoder counts to a second order polynomial with peak knee extension at the vertex. Using such a continuously generated fit, we elect to fire the solenoid once the predicted vertex position is less than 30ms in the future.

Unfortunately, the entirety of late swing is not parabolic; an inflection point exists which varies substantially between wearers and is in general difficult to predict or identify. As the region before this inflection point would skew the regression, we choose to fit to a running window rather than to all data in late swing.

While a closed form to a quadratic least squares regression exists (and in fact can be computable only from running sums), we propose a simpler, even less computationally expensive solution. Rather than fitting encoder readings to a quadratic and seeking the vertex, we fit differentials of encoder readings to a line and seek the zero crossing.

Let θ_i represent the exoskeletal knee angle i samples prior, so that θ_0 is the current angle and let $\delta\theta_i = \theta_i - \theta_{i+1}$ represent a differential angle between adjacent samples. A sliding window of the most recent W samples may be fit to a line of the form

$$\hat{\delta\theta_i} = \frac{ai + b}{d} \tag{4.1}$$

with coefficients given by

$$a = -S_0T_1 - S_1T_0 \tag{4.2}$$

$$b = S_2T_0 + S_1T_1 \tag{4.3}$$

$$d = S_0S_2 - S_1^2 \tag{4.4}$$

where

$$S_k = \sum_{i=0}^{W-1} i^k \tag{4.5}$$

$$T_k = \sum_{i=0}^{W-1} i^k \delta_i \tag{4.6}$$

$$\tag{4.7}$$

so that

$$S_0 = \sum_{i=0}^{W-1} 1 \quad = W \tag{4.8}$$

$$S_1 = \sum_{i=0}^{W-1} i \quad = \frac{S_0 (S_0 - 1)}{2} \tag{4.9}$$

$$S_2 = \sum_{i=0}^{W-1} i^2 \quad = \frac{S_1 (2S_0 - 1)}{3} \tag{4.10}$$

$$T_0 = \sum_{i=0}^{W-1} \delta\theta_i \quad = \theta_0 - \theta_W \tag{4.11}$$

$$T_1 = \sum_{i=0}^{W-1} i\delta\theta_i = \left(\sum_{i=1}^{W-1} \theta_i \right) - (W-1)\theta_W \tag{4.12}$$

This fit crosses zero, corresponding to the desired knee extremum, in a number of samples given by

$$\Delta n_{eta} = - \left(\frac{b}{a} \right) \tag{4.13}$$

or equivalently

$$\Delta t_{eta} = - \left(\frac{1}{f} \right) \left(\frac{b}{a} \right) \tag{4.14}$$

where f is the sampling frequency.

S_0, S_1, and S_2 are computable offline and d need not be computed at all. T_0 is trivially calculable and T_1 reduces to a running sum and requires incremental corrections only for end points of the sliding window. Thus, this approach is extremely inexpensive computationally. Figure 4-4 demonstrates its efficacy with a window 16 samples wide and a look ahead threshold of 30 samples.

4.2.3 Pulse-and-Hold Solenoid Activation

In order to minimize clutch engagement time, the solenoid may be driven at $D_{open} = 100\%$ duty cycle, but it is desirable to reduce this voltage once the clutch is fully engaged in order to reduce power consumption and maximize battery life. To this end, a pulse-and-hold strategy is used, settling to an experimentally determined $D_{closed} = 24\%$ duty cycle sufficient to overcome the return spring once the break beam sensor reports full engagement.

Chapter 5

Clinical Testing and Results

In order to determine the effect of parallel elasticity at the knee joint on running, an experiment was undertaken in which subjects ran on a treadmill with and without the exoskeleton while instrumented for joint kinematics and kinetics, electromyography, and metabolic demand.

5.1   Experimental Design

The proposed exoskeleton provides an elastic element in parallel with the knee during stance phase, but unfortunately a practical device, like that outlined in Chapter 3, also influences the body in several other ways due to its mass and means of attachment. Additional mass of the exoskeleton has a gravitational effect as hip extensors and knee flexors must lift the mass during early swing and an inertial effect as hip flexors must accelerate the mass during swing. Finally, attachment to the body, as discussed in Chapter 2, is difficult to accomplish without some constriction, which limits range of motion and causes discomfort. In order to isolate the effect of elasticity, experiments were conducted in three conditions - control, in which subjects ran in self selected footwear with no experimental apparatus other than those required for instrumentation, inactive, in which subjects wore the investigational knee brace with the power off, contributing zero stiffness but offering the same secondary affects associated with mass and restricted movement, and active, in which subjects wore

	Age yr	Height cm	Leg Length cm	Mass kg	Cadence Steps/s	Control Steps	Inactive Steps	Active Steps
S1	27	175	96	57	172	30	30	11
S2	19	196	107	61	152	50	50	50
S3	44	180	99	74	175	50	50	50
S4	25	185	102	82	162	50	50	50
S5	20	180	85	77	162	50	50	28
S6	34	170	93	66	166	50	33	37

Table 5-1: Descriptive measurements of the six recruited subjects and the number of steps analyzed for each in the three trials. Fewer steps than expected were available for S1 due to lost markers, for S5 due to an equipment failure, and for S6 due to early exhaustion.

the investigational knee brace with the power on, contributing a non-zero parallel stiffness during stance phase.

Human testing was conducted in accordance with MIT COUHES protocol number 0801002566 and UNC IRB protocol number 10-0691. Pilot trials and device tested was conducted in the MIT Biomechatronics Group. Experimental trials discussed in this chapter were conducted in the North Carolina State University PoWeR Laboratory.

Six male subjects (Mass $69\pm8kg$, Height $181\pm8cm$), described in Table Table 5-1, were recruited from a pool of healthy recreational runners having leg length (>90cm) and circumference (45-55cm at the thigh, 20-30cm at the shin) consistent with the investigational knee brace.

Each subject ran with the device active for a training session of at least thirty minutes on a day prior to instrumented trials. Subjects trained initially on open ground then continued on a treadmill wearing a fall prevention harness (Bioness, Valencia, CA, USA). During this training session, subjects with a gait insufficiently wide to prevent collision between the braces or with stance knee extension insufficient to ensure disengagement of the clutch were disqualified on the basis of safety.

During the experimental session, a nominal 0.9 Nm/^{o} elastic element was used. This relatively small stiffness proved necessary due to the effects of series compliance in the harness and the tendency of the biological knee to resist a stiffer exoskeleton by shifting anteriorly in the brace.

At the start of the experimental session, each subject's self-selected step frequency was measured while running on the treadmill at 3.5m/s without the investigational knee brace. The time necessary to complete 30 strides was measured by stopwatch after approximately one minute of running. This cadence (166 ± 9 steps/s) was enforced by metronome for all subsequent trials.

After being instrumented for electromyography and motion capture, subjects then ran on the instrumented treadmill at 3.5m/s in the control, inactive, and active conditions. Trial order was randomized, excepting that inactive and active conditions were required to be adjacent, so as to require only a single fitting of the investigational device in each session. Each running trial was seven minutes in length, with an intervening rest period of at least as long. Resting metabolism was also measured for five minutes at both the start and end of the experimental session. Sessions lasted approximately three hours, including 21 minutes of treadmill running.

5.2   Instrumentation and Processing

During the experimental session, each subject was instrumented for joint kinematics and kinetics, electromyography, and metabolic demand.

Subject motion was recorded using an 8 camera passive marker motion capture system (VICON, Oxford, UK). Adhesive-backed reflective markers were affixed to subjects using a modified Cleveland Clinic marker set for the pelvis and right leg (Left and right ASIS and Trochanter, three marker pelvis cluster, four marker thigh cluster, medial and lateral epicondyle, four marker shin cluster, medial and lateral malleolus, calcaneus, foot, fifth metatarsal). For inactive and active trials, the termination points of the exoskeletal spring were also marked. The marker set for the right leg is shown in Figure 5-1. Motion data was recorded at 120Hz and low filtered using a 2nd order Butterworth filter with a 10Hz cutoff. Ground reaction forces were recorded at 960Hz using a dual belt instrumented treadmill (BERTEC, Columbus, OH, USA) and low pass filtered using a 2nd order Butterworth filter with a 35Hz cutoff. Following calibration using a static standing trial, Visual3D (C-Motion Inc, Germantown, MD,

USA) modeling software was used to reconstruct joint kinematics and kinetics and center of mass trajectories, with right-left leg symmetry assumed.

Fifty steps from each trial were analyzed to determine average leg and joint stiffness. Due to technical difficulties associated with loss or migration of motion capture markers and the appearance of false markers due to reflectivity of the exoskeleton, some motion capture recordings proved unusable. Consequently, the exact timing of the steps used varies between subjects and it was not possible to analyze fifty steps for all trials, as indicated in Table 5-1. In general, the earliest available reconstructions a minimum of one minute into the trial were used, to minimize effects of fatigue.

k_{leg} and k_{vert} were calculated for each step using Equation 1.2 and Equation 1.1 with center of mass displacements determined by Visual3D through integration of reaction forces as in [7]. Unlike the effective leg spring, the knee and ankle experience different stiffnesses in absorptive (early) stance and generative (late) stance. Consequently, stiffnesses of these joints were estimated individually for the two phases using

$$\kappa_{joint,abs} = \frac{M_{joint,peak} - M_{joint,HS}}{\theta_{point,peak} - \theta_{joint,HS}} \tag{5.1}$$

$$\kappa_{joint,gen} = \frac{M_{joint,peak} - M_{joint,TO}}{\theta_{point,peak} - \theta_{joint,TO}} \tag{5.2}$$

where *peak* represents the instant of peak torque in the joint and HS and TO represent heel-strike and toe-off respectively.

Muscle activation was gauged noninvasively using surface electromyography (EMG), which responds to the membrane potential of a muscle beneath skin. Electrodes were placed as shown in Figure 5-2 above the right soleus, lateral gastrocnemius, tibialis anterior, vastus lateralis, rectus femoris, biceps femoris, gluteus maximus, and illiopsoas. Wires were taped to skin and routed an amplifier (Biomectrics Ltd, Ladysmith, VA, USA) clipped to the chest harness containing the cardiopulmonary test system. An EMG system with low profile electrodes was used to facilitate placement around the harness. Nonetheless, placement of the electrode on the lateral gastrocnemius was suboptimal due to the positioning of harness straps. A reference electrode was at-

Figure 5-1: Right leg instrumented for motion capture. Black tape covers all reflective surfaces.

(a) Soleus   (b) Lateral Gastrocnemius   (c) Tibialis Anterior   (d) Vastus Lateralis

(e) Rectus Femoris   (f) Biceps Femoris   (g) Gluteus Maximus   (h) Iliopsoas
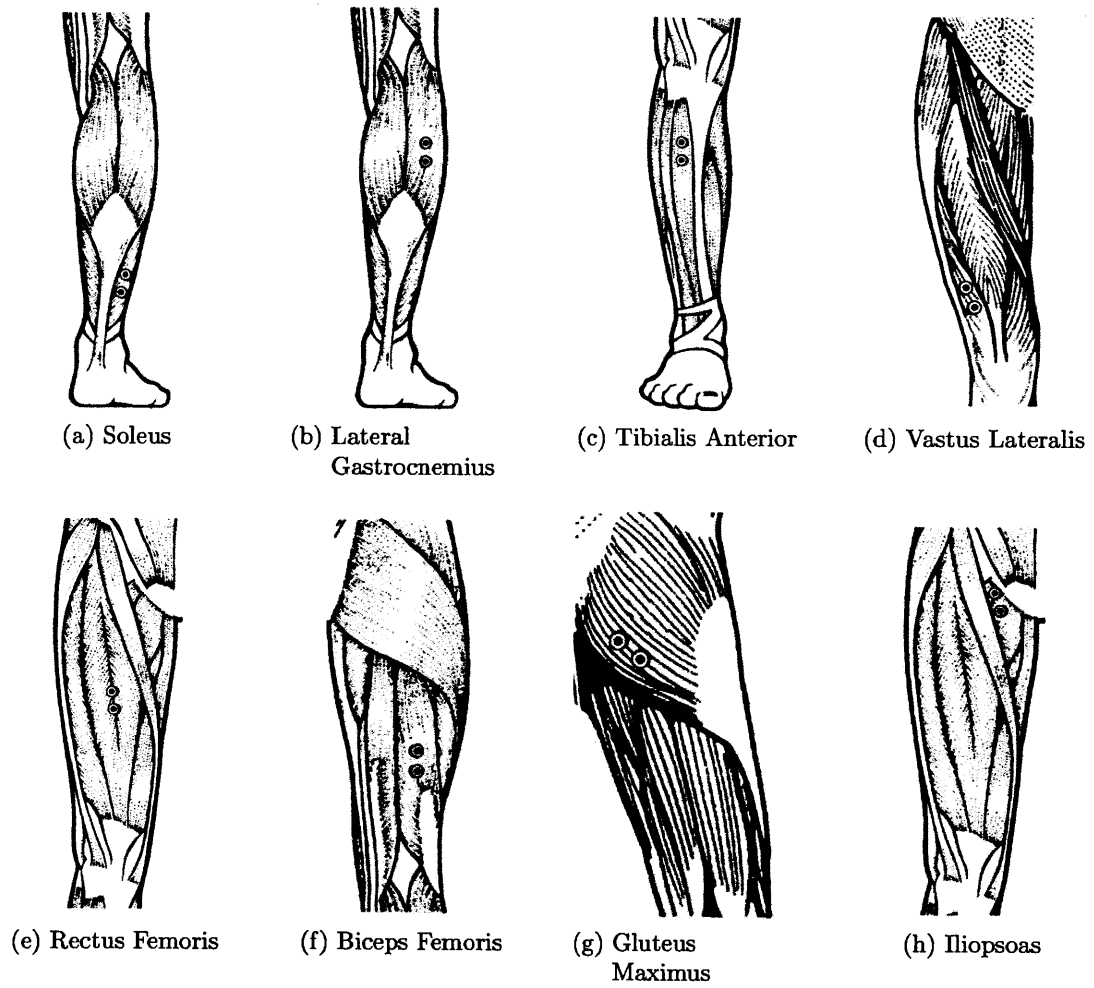
Figure 5-2: Placements of surface electromyography electrodes on the right leg. Adapted from [11].
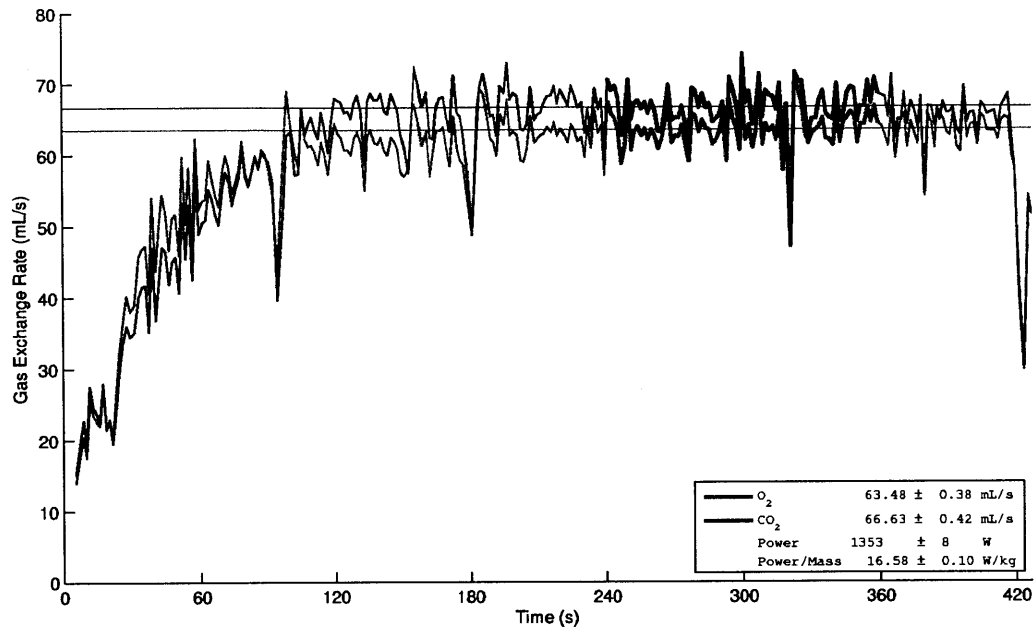
Figure 5-3: Example metabolic demand calculation

tached to the wrist. Prior to the first running trial, recordings were made of maximal voluntary contractions (MVCs) in each muscle.

Electromyography was recorded at 960Hz then filtered into a low bandwidth signal indicative of activation by the following filter chain[34][9]: DC block, 60Hz notch filter to eliminate mains hum, a 50ms moving average filter to eliminate motion artifacts, and rectification with a 200ms moving average filter to recover the envelope. Finally, activation for each muscle was normalized to the maximum activation seen in stride averaged control trials for that subject.

Metabolic demand was measured noninvasively using a mobile cardiopulmonary exercise test system (VIASYS Healthcare, Yorba Linda, CA, USA), which measures rates of oxygen consumption and carbon dioxide production through a face mask. Once sub-maximal steady state metabolism was achieved, total metabolic power was deduced from linear expressions of the form

$$P = K_{O_2}V'_{O_2} + K_{CO_2}V'_{CO_2} \qquad (5.3)$$

87

where V'_{O_2} and V'_{CO_2} represent average rates of oxygen inhalation and carbon dioxide exhalation and K_{O_2} and K_{CO_2} are constants which have been well documented. Brockway's[6] values $K_O = 16.58kW/L$ and $K_{CO_2} = 4.51kW/L$ were used. Average rates were calculated over a two minute window during steady state metabolism from 4:00 to 6:00 within each seven minute trial, as shown in Figure 5-3. In addition to the running conditions, resting metabolic power was also measured with the subject standing for five minutes.

Such measures of metabolic power are only valid if the contributions of anaerobic metabolism are small. This was assured by monitoring the ratio of volume of carbon dioxide exhaled to oxygen inhaled, known as the respiratory exchange ratio. Oxidative metabolism was presumed to dominate while this ratio was below 1.1.

More details of the instrumentation used here can be found in [16], in which identical instrumentation and signal processing was used, with the omission of electromyography.

5.3 Results

Joint and leg stiffnesses calculated for each of the six subjects as described in Section 5.2 are presented in Table 5-2 and Table 5-3, with averaged stiffnesses presented in Table 5-5 . Subjects S1, S2, S3, and S4 exhibited similar gross kinematics in all three conditions. S5 exhibited similar kinematics in the inactive condition, but transitioned to a toe-striking gait, with significant ankle plantar flexion at strike in the active condition. Consequently, S5's active mechanics are not considered in population averages. S6's mechanics are similarly omitted, as he was visibly fatigued and failed to complete either the active or inactive trials.

Metabolic demand, calculated using Equation 5.3 is presented in Table 5-4 for resting, control, inactive, and active conditions, with averaged demand presented in Table 5-5.

	Control		Inactive		Active	
	$K_{ankle,Abs}$ $\frac{Nm/kg}{°}$	$K_{ankle,Gen}$ $\frac{Nm/kg}{°}$	$K_{ankle,Abs}$ $\frac{Nm/kg}{°}$	$K_{ankle,Gen}$ $\frac{Nm/kg}{°}$	$K_{ankle,Abs}$ $\frac{Nm/kg}{°}$	$K_{ankle,Gen}$ $\frac{Nm/kg}{°}$
S1	0.136±0.012	0.078±0.003	0.134±0.012	0.087±0.003↑	0.183±0.022↑	0.094±0.012
S2	0.182±0.012	0.079±0.006	0.165±0.012↓	0.083±0.005↑	0.174±0.016↑	0.085±0.007
S3	0.181±0.013	0.077±0.003	0.165±0.010↓	0.079±0.003↑	0.174±0.013↑	0.086±0.005↑
S4	0.176±0.014	0.065±0.003	0.148±0.012↓	0.069±0.002↑	0.160±0.011↑	0.068±0.003
S5	0.153±0.009	0.075±0.004	0.138±0.006↓	0.081±0.005↑	0.142±0.017	0.096±0.004↑
S6	0.110±0.017	0.059±0.007	0.185±0.015↑	0.085±0.002↑	0.123±0.011↓	0.078±0.004↓

(a) Ankle stiffnesses, measured in absorptive and generative stance, normalized by body mass

	Control		Inactive	
	$K_{knee,Abs}$ $\frac{Nm/kg}{°}$	$K_{knee,Gen}$ $\frac{Nm/kg}{°}$	$K_{knee,Abs}$ $\frac{Nm/kg}{°}$	$K_{knee,Gen}$ $\frac{Nm/kg}{°}$
S1	0.120±0.022	0.081±0.007	0.105±0.016↓	0.066±0.009↓
S2	0.113±0.022	0.106±0.010	0.111±0.019	0.087±0.011↓
S3	0.132±0.021	0.140±0.018	0.106±0.017↓	0.092±0.005↓
S4	0.088±0.011	0.091±0.007	0.114±0.016↑	0.089±0.007
S5	0.093±0.016	0.077±0.009	0.088±0.012	0.061±0.006↓
S6	0.099±0.021	0.066±0.007	0.145±0.018↑	0.103±0.010↑

	Active					
	$K_{knee,Abs}$ $\frac{Nm/kg}{°}$	$K_{knee,Gen}$ $\frac{Nm/kg}{°}$	$K_{exo,Abs}$ $\frac{Nm/kg}{°}$	$K_{exo,Gen}$ $\frac{Nm/kg}{°}$	$K_{bioknee,Abs}$ $\frac{Nm/kg}{°}$	$K_{bioknee,Gen}$ $\frac{Nm/kg}{°}$
S1	0.124±0.023	0.085±0.013↑	0.019±0.005	0.014±0.005	0.108±0.021	0.072±0.013
S2	0.113±0.016	0.089±0.011	0.025±0.006	0.020±0.003	0.089±0.015↓	0.069±0.011↓
S3	0.130±0.024↑	0.107±0.010↑	0.017±0.002	0.016±0.002	0.114±0.024	0.091±0.009
S4	0.110±0.015	0.088±0.006	0.011±0.001	0.010±0.002	0.100±0.015↓	0.078±0.006↓
S5	0.062±0.014↓	0.056±0.007↓	0.015±0.062	0.041±0.053	0.060±0.070	0.041±0.019↓
S6	0.093±0.030↓	0.073±0.008↓	0.020±0.027	0.020±0.014	0.070±0.030↓	0.056±0.009↓

(b) Knee stiffnesses, measured in absorptive and generative stance, normalized by body mass

Table 5-2: Effective joint stiffnesses, normalized by subject mass, calculated for the six subjects. Uncertainties reflect the standard deviation associated with step-to-step variation. Because the control and inactive condition impose zero exoskeletal stiffness and therefore result in equal total and biological knee stiffnesses, exoskeletal and biological contributions at the knee are listed only for the active condition. Arrows indicate the direction of statistically significant differences at the 1% level within a given subject from the control to inactive condition or from the inactive to active condition. Significance was computed using a two sided t-test. Because the uncertainties reported here do not reflect trial-to-trial variation and due to the large number of comparisons (60) made within this table, these marks should be taken as suggestive of greater trends and not treated as meaningful in isolation.

	Control		Inactive		Active	
	k_{leg} $\frac{N/kg}{m/m}$	k_{vert} $\frac{N/kg}{m/m}$	k_{leg} $\frac{N/kg}{m/m}$	k_{vert} $\frac{N/kg}{m/m}$	k_{leg} $\frac{N/kg}{m/m}$	k_{vert} $\frac{N/kg}{m/m}$
S1	196±14	692±122	204±16	820±165↑	218±26	793±182
S2	191±16	608±104	198±15	688±138↑	204± 9	708±115
S3	241±15	733±100	249±16↑	815±135↑	280±23↑	956±210↑
S4	153± 8	499± 57	165±11↑	592±125↑	155± 7↓	530± 52↓
S5	166±16	626±130	169±15	716±260	205±16↑	694±200
S6	182±11	727±115	185±10	664±105	193±15	734±109↑

Table 5-3: Effective leg stiffnesses, normalized by subject mass and leg length, calculated for the six subjects. Uncertainties reflect the standard deviation associated with step-to-step variation. Arrows indicate the direction of statistically significant differences at the 1% level within a given subject from the control to inactive condition or from the inactive to active condition. Significance was computed using a two sided t-test. Because the uncertainties reported here do not reflect trial-to-trial variation and due to the large number of comparisons (60) made within this table, these marks should be taken as suggestive of greater trends and not treated as meaningful in isolation.

	Resting W/kg	Control W/kg	Inactive W/kg	Active W/kg
S1	1.7±0.2	15.7±0.1	21.2±0.1↑	20.7±0.1↓
S2	1.3±0.2	17.2±0.2	19.6±0.3↑	19.7±0.3
S3	1.1±0.1	16.6±0.1	20.6±0.0↑	20.3±0.1↓
S4	1.4±0.1	16.6±0.1	19.6±0.1↑	20.4±0.1↑
S5	1.2±0.1	17.2±0.3	16.9±0.1	-
S6	1.7±0.1	16.2±0.2	-	-

Table 5-4: Metabolic demands, normalized by subject mass, calculated for the six subjects. Uncertainties reflect the standard error associated with breath-to-breath variation. Arrows indicate the direction of statistically significant differences at the 1% level within a given subject from the control to inactive condition or from the inactive to active condition. Significance was computed using a two sided z-test. Because the uncertainties reported here do not reflect trial-to-trial variation, these marks should be taken as suggestive of greater trends and not treated as meaningful in isolation.

		Control	Inactive	Active
$K_{ankle,Abs}$	$\left(\frac{Nm/kg}{°}\right)$	0.169±0.022	0.153±0.015	0.173±0.010
$K_{ankle,Gen}$	$\left(\frac{Nm/kg}{°}\right)$	0.075±0.006	0.079±0.008†	0.083±0.011
$K_{knee,Abs}$	$\left(\frac{Nm/kg}{°}\right)$	0.113±0.019	0.109±0.004	0.119±0.009
$K_{knee,Gen}$	$\left(\frac{Nm/kg}{°}\right)$	0.105±0.026	0.084±0.012	0.092±0.010
$K_{exo,Abs}$	$\left(\frac{Nm/kg}{°}\right)$	-	-	0.018±0.006
$K_{exo,Gen}$	$\left(\frac{Nm/kg}{°}\right)$	-	-	0.015±0.004
$K_{bioknee,Abs}$	$\left(\frac{Nm/kg}{°}\right)$	0.113±0.019	0.109±0.004	0.102±0.011
$K_{bioknee,Gen}$	$\left(\frac{Nm/kg}{°}\right)$	0.105±0.026	0.084±0.012	0.078±0.010
k_{leg}	$\left(\frac{N/kg}{m/m}\right)$	195± 36	204± 35	214± 52
k_{vert}	$\left(\frac{N/kg}{m/m}\right)$	633± 103	729± 110†	747± 178
P_{met}	$\left(\frac{W}{kg}\right)$	16.5± 0.7	20.3± 0.8	20.3± 0.4

Table 5-5: Mean joint stiffnesses, leg stiffnesses, and metabolic demands. Uncertainties reflect the standard deviation associated with subject-to-subject variation. Arrows indicate the direction of statistically significant differences at the 5% level from the control to inactive condition or from the inactive to active condition. Significance was determined using a post-hoc paired two-sided Šidák-corrected t-test, following a repeated measures ANOVA. Due to atypical kinematics, results for S5 and S6 are omitted, though S5's data are used to compare control and inactive conditions; see text for details.

5.3.1 Average Mechanics and Metabolic Demand

For each stiffness as well as metabolic demand, a repeated measures ANOVA was conducted to determine significance of trends apparent in Section 5.3. Due to the outlying nature of S6's inactive trial and S5's active trial, their data for all conditions was omitted from this test. For each stiffness found to vary among the three groups, a post-hoc two-sided paired t-test was conducted using Šidák correction to compare the control and inactive conditions and inactive and active conditions, so that $P = 0.0253$ is considered significant.

ANOVA suggests total leg stiffness varies among the conditions ($P = 0.08$), with post-hoc paired t-testing revealing that the observed increase in k_{leg} due to inactive mass is significant ($P < 0.01$), but that no significant difference exists between the

inactive and active conditions. This suggestion that increased mass at the knee increases leg stiffness is interesting, particularly in light of He's[22] finding that leg stiffness does not vary when gravity is reduced. Moreover, if leg stiffness is normalized by total mass rather than by subject mass (as was not necessary in [22]), no evidence of increase is found.

ANOVA suggests variation in total generative phase knee stiffness ($P = 0.10$) and finds significant variation in biological generative phase knee stiffness ($P = 0.04$). Post-hoc testing suggests that generative phase knee stiffness decreases due to the additional mass ($P = 0.10$), but does not find evidence of difference between the inactive and active conditions.

Additionally, a significant variation in ankle stiffness in generation ($P = 0.02$), with post-hoc testing suggesting a difference between the control and inactive conditions ($P = 0.06$) but not between inactive and active conditions.

A suggestive difference exists in metabolic demand between the control and inactive conditions for all subjects for whom metabolic data was available in these conditions ($P = 0.04$, not quite significant at the 5% level with the Šidák correction). This is misleading, however, as the respiratory exchange ratio is notably higher for trials in the inactive and active condition than for trials in the control condition. Though always below 1.1, this shift in respiratory exchange ratio implies that some anaerobic contribution is present when the brace is worn, making comparisons between the control and inactive case tenuous. It is worth noting that if S5's anomalously low demand in the inactive condition is omitted as an outlier, the difference between these conditions becomes significant, as is expected from subjective reactions to running with the additional mass.

There is no evidence against the null hypotheses that leg stiffness and knee stiffness are each unchanged by the presence of an external parallel spring at the knee.

5.3.2 Subject Variation in Response to Intervention

Closer examination of Table 5-2 suggests that the population may be divided into two groups according to level of training. As shown in Figure 5-4, trained compet-
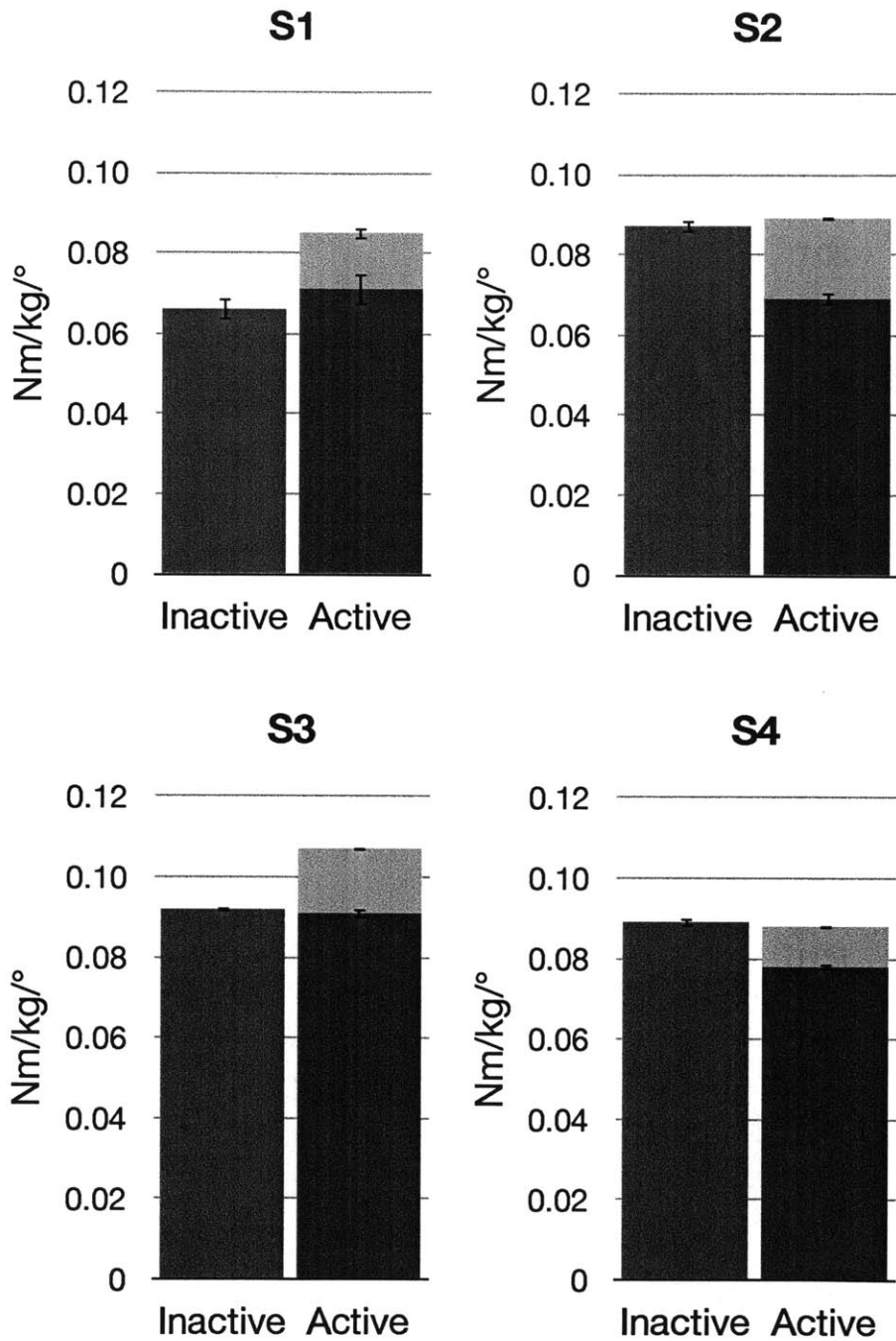
Figure 5-4: Biological (dark) and exoskeletal (light) generative phase knee stiffness for several subjects in the inactive (green) and active (blue) conditions. Subjects S1 and S3 are trained competitive marathon runners and appear to maintain biological stiffness while recreational runners S2 and S4 appear to maintain total stiffness.

itive marathoners S1 and S3 appear to exhibit increased total knee stiffness in the active condition, while recreational runners S2 and S4 exhibit unchanged knee stiffness despite the external stiffness. While statistics for such a small sample must be approached cautiously, a two sided paired t-test suggests increased total knee stiffness in both absorption and generation in marathoners ($P = 0.07$ in both cases) with no corresponding effect in recreational runners ($P = 0.80$ in both cases). Ankle stiffness in generation is also found to increase in the active case in marathoners ($P < 0.01$) but not in recreational runners ($P = 0.50$). Marathoners S1 and S3 also exhibit small (2%) reductions in metabolic demand above resting while S2 and S4 do not, though this effect is not statistically significant. Verifying these apparent differences in stiffness and metabolic demand based on runner training would require subsequent investigation with larger samples of recreational and trained runners, however.

Chapter 6

Discussion

6.1 Conclusions

There is no evidence of a change in leg stiffness in response to the addition of a parallel knee spring during running stance. The mechanism by which this is accomplished varies; there is suggestive evidence that the population is divided by training, so that recreational runners regulate total knee stiffness while marathon runners allow total knee stiffness to increase.

There is also evidence linking the addition of mass to the leg to an increase in leg stiffness.

6.2 Implications

The suggestion that the body's reaction to a parallel stiffness varies between recreational and marathon runners is particularly interesting. It is plausible that plasticity varies with level of training, so that recreational runners can reduce biological knee stiffness to preserve total stiffness in the presence of the external spring, while trained marathon runners cannot.

It has been suggested that running dynamics arise predominantly from tuned morphology, with knee stiffness representing primarily passive tendon stiffness. If this is the case, marathoners may have muscle fascicles optimized for low-speed, largely

isometric contractions and therefore be physiologically less capable of modulating knee stiffness downward through spring-like muscle activation.

Alternatively, it is possible that trained runners and recreational runners optimize different parameters while running. Recreational runners may optimize their gait for load reduction in joints or minimal center of mass displacement, while marathon runners may instead optimize their gait for metabolic demand. Subsequent investigation of the effects of training on gait plasticity is warranted.

If total leg stiffness is maintained despite increases in ankle and knee stiffnesses, the hip is presumably responsible for regulating total leg stiffness in these cases. The total work at the hip, which is difficult to measure by inverse dynamics as errors accumulate with each proximal to ground contact, may therefore account for the observed negative correlation between total knee stiffness and metabolic demand.

For patients who are able to reduce biological knee torque to accommodate a parallel spring, a device of this kind holds promise as an orthosis for reducing load, and therefore pain, in the knee.

6.3 Future Improvements

Though beyond the scope of this work, there are several ways in which the designed exoskeleton could be improved.

First, it is unfortunate that human attachment technologies are unable to accommodate the loads associated with the intended intervention. Notably, in its use in the knee brace, the exoskeletal clutch operates at less than 10% its rated torque to avoid deformation of the harness and movement of the biological limb independently of the harness. In order to increase the applicable intervention, the harness could be improved in several ways:

- **Reinforcement of the lateral support:** Exoskeletal spring forces cause elastic deformation of the harness itself in the coronal plane. This series elasticity limits the maximum net spring stiffness experienced by the body. Using stiffer

materials for the lateral wall of the brace or reducing the moment arm by which the exoskeletal protrudes laterally would reduce this effect.

- **Improved posterior loading:** Posterior soft tissue compression, particularly in the thigh, allows the biological knee to flex without an equivalent harness flexion. This problem may be mitigated by increasing the surface area over which load is applied, as by a thermoplastic insert molded to each wearer.

- **Improved anterior constraint:** As pain prevents loading directly through the patella, the biological knee itself is unrestricted by the harness. When large stiffnesses are applied, the biological knee may translate anteriorly, effectively leaving the harness and again allowing larger biological knee flexion than harness flexion. Molded inserts on the anterior face of the brace, as close as possible to the patella, would reduce this effect.

- **Reduction of migration:** Over time, the knee brace tends to slip distally, though the act of flexing the knee in swing ultimately limits total migration. This movement causes discomfort and a poor interface for force transduction between the exoskeleton and the body. In trials, this problem was mitigated using tape to secure the brace to pants. A more elegant solution could integrate the proximal harness into a hip spanning structure or the integrate the distal harness into an ankle spanning structure, as by stirrups.

One solution to the first of these problems involves abandoning the robust linear spring designed to span arbitrary sets of joints in favor of a rotary design intended specifically for the knee. The existing clutch could be adapted to use either a torsional leaf spring or a linear compression spring on a moment arm, without the lateral moment arm necessary to use the linear bow-style spring. This design would also place the mass of the clutch less laterally, reducing the hip adductor torque experienced in swing, though the spring elements would likely have higher mass than those used currently.

The total mass of the device is a grave concern in running. The substantial increase in metabolic demand associated with carrying the inactive mass of the harness and

clutch will be difficult to surmount. While dramatically increasing spring stiffness may result in a sufficiently large decrease in metabolic demand, a reduction in total mass will likely be necessary if the device is to decrease total metabolic demand relative to unaffected running. This may require substantially derating the clutch - possibly an acceptable tradeoff if use exclusively at the knee is desired.

Metabolically, spanning the ankle as well at the knee makes mass an even greater concern. In preliminary experiments with such a full leg spring, a highly active athlete was unable to maintain aerobic metabolism at running speeds greater than $2.5m/s$. It may prove impossible to reduce the total mass of such a system sufficiently to permit use of a single full-leg spring, though multiple single-joint springs could implement an equivalent system.

Additionally, it is conceivable that this device could be made to operate without the need for battery charging. The addition of pulse-and-hold solenoid activation reduces the average power consumed by the solenoid to below 300mW, bringing it within an order of magnitude of the sensors and control electronics. Such a small amount of power could be derived from the biological knee itself during deceleration in late swing. Biomechanically, the negative power seen during braking likely represents storage in elastic elements, so we must assume that such power scavenging represents a net loss to the body. Nonetheless, if the needed power is sufficiently small and the generator sufficiently efficient, the exoskeleton could still provide net augmentation. Such a device would be completely passive energetically - a system which merely adjusts natural bias points.

For this reason, it is desirable to lower the electrical cost as much as possible. With an understanding of effective control strategies and the usage model of the sensors, the cost of onboard electronics could be reduced significantly. Unfortunately, the nature of a spring return solenoid ensures that power must be used to keep the clutch engaged. While the pulse-and-hold approach reduces this power and turning off the solenoid after midstance eliminates it for a significant fraction of stance, a bistable actuator could eliminate it completely. Bistable solenoids can be constructed, using permanent magnets or non-linear spring systems to construct a potential barrier, but

were not considered for this version due to the associated complexity.

Finally, a purely elastic exoskeleton is poorly suited for traversal of uneven terrain. In stair or ramp descent, for instance, energy absorption in an exoskeletal knee joint would likely be beneficial. To achieve this versatility, the clutch could be replaced or assisted by a brake, to enable dissipative operation as well as elastic operation.

Such uneven environments also dramatically worsen the problem of disengagement. The purely elastic exoskeleton is dependent on achieving a spring length at toe off greater than the length at clutch engagement, so that all spring energy is released. In typical level ground running, knee extension at toe off exceeds the peak extension seen in swing, so this problem rarely manifests in steady state. However, in less consistent gaits, it may become a dominant concern and some mechanism, such as a parallel brake, will be necessary to dissipate stored spring energy so that the clutch may be safely disengaged.

6.4   Future Research

Once the changes to the harness discussed in Section 6.3 are achieved and it is possible to proceed with larger interventions several interesting questions become answerable:

- **Do marathon runners and recreational runners respond differently to the presence of parallel stiffness?** Though this works suggests this to be the case, the sample size of each class is too small to be conclusive.

- **How do joint and leg stiffnesses vary with exoskeleton stiffness?** This experiment may be repeated with several increasing stiffnesses in order to determine the kinetic effects over a range of stiffnesses. In particular, if trained runners conclusively do allow total knee stiffness to increase in the presence of a parallel spring, does this effect saturate?

- **How does metabolic demand vary with exoskeleton stiffness?** An original goal of this work was to investigate the possibility of significantly reducing

metabolic demand through the use of parallel elasticity. With the ability to couple larger moments to the body, such an achievement may be possible.

Additionally, following the discussion in Chapter 2, this clutched spring exoskeleton may be attached to any of several combinations of joints, allowing similar questions to be answered through interventions elsewhere on the leg:

- **What are the effects of parallel stiffness at the ankle?** A similar device acting at the ankle has shown promise in reducing the metabolic demand of level ground walking[44] while a passive spring at the ankle has demonstrated conservation of total leg stiffness and total ankle stiffness in hopping[17].

- **What are the effects of parallel stiffness across the full leg?** Following a successful reduction in the metabolic demand of hopping using a full leg spring[20], an initial effort was made to replicate the system for running. Both toe running and traditional striking with a modified ground interface were attempted, but ultimately the burden of the exoskeleton mass proved too significant in this configuration.

6.5 Other Applications

A high torque clutch, potentially in tandem with a motor, could potentially surrogate any muscle which largely acts isometrically. Several modern robotic prostheses and orthoses incorporate biomimetic structures emulating the interactions between muscles and tendons[2][30], but even the most robust devices consume significant energy to simply immobilize elements. The low weight clutch design presented here could be incorporated into existing biomimetic ankles and knees, potentially yielding drastic battery life improvements, and could make possible previously discarded architectures.

100

6.6 Concluding Thoughts

Human legged locomotion is efficient and robust, making it nearly ideal for traversing uneven terrain. It is, however, human nature to press limits and new solutions are needed if human locomotion is to conquer the ravages of hostile environments, prolonged activity, and simple old age. The parallel exoskeleton architecture described here offers a first step towards that goal.

Bibliography

[1] R M Alexander. Energy-saving mechanisms in walking and running. *Journal of Experimental Biology*, 160:55–69, 1991.

[2] Samuel Au. *Powered ankle-foot prosthesis for the improvement of amputee walking economy*. PhD thesis, Massachusetts Institute of Technology, 2007.

[3] A Belli, H Kyrolainen, and P V Komi. Moment and power of lower limb joints in running. *International Journal of Sports Medicine*, 23:136–141, 2002.

[4] Andrew A Biewener. Muscle function in vivo: A comparison of muscles used for elastic energy savings versus muscles used to generate mechanical power. *American Zoology*, 38:703–717, 1998.

[5] Alexander Bock. *Device for Helping a Person to Walk*. US Patent, 2004. 6719671.

[6] J M Brockway. Derivation of formulae used to calculate energy expenditure in man. *Human Nutrition Clinical Nutrition*, 41:463–471, 1987.

[7] G A Cavagna. Force plates as ergometers. *Journal of Applied Physiology*, 39(1):174–179, 1975.

[8] Giovanni A Cavagna, Normal C Heglund, and C Richard Taylor. Mechanical work in terrestrial locomotion: Two basic mechanisms for minimizing energy expenditure. *American Journal of Physiology Regulatory, Integrative, and Comparative Physiology*, 233:243–261, 1977.

[9] E A Clancy, E L Morin, and R Merletti. Sampling, noise-reduction, and amplitude estimation issues in surface eletromyography. *Journal of Electromyography and Kinesiology*, 12:1–16, 2002.

[10] Jack A Collins. *Mechanical Design of Machine Elements and Machines*. John Wiley and Sons, Hoboken, NJ, 2003.

[11] Jeffrey R Cram, Glann S Kasman, and Jonathan Holtz. *Introduction to Surface Electromyography*. Aspen Publishers, Inc., 1998.

[12] G John Dick and Eric A Edwards. *Human Bipedal Locomotion Device*. US Patent, 1991. 5016869.

[13] Aaron M. Dollar and Hugh Herr. Lower extremity exoskeletons and active orthoses: Challenges and state-of-the-art. *IEEE Transactions on Robotics*, 24(1):144–158, 2008.

[14] Clair T Farley and Daniel P Ferris. Biomechanics of walking and running: From center of mass movement to muscle action. *Exercise and Sport Sciences Reviews*, 26:253–285, 1998.

[15] Claire T Farley and Octavio Gonzalez. Leg stiffness and stride frequency in human running. *Journal of Biomechanics*, 29(2):181–186, 1996.

[16] Dominic James Farris and Gregory S Sawicky. The mechanics and energetics of human walking and running: A joint level perspective. *Journal of the Royal Society Interface*, 9(66):110–118, 2011.

[17] D P Ferris, Z A Bohra, J R Lukos, and C R Kinnaird. Neuromechanical adaptation to hopping with an elastic ankle-foot orthosis. *Journal of Applied Physiology*, 100:163–170, 2006.

[18] Daniel P Ferris. Running in the real world: Adjusting leg stiffness for different surfaces. *Proceedings Biological Sciences*, 265:989–994, 1998.

[19] Daniel P Ferris, Kailine Liang, and Claire T Farley. Runners adjust leg stiffness for their first step on a new running surface. *Journal of Biomechanics*, 32:787–794, 1999.

[20] Alena M Grabowski and Hugh M Herr. Leg exoskeleton reduces the metabolic cost of human hopping. *Journal of Applied Physiology*, 107:670–678, 2009.

[21] What's HAL (hybrid assistive limb)? http://www.cyberdyne.jp/english/robotsuithal/.

[22] Jiping He, Roger Kram, and Thomas A. McMahon. Mechanics of running under simulated low gravity. *Journal of Applied Physiology*, 71:863–870, 1991.

[23] Hugh Herr. Exoskeletons and orthoses: classification, design challenges and future directions. *Journal of NeuroEngineering and Rehabilitation*, 6(1), June 2009.

[24] Hulc. www.lockheedmartin.com/products/hulc/.

[25] Hiroaki Kawamoto and Yoshiyuki Sankai. Power assist method based on phase sequence and muscle force condition for HAL. *Advanced Robotics*, 19(7):717–734, 2005.

[26] H Kazerooni and S Kim. Contact instability of the direct drive robot when constrained by a rigid environment. In *ASME Winter Annual Meeting*, December 1989.

[27] H Kazerooni, Jean-Louis Racine, Lihua Huang, and Ryan Steger. On the control of the Berkeley lower extremity exoskeleton (BLEEX). In *IEEE International Conference on Robotics and Automation*, April 2005.

[28] Amy E Kerdok, Andrew A Biewener, Thomas A McMahon, Peter G Weyand, and Hugh M Herr. Energetics and mechanics of human running on surfaces of different stiffnesses. *Journal of Applied Physiology*, 92:469–478, 2002.

[29] Cynthia R Lee and Claire T Farley. Determinants of the center of mass trajectory in human walking and running. *Journal of Experimental Biology*, 201:2935–2944, 1998.

[30] Ernesto C Martinez, Jeff Weber, Grant Elliott, and Hugh Herr. Design of an agonist-antagonist active knee prosthesis. *Biomedical Robotics and Biomechatronics*, 2:529–534, 2008.

[31] Matweb online materials information resource. http://www.matweb.com.

[32] Thomas A McMahon. *Muscles, Reflexes, and Locomotion.* Princeton University Press, Princeton, NJ, 1984.

[33] Thomas A McMahon and George C Cheng. The mechanics of running: How does stiffness couple with speed? *Journal of Biomechanics*, 23:65–78, 1990.

[34] Robert Merletti. Standards for reporting emg data. Technical report, Politecnico di Torino, 1999.

[35] Ralph S Mosher. Handyman to Hardiman. Technical report, General Electric Research and Development Center, 1967.

[36] Carolyn F Munro, Doris I Miller, and Andrew J. Fuglevand. Ground reaction forces in running: a reexamination. *Journal of Biomechanics*, 20(2):147–155, 1987.

[37] Tom F Novacheck. The biomechanics of running. *Gait and Posture*, 7:77–95, 1998.

[38] G A Pratt and M M Williamson. Series elastic actuators. In *IEEE International Conference on Intelligent Robots and Systems*, volume 1, pages 399–406, 1995.

[39] Stock Drive Products. *Elements of Metric Gear Technology.* New Hyde Park, NY.

[40] Raytheon company: Robotics. www.sarcos.com.

[41] Gregory S Sawicki and Daniel P Ferris. Mechanics and energetics of incline walking with robotic ankle exoskeletons. *The Journal of Experimental Biology*, 212:32–41, 2008.

[42] Andrew Valiente. Design of a quasi-passive parallel leg exoskeleton to augment load carrying for walking. Master's thesis, Massachusetts Institute of Technology, 2005.

[43] Conor James Walsh. Biomimetic design of an under-actuated leg exoskeleton for load-carrying agumentation. Master's thesis, Massachusetts Institute of Technology, 2006.

[44] M B Wiggin, S H Collins, and G S Sawicki. An exoskeleton using controlled energy storage and release to aid ankle propulsion. In *33rd Annual International Conference of the IEEE Engineering in Medicine and Biology Society*, June 2011.

[45] N Yagn. *Apparatus for Facilitating Walking, Running, and Jumping.* US Patent, 1890. 420179, 438830, and 440684.

[46] Adam Zoss, H Kazerooni, and Andrew Chu. On the mechanical design of the Berkeley lower extremity exoskeleton (BLEEX). In *IEEE International Conference on Intelligent Robots and Systems*, 2005.

Appendix A

Varying Stride Frequency

It is possible that the effect of parallel knee stiffness depends on the relationship between biological knee stiffness and passive knee stiffness. One may hypothesize that muscle activation during upward regulation of knee stiffness may be more likely to be reduced by an external parallel spring. Since leg stiffness varies with step frequency, this may be investigated by enforcing variable cadence with a metronome.

A pilot experiment was conducted recording metabolic demand and electromyography from subject S1 as he ran on a treadmill at 3.2m/s in the control, inactive, and active condition while wearing nominal 3.6 Nm/^{o} springs. It should be noted that due to the compliance of the harness, a lesser stiffness on the order of 1 Nm/^{o} was likely applied in practice. All trials were conducted in a single session.

The metabolic demand associated with running in each condition is plotted in Figure A-1. The demand associated with control and inactive running are well described by a quadratic curve ($n = 4$, $\chi^2 = 0.6$ and $n = 5$, $\chi^2 = 2.5$ respectively), but the demand of running in the active condition is not ($n = 7$, $\chi^2 = 73.8$, $P < 0.01$). Instead, the demand of running in the active condition appears to be relatively independent of cadence except at the highest and lowest achievable step frequencies.

Electromyography, shown normalized by maximal voluntary contraction in Figure A-3, confirms that muscle activation varies with stride frequency differently in the active and inactive cases. In particular, for this subject, rectus activation decreases with increasing cadence more rapidly in the active case than in the inactive

case (slopes vary with $P < 0.01$). This implies that the biological knee may begin reducing muscle work in favor of the external exoskeleton only as cadence and therefore biological stiffness increase. Somewhat contradicting this, however, no difference is found in the activation of the monarticular knee extender, vastus lateralis.

These pilot results are preliminary and represent a single subject. They are presented here only for the benefit future investigators.
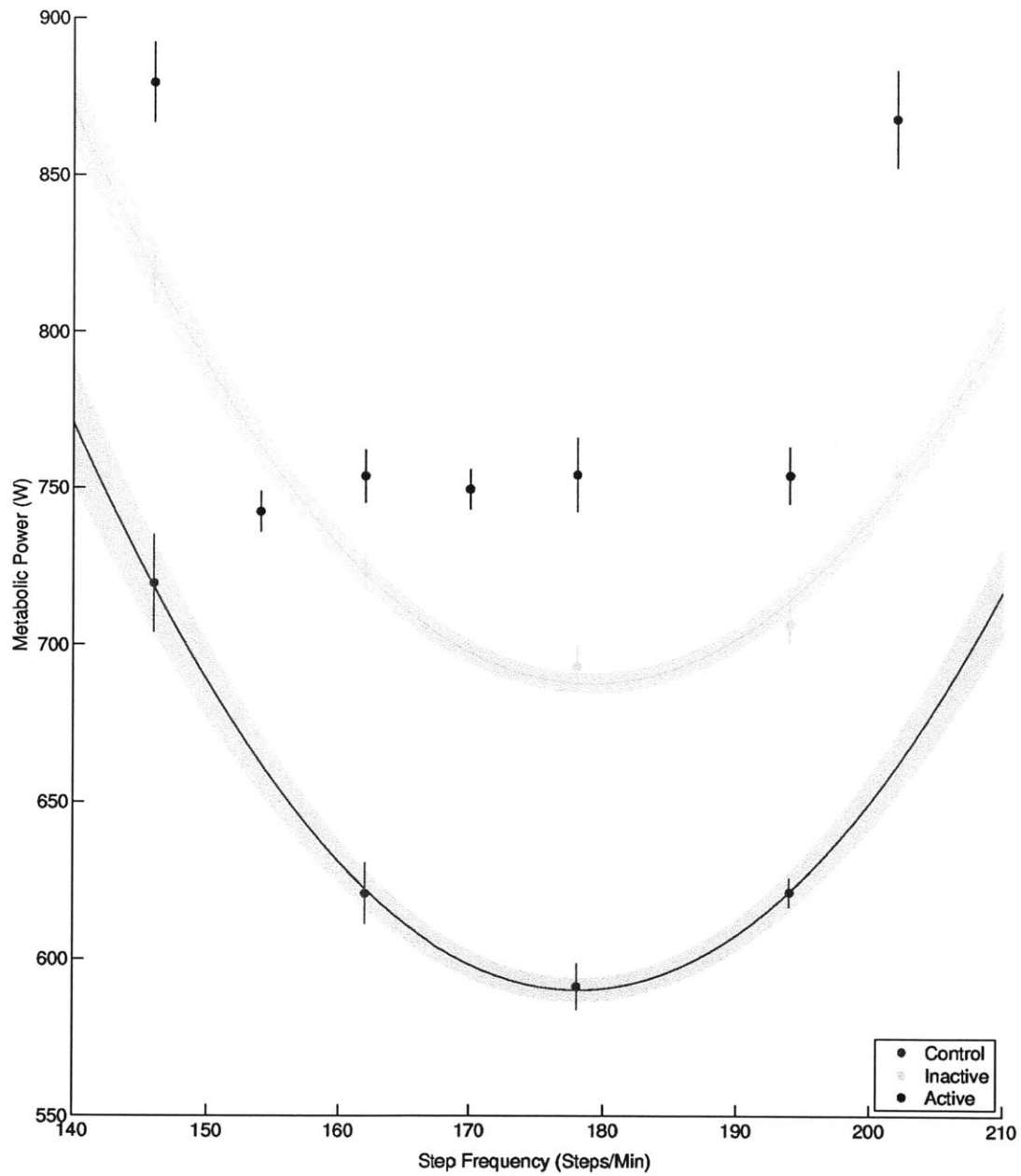
Figure A-1: Metabolic demand as a function of step frequency in the control (red), inactive (green), and active (blue) conditions for subject S1.
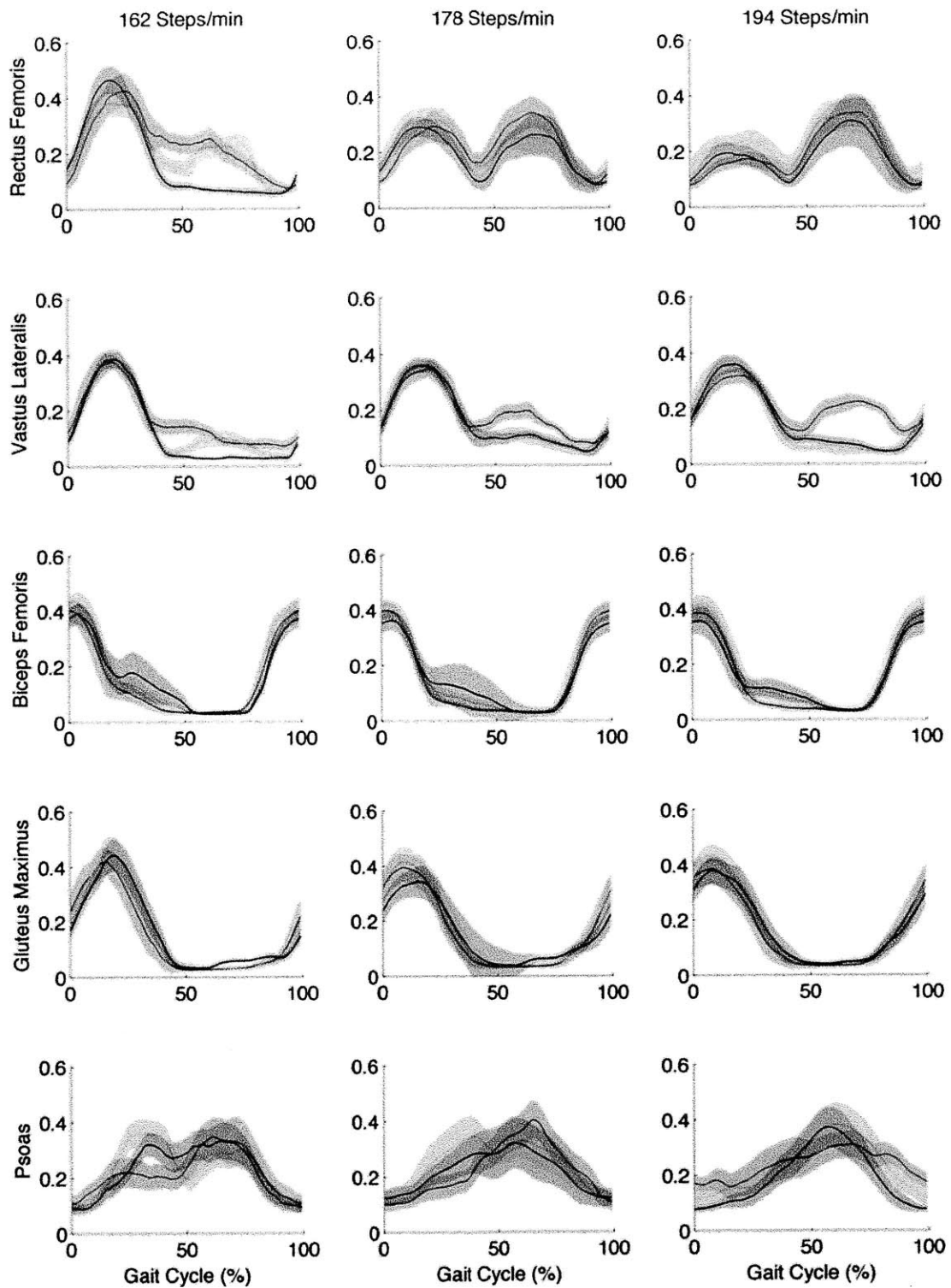
Figure A-2: Stride averaged electromyography, in six muscles for step frequencies below, at, and above metabolically optimal step frequency in the control (red), inactive (green), and active (blue) conditions for subject S1.

110
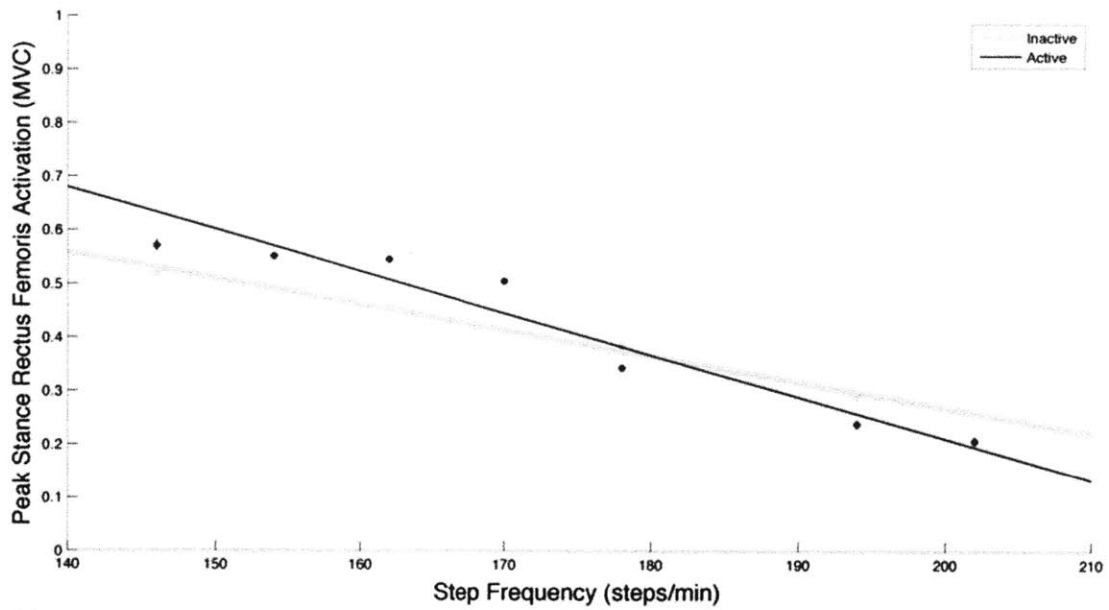
(a) Peak stance phase rectus femoris activation as a function of step frequency. Dependence on cadence is not well modeled as linear, but varies significantly from the inactive condition.
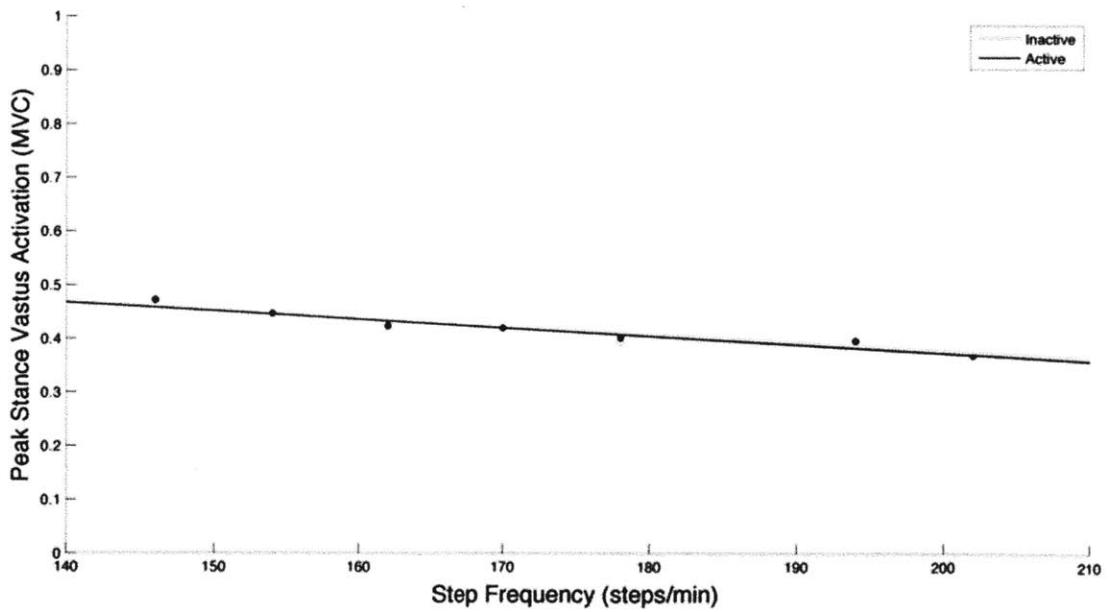
(b) Peak stance phase vastus lateralis activation as a function of step frequency. No significant difference is found.

Figure A-3: Electromyographic trends in step frequency
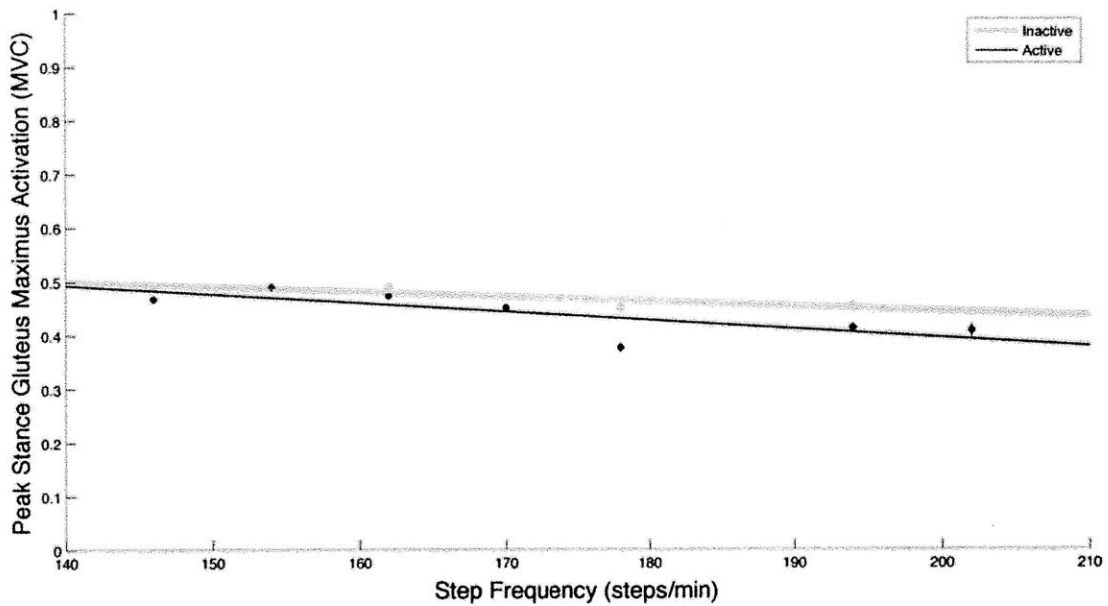
(c) Peak stance phase gluteus maximus activation as a function of step frequency. Slopes are significantly different.
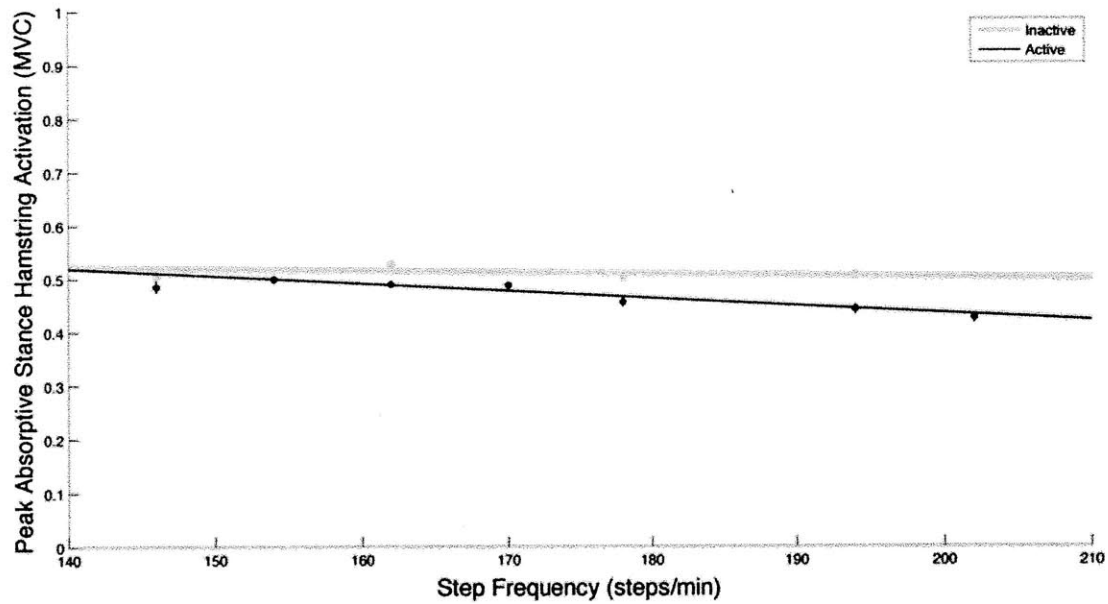
(d) Peak absorptive stance phase biceps femoris activation as a function of step frequency. Slopes are significantly different.

Figure A-3: Electromyographic trends in step frequency

Appendix B

Subject Mechanics and Electromyograhy

Stride-averaged mechanics and electromyography for each of the six subjects described in Table 5-1 are presented here. Additional plots demonstrate the spring-like dynamics of the ankle, knee, and vertical leg. In all cases, red denotes control, green denotes inactive, and blue denotes active. See Chapter 5 for methods used to produce these plots.
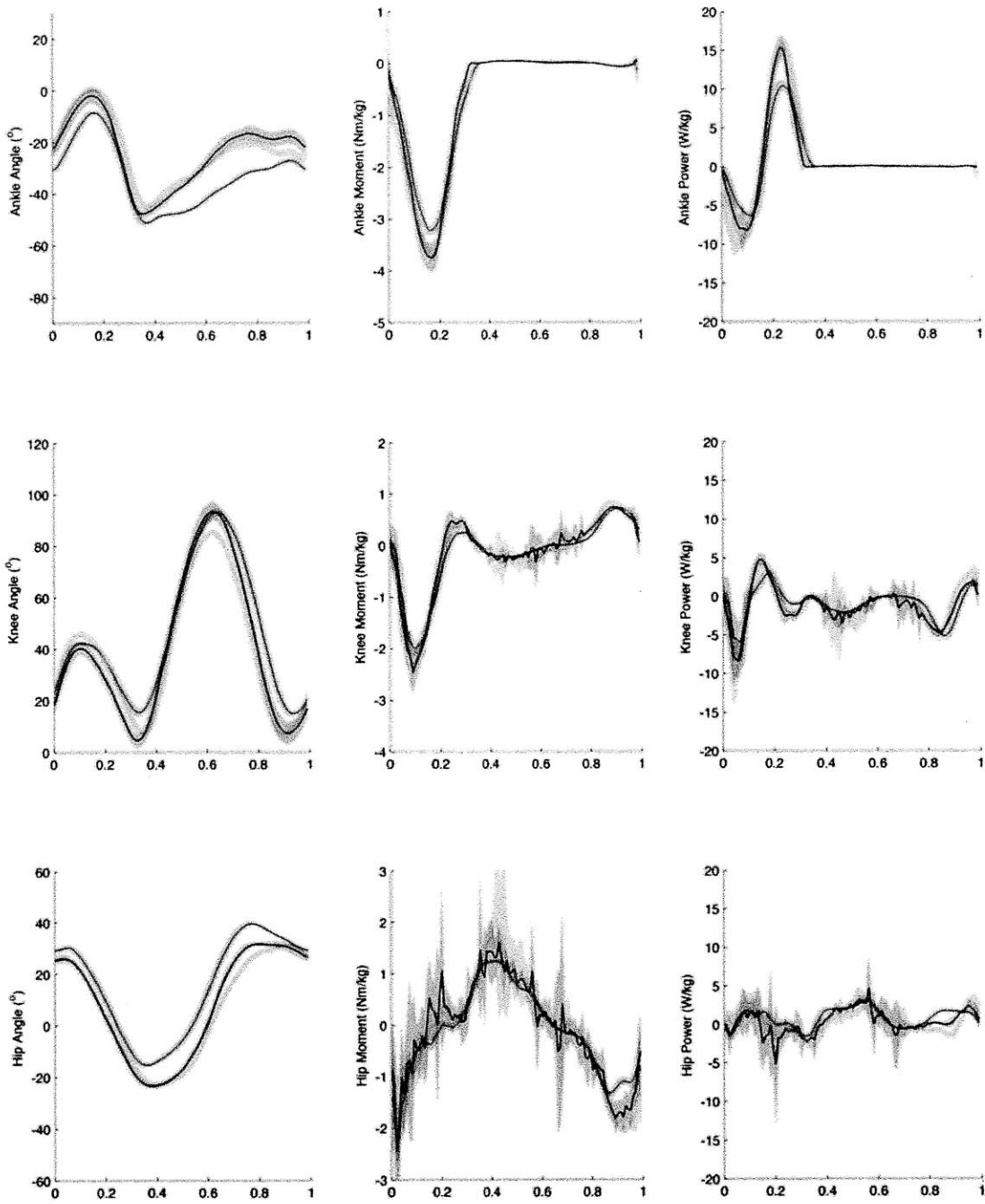
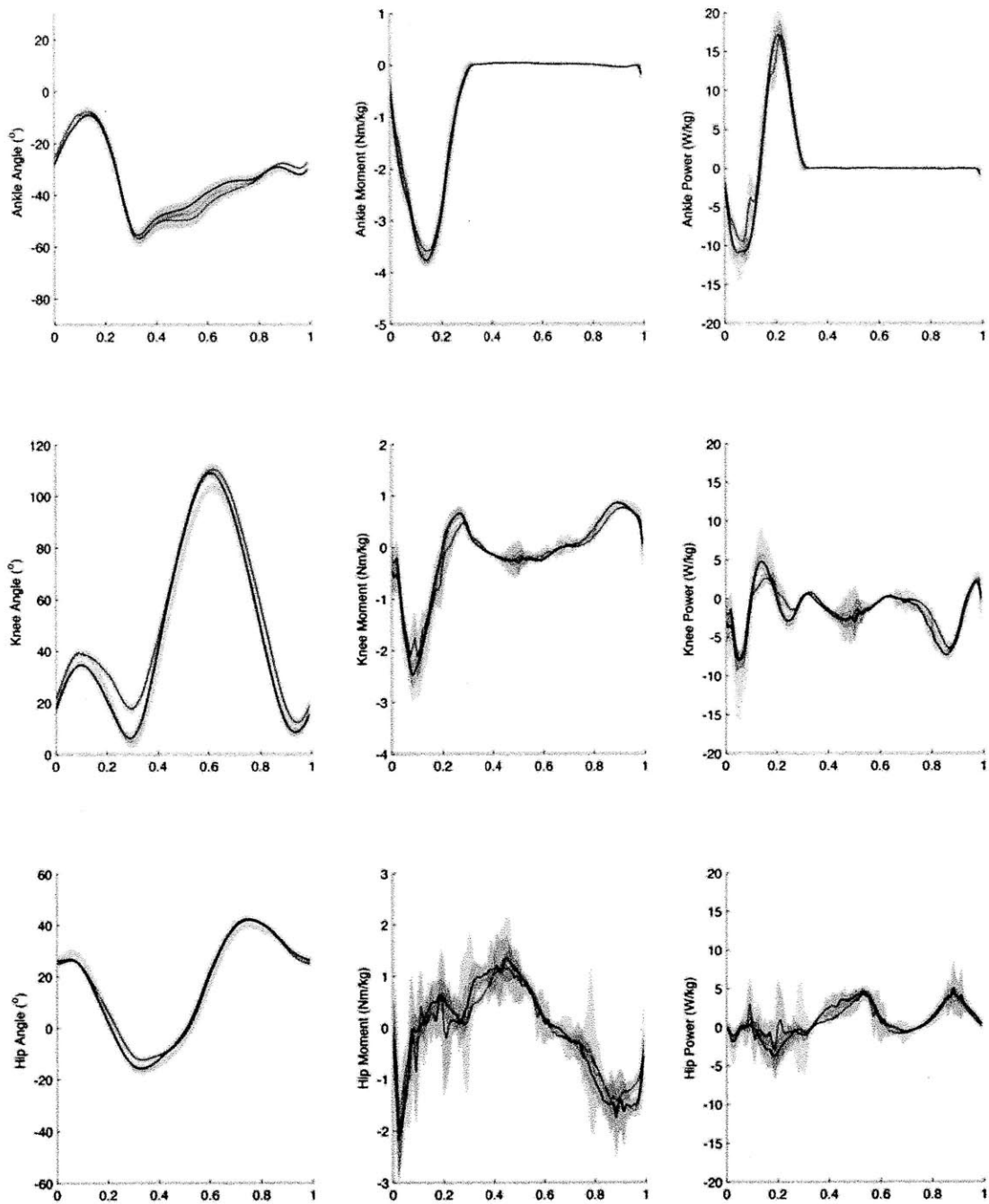(a) Joint angles, moments, and powers

Figure B-1: Subject S1
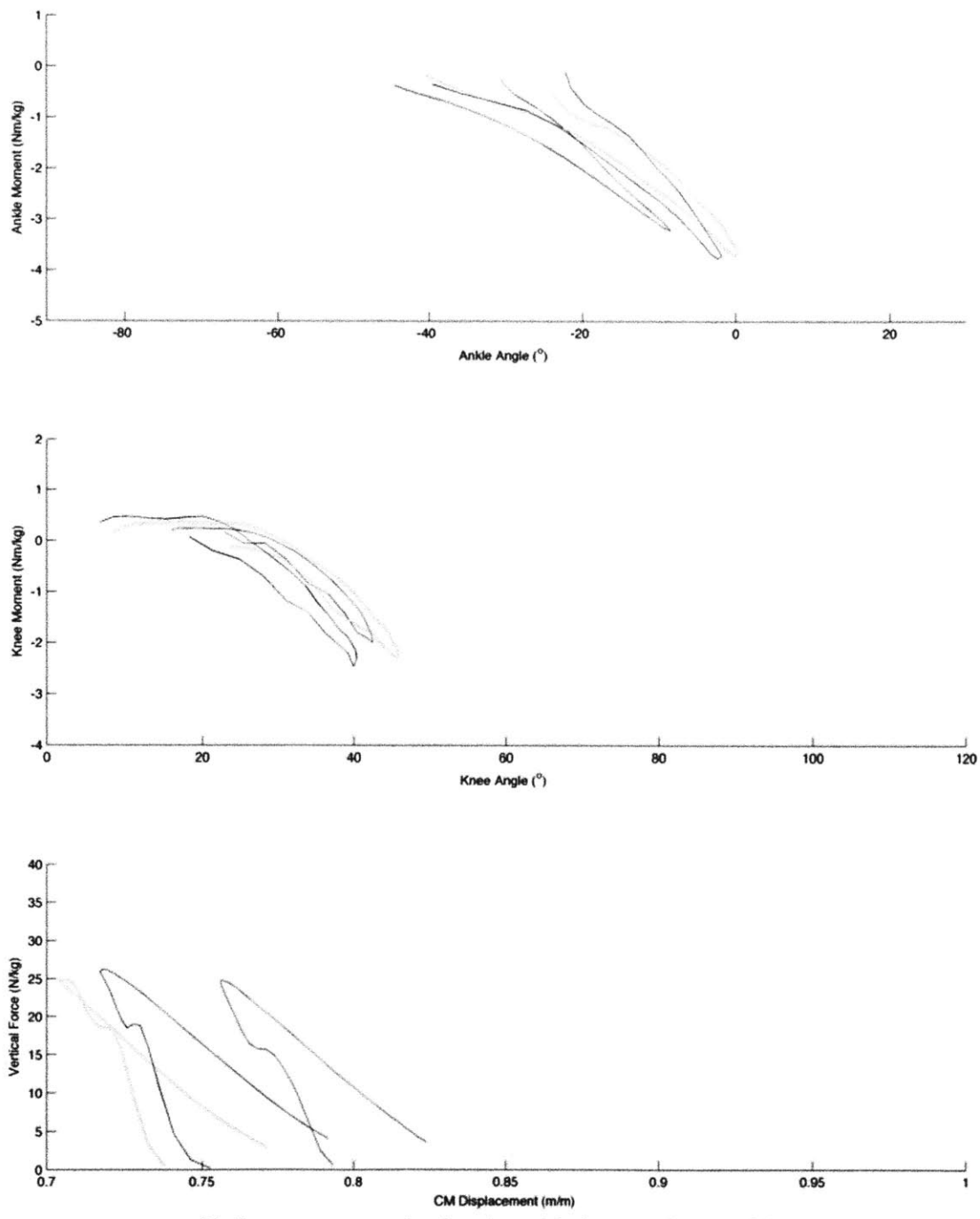
(b) Stance torque-angle plots for ankle, knee, and vertical leg
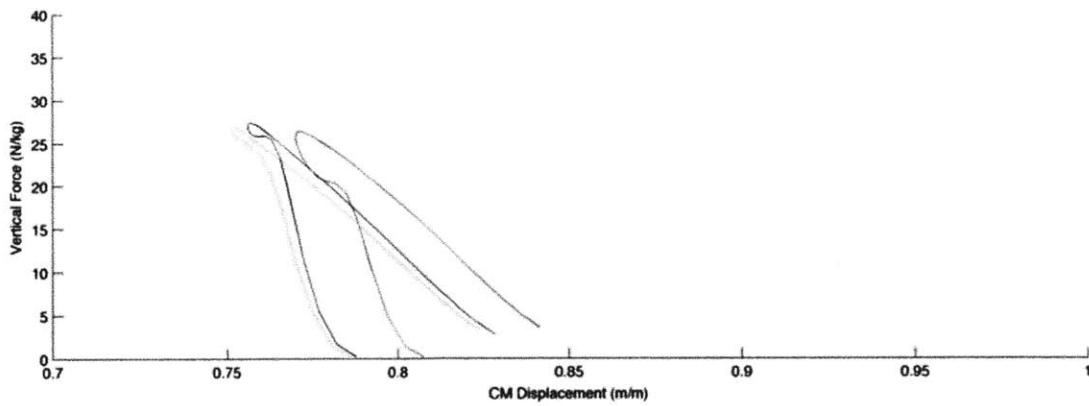
Figure B-1: Subject S1

115
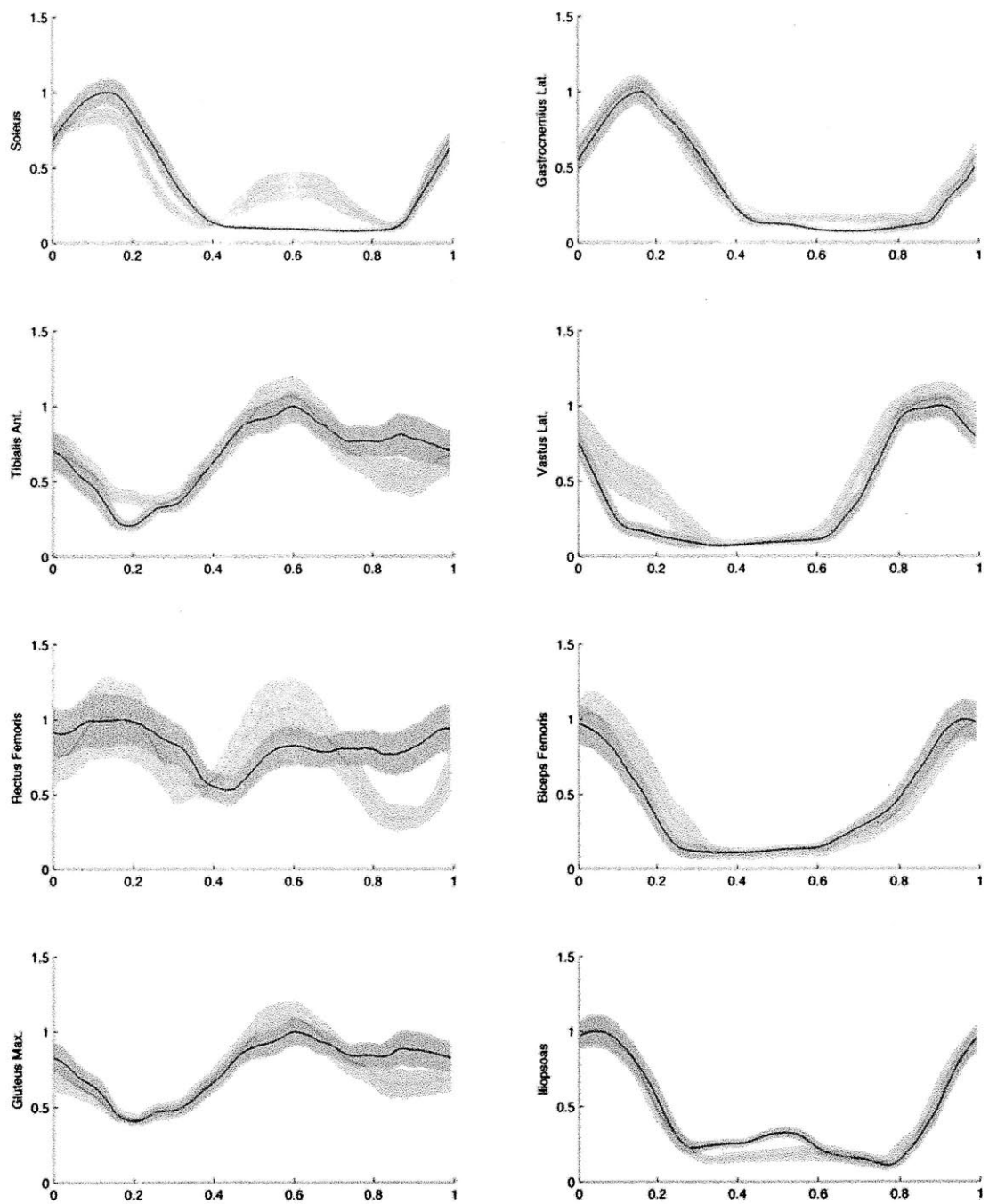
(c) Electromyography

Figure B-1: Subject S1
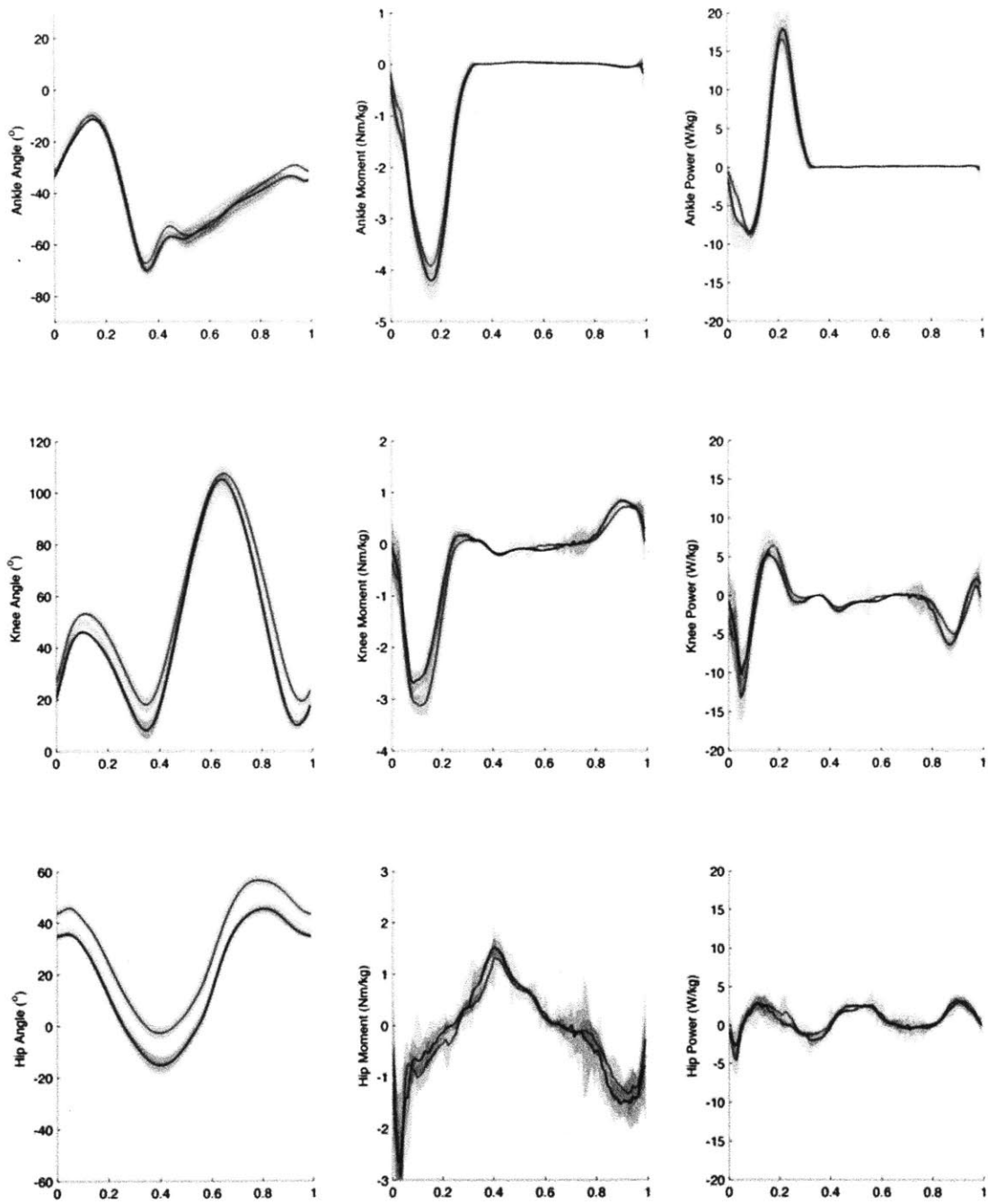
(a) Joint angles, moments, and powers

Figure B-2: Subject S2

117
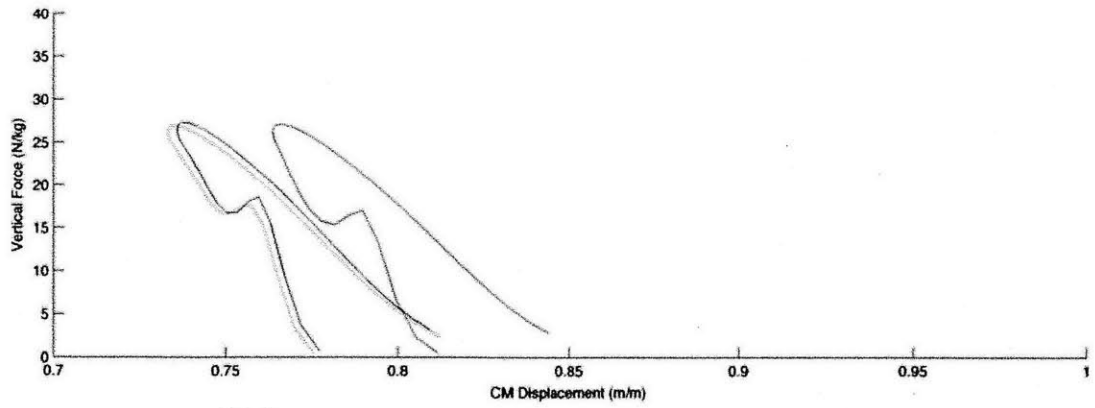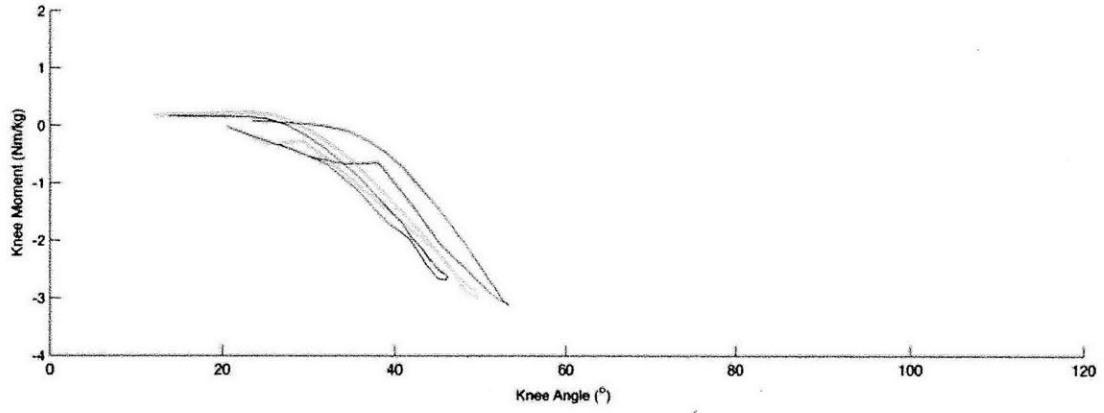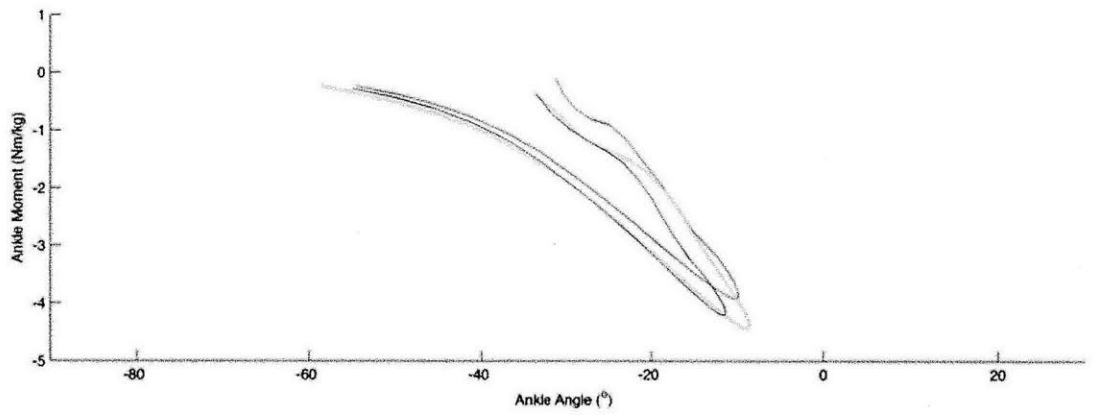
(b) Stance torque-angle plots for ankle, knee, and vertical leg
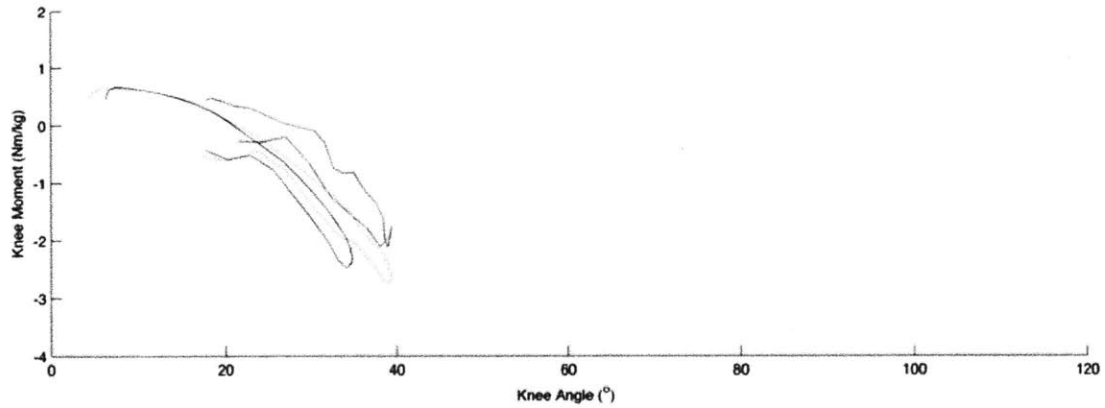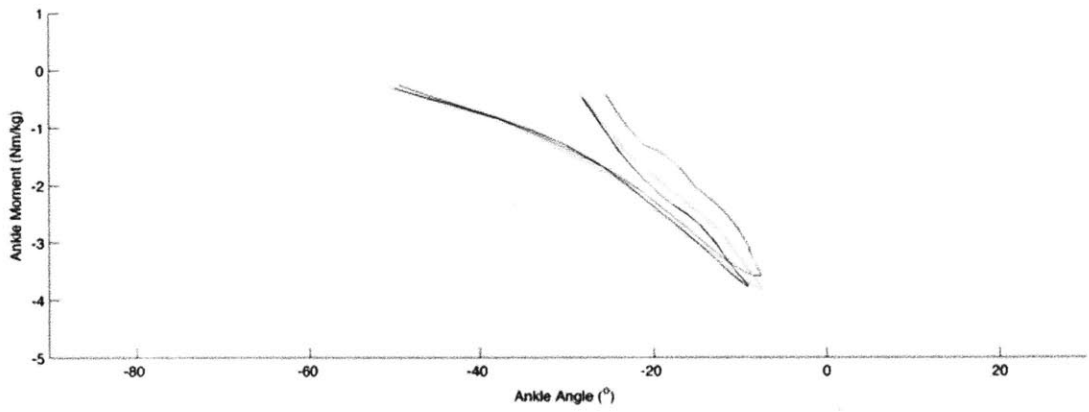
Figure B-2: Subject S2
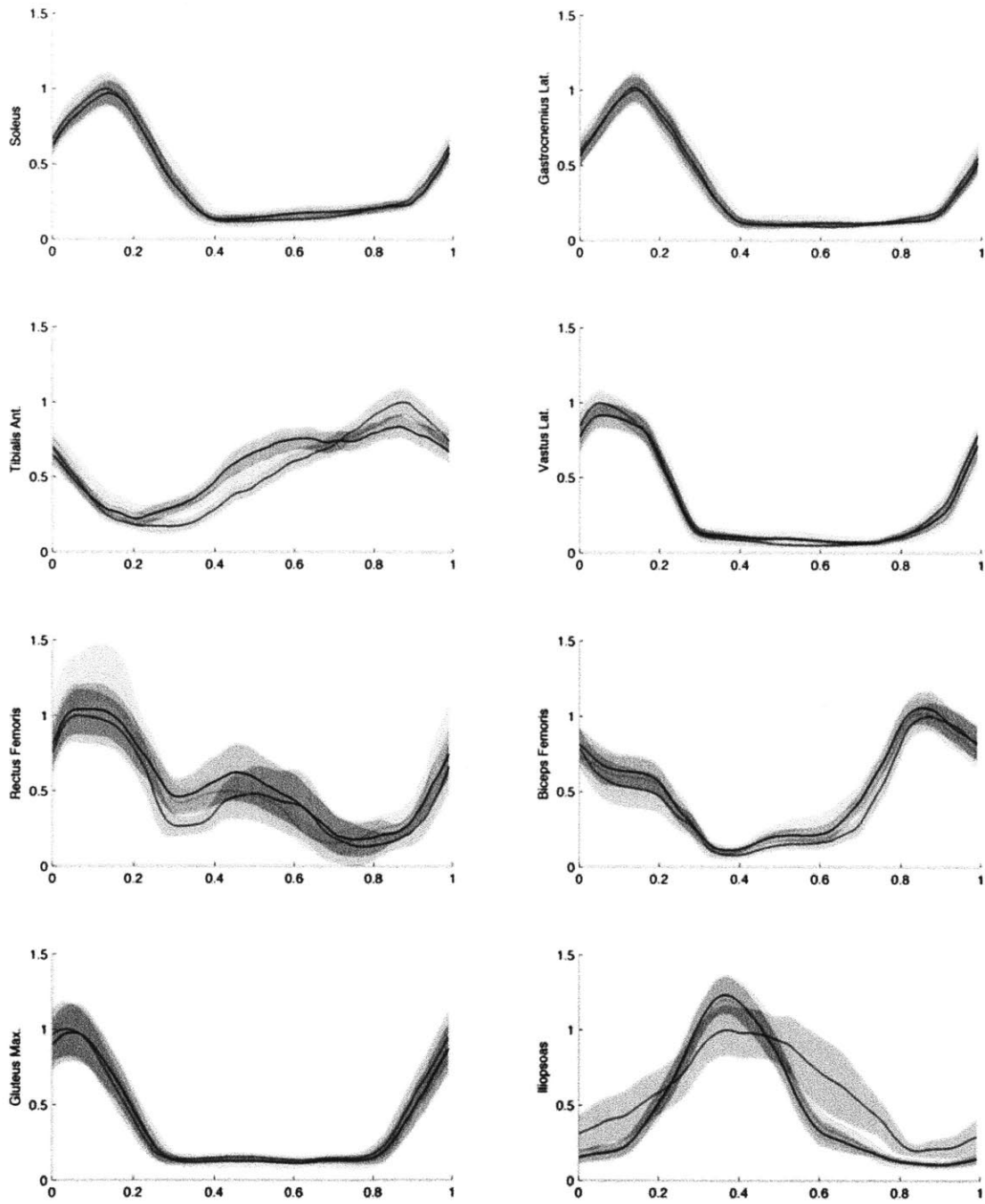
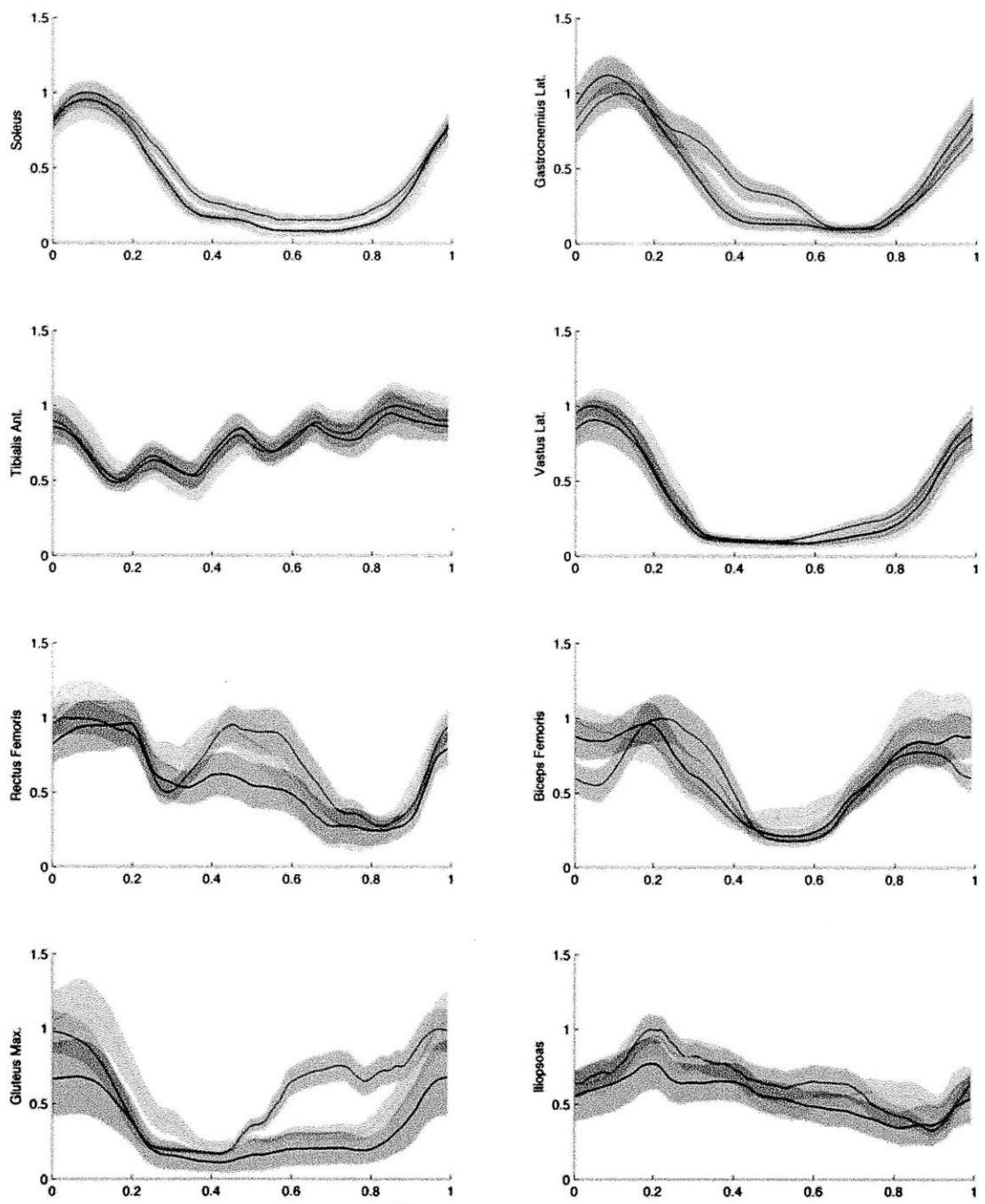(c) Electromyography

Figure B-2: Subject S2

(a) Joint angles, moments, and powers

Figure B-3: Subject S3

(b) Stance torque-angle plots for ankle, knee, and vertical leg

Figure B-3: Subject S3

(c) Electromyography

Figure B-3: Subject S3

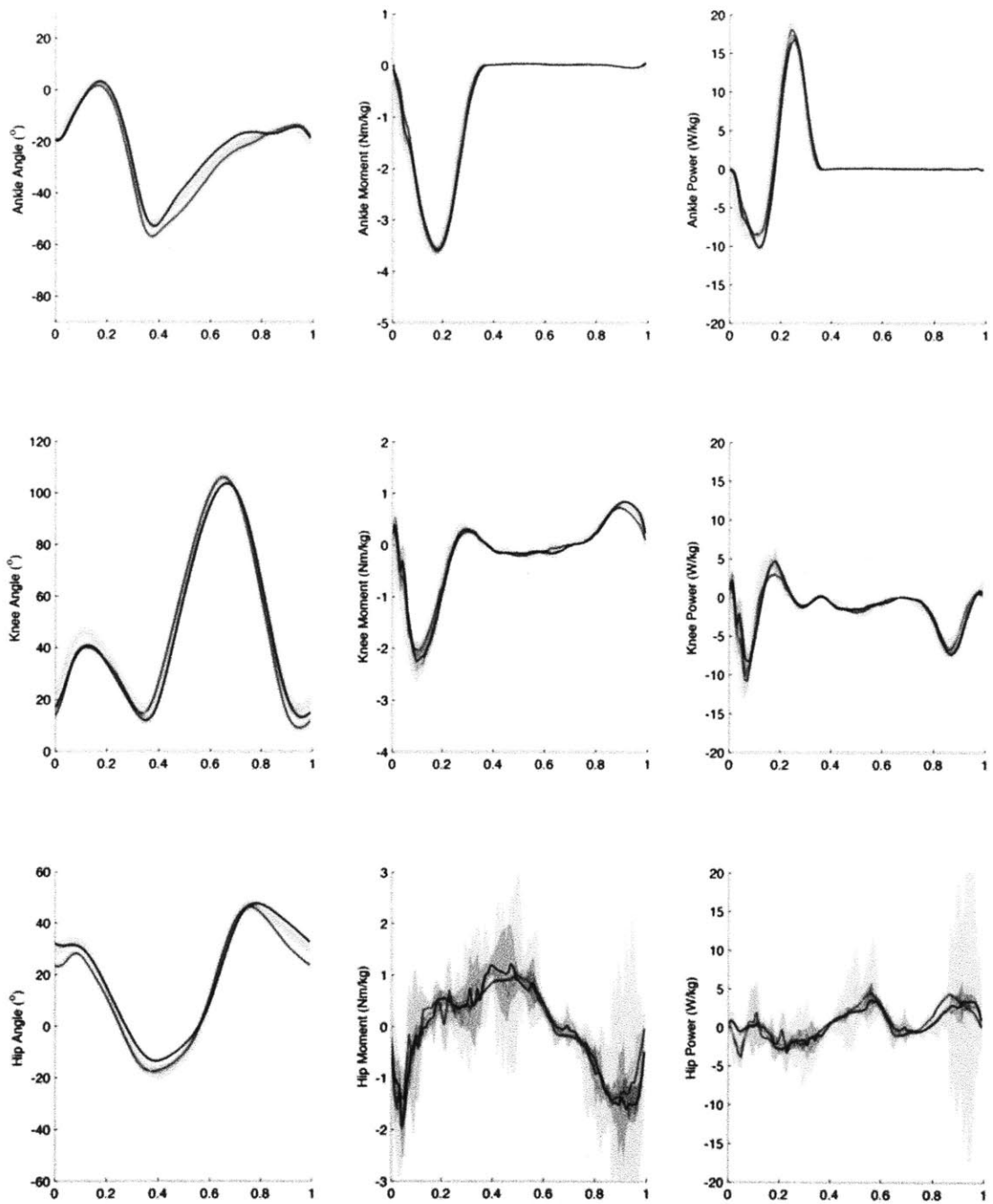(a) Joint angles, moments, and powers

Figure B-4: Subject S4

(b) Stance torque-angle plots for ankle, knee, and vertical leg
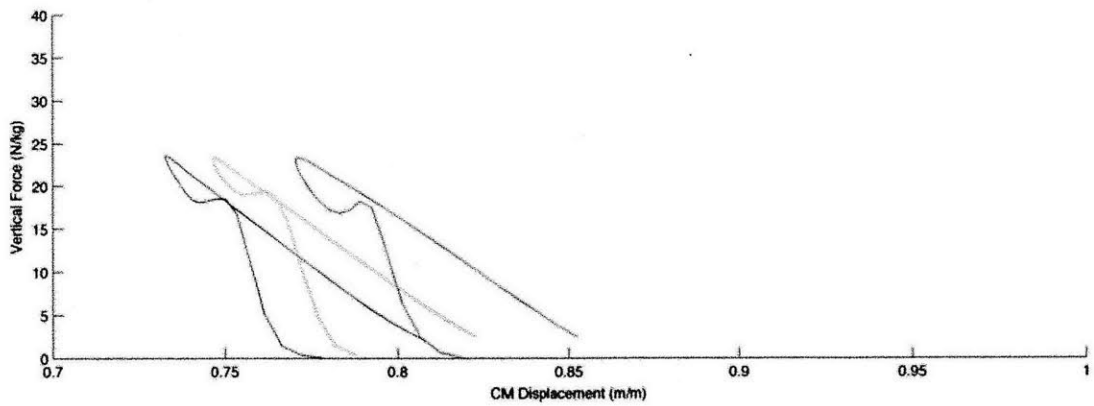
Figure B-4: Subject S4

124

(c) Electromyography

Figure B-4: Subject S4

(a) Joint angles, moments, and powers

Figure B-5: Subject S5

(b) Stance torque-angle plots for ankle, knee, and vertical leg

Figure B-5: Subject S5

(c) Electromyography

Figure B-5: Subject S5

128

(a) Joint angles, moments, and powers

Figure B-6: Subject S6

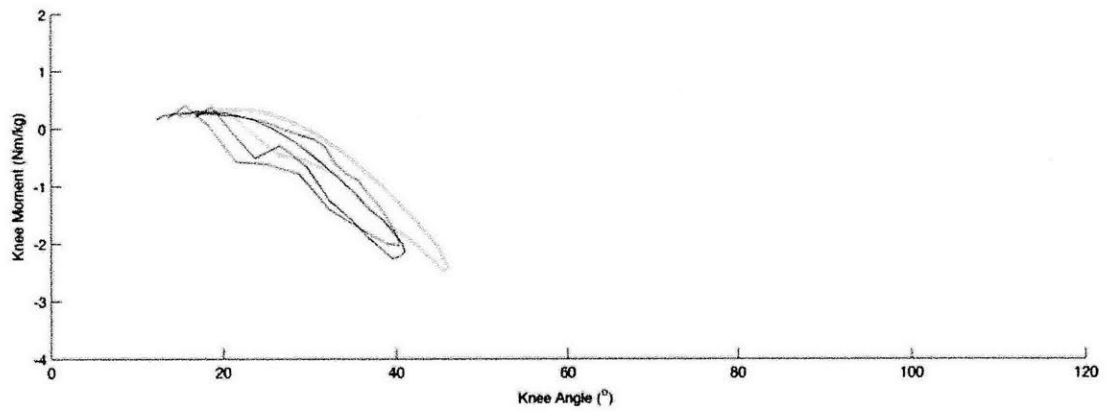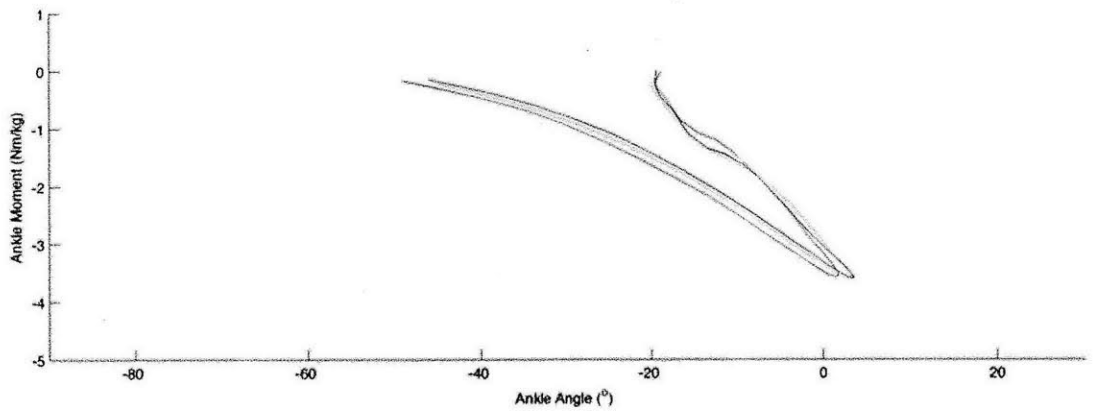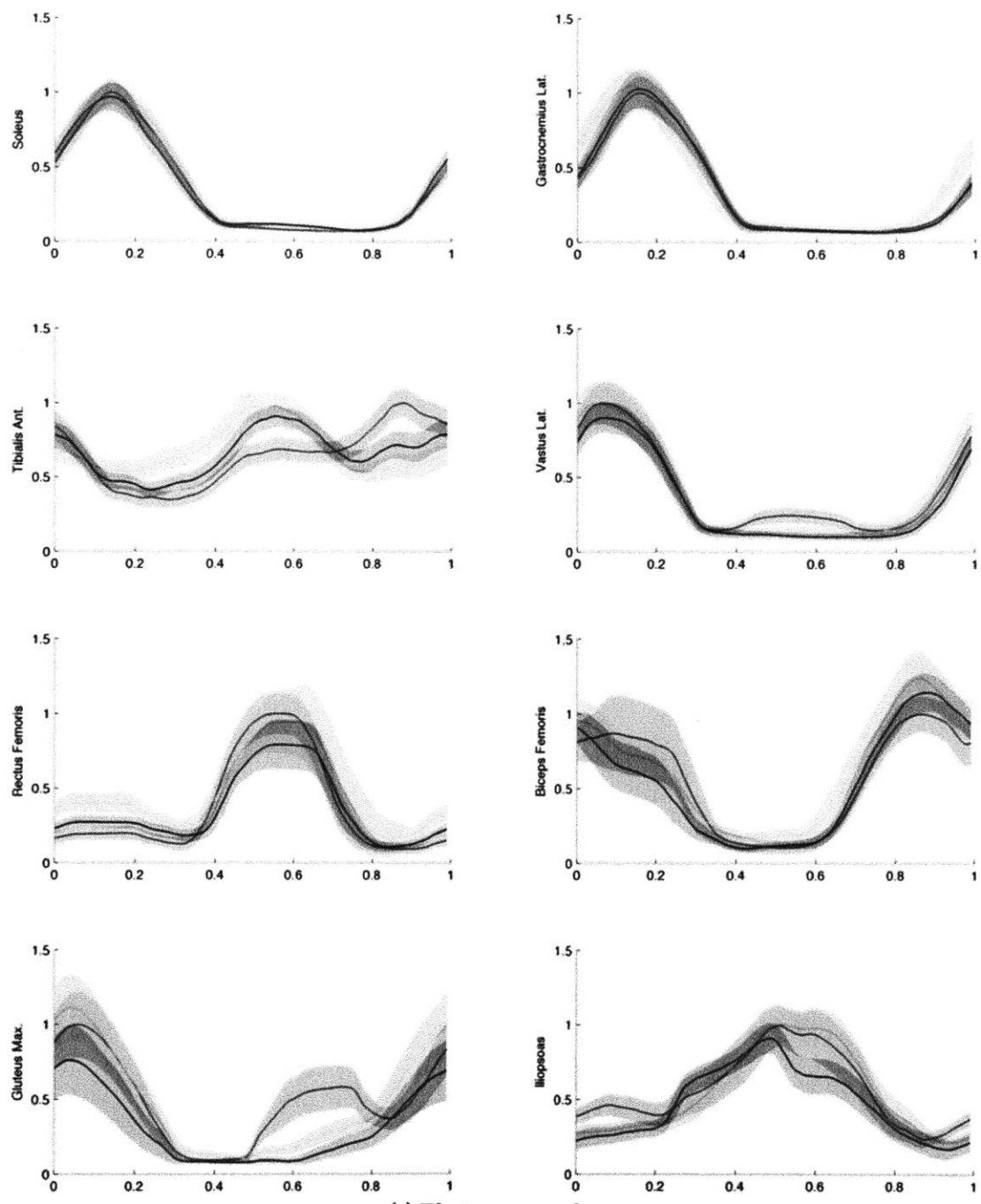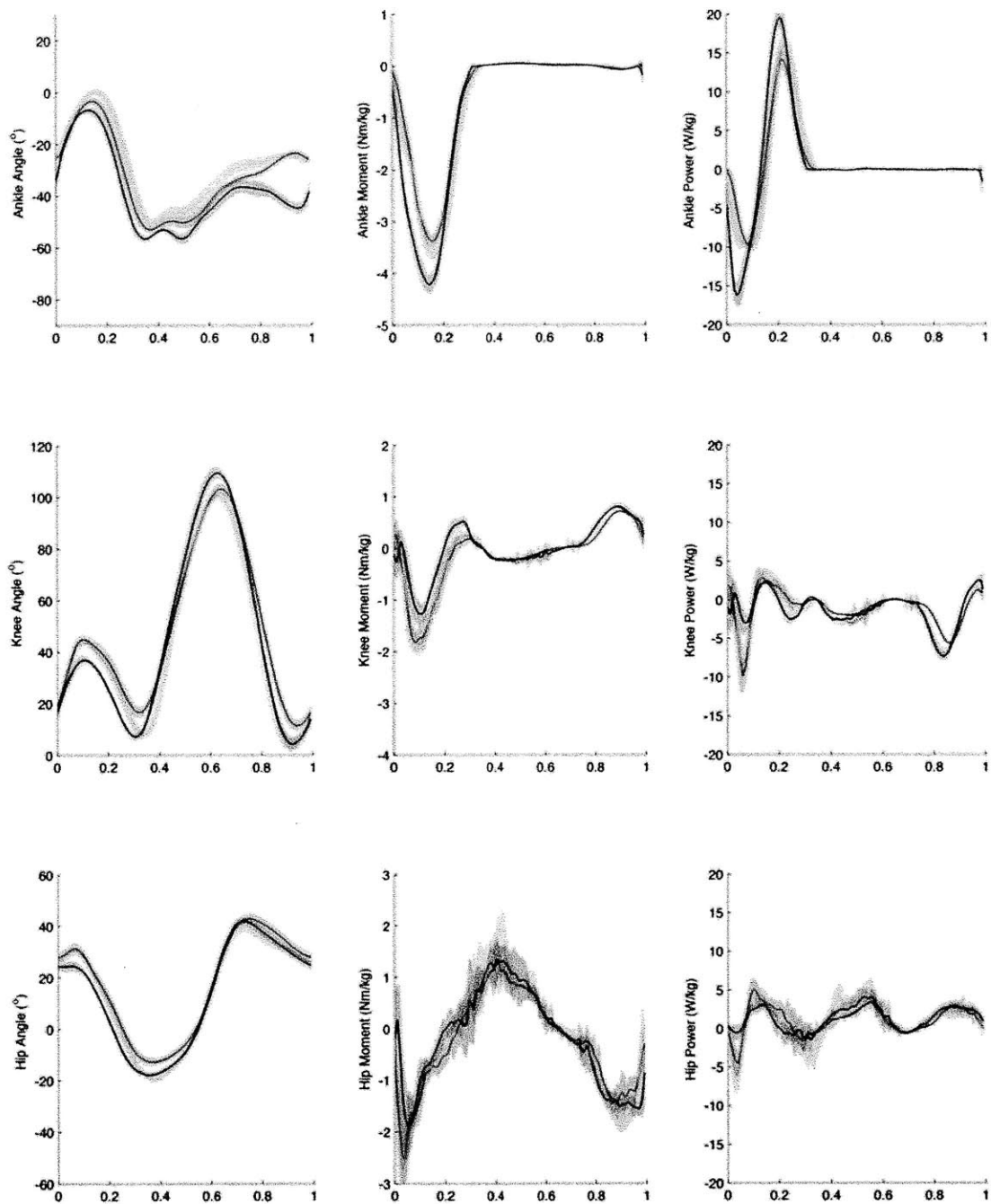(b) Stance torque-angle plots for ankle, knee, and vertical leg

Figure B-6: Subject S6

130

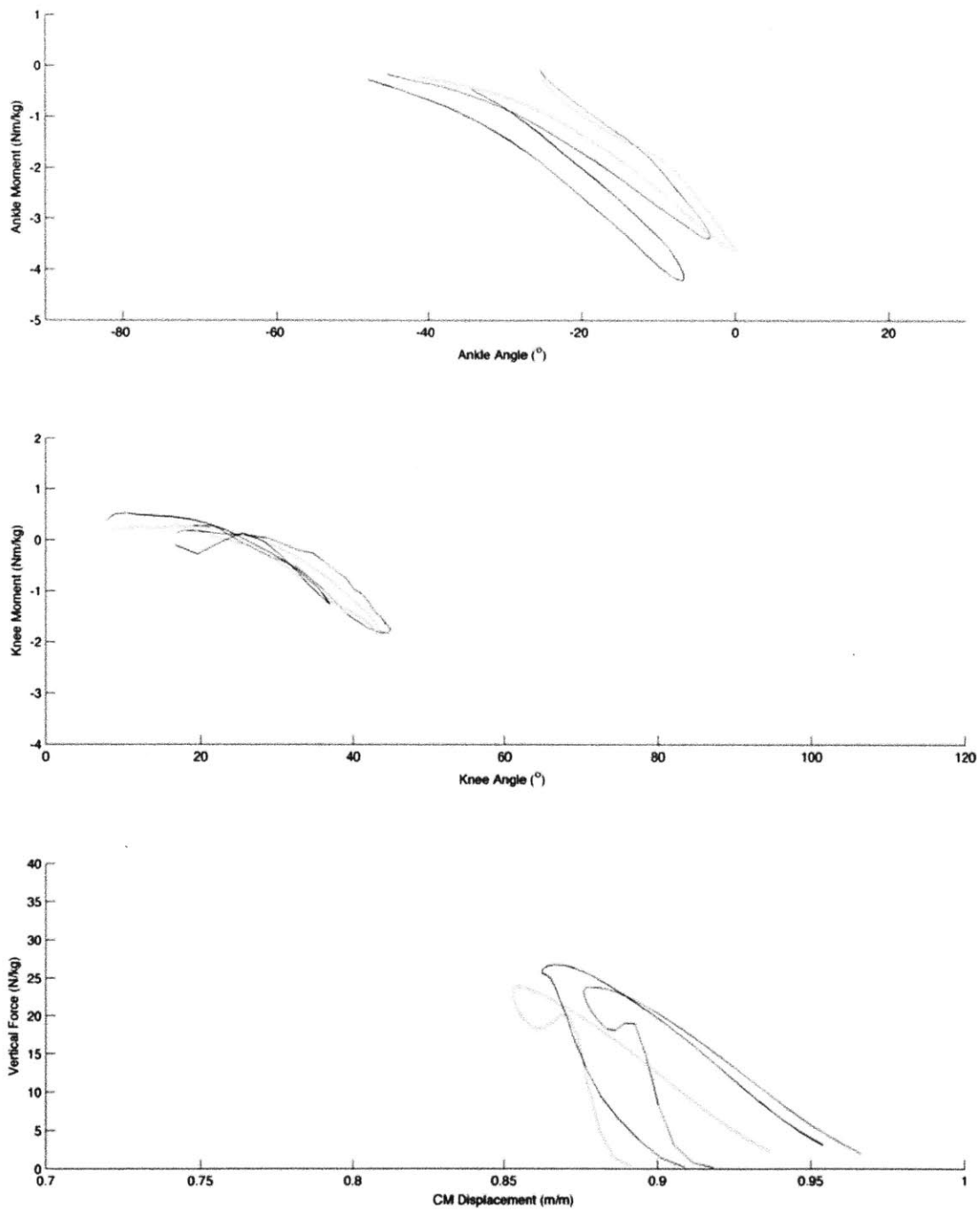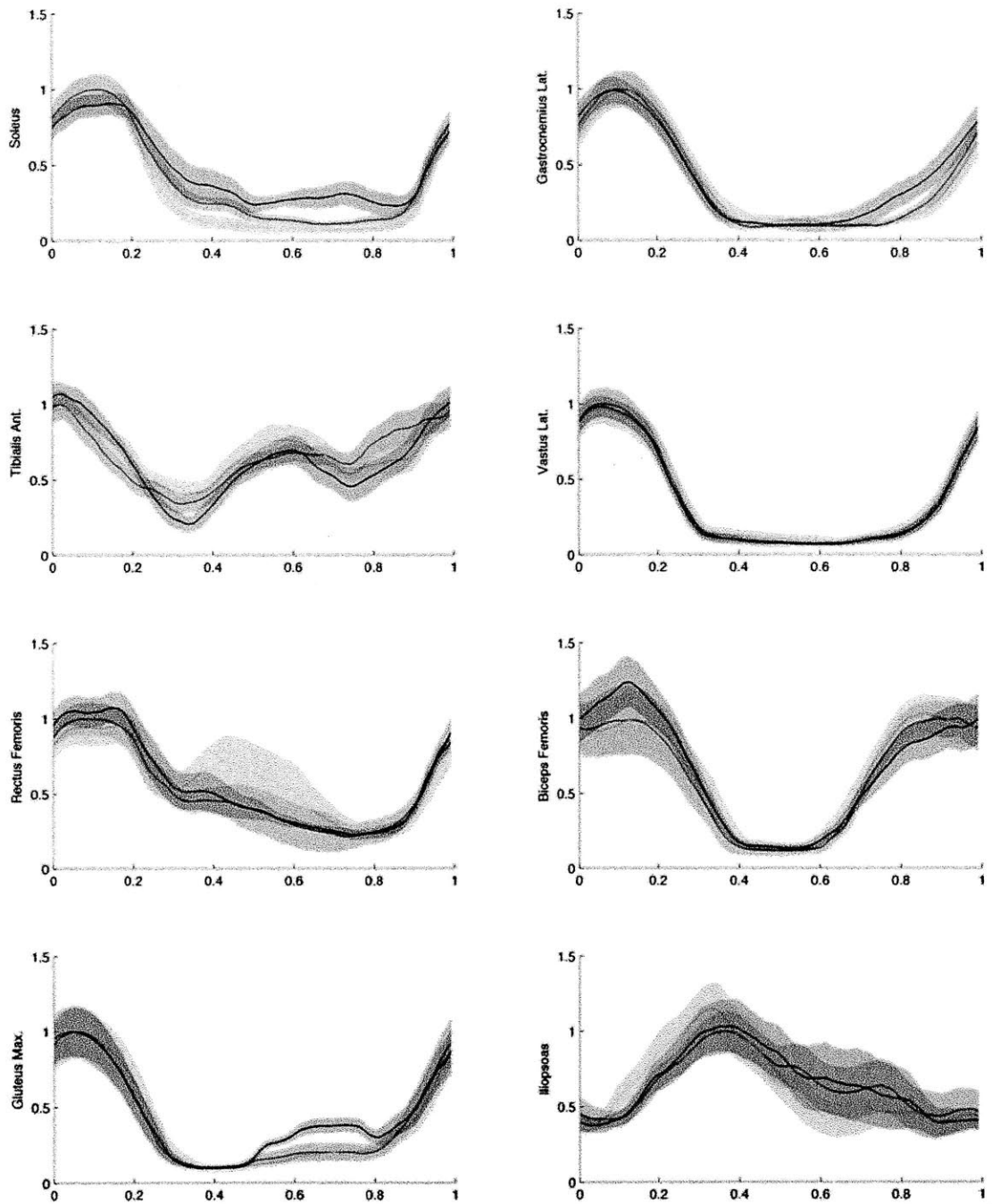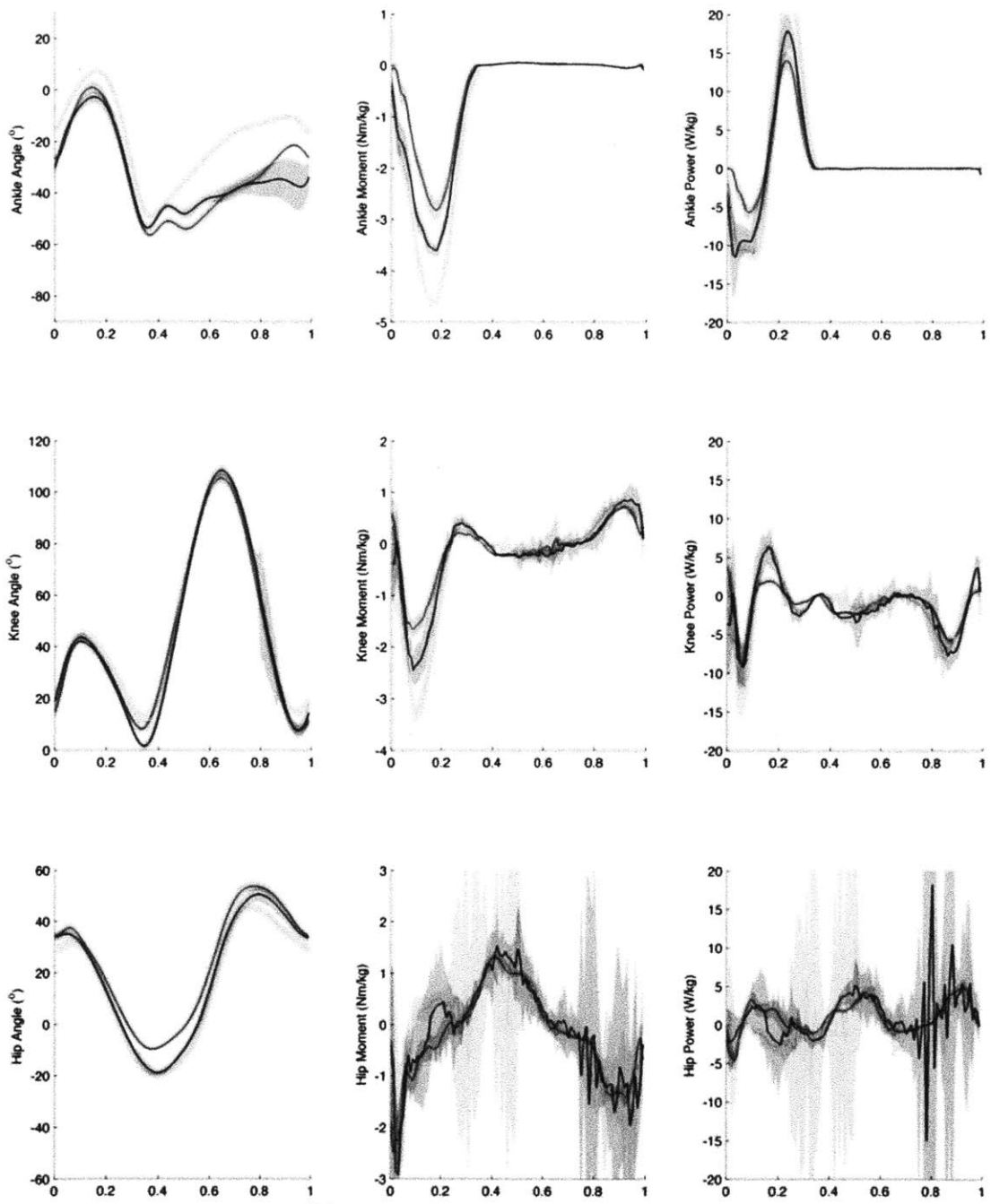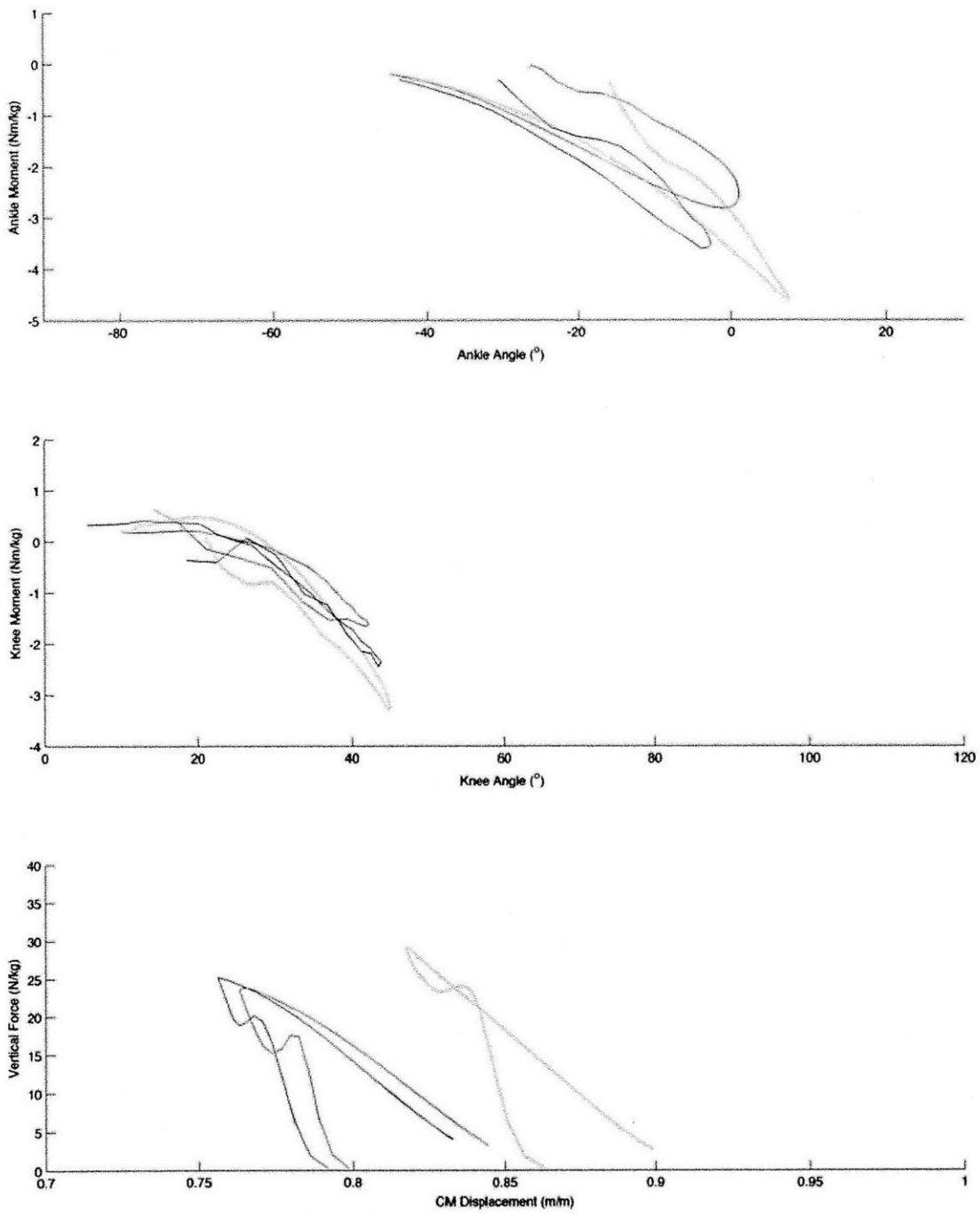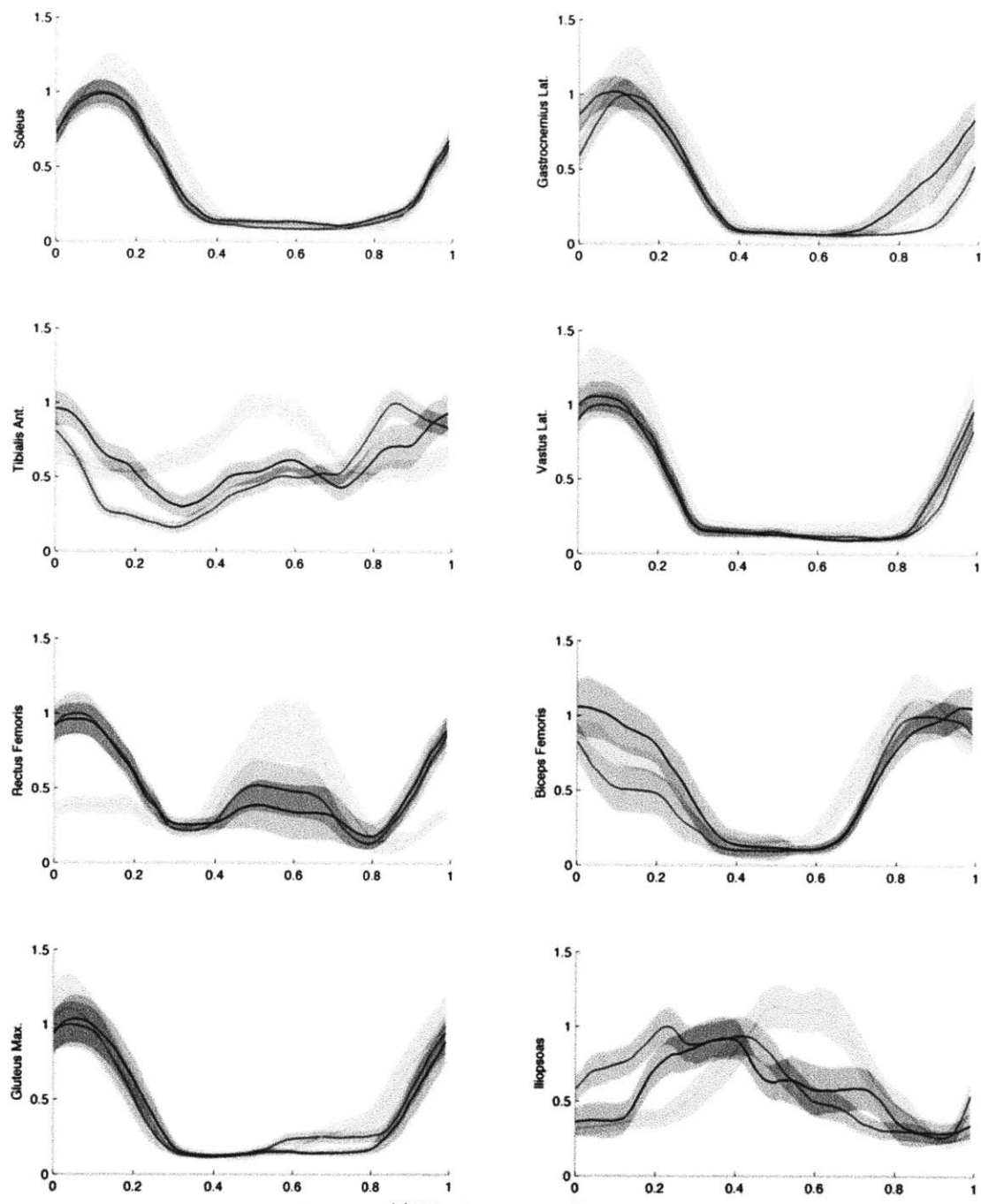(c) Electromyography

Figure B-6: Subject S6

131

Appendix C

Selected Source Code Listing

Source code is provided here for the project-level firmware running on the exoskeletal knee joint. For questions regarding lower level code, contact the author.

project/mystatelist.h

```
1   /*mystatelist.h
2   List all of your states here.  SLEEP and POWERON are implicitly defined;  Do not list them
3   End each line with a \ except the last last line.
4   The first state listed here will be state 2, after SLEEP (0) and POWERON (1)
5   Example:
6   ****************************
7   #define STATELIST(S)      \
8       S(RUN)                \
9       S(JUMP)               \
10      S(SKIP)               \
11      S(FALL)
12  ****************************
13  */
14
15  #define STATELIST(S)        \
16      S(ON)                   \
17      S(OFF)                  \
18      S(TERMINALSTANCE)       \
19      S(EARLYSWING)           \
20      S(MIDSWING)             \
21      S(SWING)                \
22      S(TERMINALSWING)        \
23      S(EARLYSTANCE)          \
```

project/mystates.c

```
1   /*mystates.c
2   Fill in all of your states code here (and no other functions!)
3   If you need to, you can also define global variables here (they should be declared as static)
4   You must implement a behavior for every state defined in mystatelist.h (and vice-versa).
5   The SLEEP state is implicit.  Do not define its behavior here
6   The POWERON state's existance is implicit, but you need to provide its behavior.
7   */
8
9   #define ACCLSTRIKETHRESHOLD          accl_mmps2_to_arb(-30000)
10  #define GYROFLEXIONTHRESHOLD         gyro_degps_to_arb( 200)
11  #define GYROMIDSTANCETHRESHOLD       gyro_degps_to_arb(-200)
12  #define MINKNEEDIFFERENTIAL          knee_deg_to_arb(40)
13  #define KNEEFLEXIONEPSILON           knee_deg_to_arb(2)
14  #define LOOKAHEAD                    time_ms_to_periods(30)
15
16  #define TERMINALSTANCETIMEIN         time_ms_to_periods( 20)
17  #define MIDSWINGTIMEOUT              time_ms_to_periods(200)
18  #define SWINGTIMEOUT                 time_ms_to_periods(320)
19  #define TERMINALSWINGTIMEOUT         time_ms_to_periods(250)
20  #define EARLYSTANCETIMEIN            time_ms_to_periods( 20)
21  #define EARLYSTANCETIMEOUT           time_ms_to_periods(200)
22
23  #define WINDOWSIZE                   32L
24  #define S0                           (WINDOWSIZE)
25  #define S1                           (S0*(S0-1)/2)
26  #define S2                           (S1*(2*S0-1)/3)
27
28  State state_POWERON(void)
29  {
30      //return OFF;
31      return TERMINALSTANCE;
32  }
33
34  State state_OFF(void)
```

```
35  {
36      if (state_timer_read()>time_ms_to_periods(2500))
37          return ON;
38      return OFF;
39  }
40
41  State state_ON(void)
42  {
43      if (state_timer_read()>time_ms_to_periods(500))
44          return OFF;
45      return ON;
46  }
47
48  State state_TERMINALSTANCE(void)
49  {
50      if (breakbeam_open() && state_timer_read()>TERMINALSTANCETIMEIN)
51          return EARLYSWING;
52      return TERMINALSTANCE;
53  }
54
55  State state_EARLYSWING(void)
56  {
57      if (state_timer_read()==0)
58          knee_max_clear();
59      if (gyro_read()>GYROFLEXIONTHRESHOLD)
60          return MIDSWING;
61      return EARLYSWING;
62  }
63
64  State state_MIDSWING(void)
65  {
66      if (state_timer_read()>MIDSWINGTIMEOUT)
67          return TERMINALSTANCE;
68      if (knee_max()>knee_min()+MINKNEEDIFFERENTIAL && knee_read()<knee_max()-KNEEFLEXIONEPSILON)
69          return SWING;
70      return MIDSWING;
71  }
72
73  unsigned char origin=0, go=0;
74  State state_SWING(void)
75  {
76      if (state_timer_read()==0)
77      {
78          knee_min_clear();
79          go=0;
80          origin=0;
81      }
82      if (state_timer_read()>SWINGTIMEOUT)
83          return TERMINALSTANCE;
84      static int window[WINDOWSIZE];
85      window[origin] = knee_vel();
86      if (origin==WINDOWSIZE-1)
87          go=1;
88      if (go)
89      {
90          long t0=0,t1=0;
91          for (unsigned char k=0;k<WINDOWSIZE;k++)
92          {
93              int dat = window[(origin+1+k)%WINDOWSIZE];
94              t0+=(long)dat;
95              t1+=(long)k*(long)dat;
```

```
96              }
97              long a = S0*t1 - S1*t0;
98              long b = S2*t0 - S1*t1;
99              eta_set(-b/a-S0+1);
100             if (eta_get()>=0 && eta_get()<=LOOKAHEAD && knee_read()<knee_max()-MINKNEEDIFFERENTIAL)
101                 return TERMINALSWING;
102         }
103         origin=(origin+1)%WINDOWSIZE;
104         return SWING;
105 }
106
107 State state_TERMINALSWING(void)
108 {
109     if (state_timer_read()>TERMINALSWINGTIMEOUT)
110         return TERMINALSTANCE;
111     if (accl_horiz_read()<ACCLSTRIKETHRESHOLD)
112         return EARLYSTANCE;
113     return TERMINALSWING;
114 }
115
116 State state_EARLYSTANCE(void)
117 {
118     if (state_timer_read()>EARLYSTANCETIMEOUT || (state_timer_read()>EARLYSTANCETIMEIN && gyro_read()<
            GYROMIDSTANCETHRESHOLD))
119         return TERMINALSTANCE;
120     return EARLYSTANCE;
121 }
```

project/myhelpers.h

```
1   //systemhelpers.h
2   //Provides a home for misc helper functions needed by the user
3
4   #define SOLCLOSEPOWER         255
5   #define SOLHOLDPOWER          150
6
7   #define CAGEOPENTHRESHOLD     200
8   #define CAGECLOSEDTHRESHOLD   900
9
10  static inline int accl_horiz_read(void) {return accl_y_read();}
11  static inline int accl_vert_read(void) {return accl_x_read();}
12  static inline int gyro_read(void) {return gyro_z_read();}
13  static inline int knee_read(void) {return (int)enc_read();}
14
15  void knee_filter_update(void);
16  int knee_max(void);
17  void knee_max_clear(void);
18  int knee_min(void);
19  void knee_min_clear(void);
20  int knee_vel(void);
21
22  static inline int knee_arb_to_deg(int a) {return enc_arb_to_mdeg(a)*24L/(88L*1000L);}
23  static inline int knee_deg_to_arb(int a) {return enc_mdeg_to_arb(a*88L*1000L/24L);}
24
25  void eta_set(long);
26  long eta_get(void);
27
28  unsigned char solenoid_feedback(unsigned char);
29
30  static inline unsigned char breakbeam_open(void) {return breakbeam_read()<CAGEOPENTHRESHOLD;}
31  static inline unsigned char breakbeam_closed(void) {return breakbeam_read()>CAGECLOSEDTHRESHOLD;}
```

project/myhelpers.c

```c
1    //systemhelpers.c
2    //Provides a home for misc helper functions needed by the user
3
4    #include "../core/config.h"
5    #include "../core/misc.h"
6    #include "../core/hardware.h"
7    #include "../system/systemhelpers.h"
8    #include "myhelpers.h"
9
10   //Solenoid Feedback
11   unsigned char solenoid_feedback(unsigned char on)
12   {
13       return on ? (breakbeam_closed() ? SOLHOLDPOWER : SOLCLOSEPOWER) : 0;
14   }
15
16   //Encoder Filtering and Extrema
17   int knee_max_value=0;
18   int knee_min_value=0;
19   int knee_vel_value=0;
20   void knee_filter_update(void)
21   {
22       static long history=0;
23       if (knee_read()>knee_max_value)
24           knee_max_value=knee_read();
25       if (knee_read()<knee_min_value)
26           knee_min_value=knee_read();
27       knee_vel_value=knee_read()-history;
28       history=knee_read();
29   }
30   int knee_max(void) {return knee_max_value;}
31   void knee_max_clear(void) {knee_max_value=knee_read();}
32   int knee_min(void) {return knee_min_value;}
33   void knee_min_clear(void) {knee_min_value=knee_read();}
34   int knee_vel(void) {return knee_vel_value;}
35
36   //ETA Accessor and Mutator
37   long eta=0;
38   void eta_set(long t) {eta=t;}
39   long eta_get(void) {return eta;}
```

project/mybehaviors.c

```c
1    //mybehaviors.c
2    //Contains definitions for
3    //void dead_man_switch(void)
4    //void lead_in(void)
5    //void lead_out(void)
6
7    #define ENCVELKEEPALIVETHRESH    2
8    #define ACCLKEEPALIVETHRESH      400
9    #define GYROKEEPALIVETHRESH      40
10
11   //The Lead In is executed immediately after latching in all sensors
12   //but before advancing the state machine
13   //Its execution counts against the user space timeout.
14   //
15   //Lead in is intended as a home for filter updates which must occur
16   //every cycle regardless of state
17
18   void lead_in(void)
```

137

```
19  {
20      knee_filter_update();
21      if (accl_x_read() > ACCLKEEPALIVETHRESH || accl_x_read() < -ACCLKEEPALIVETHRESH ||
22          accl_y_read() > ACCLKEEPALIVETHRESH || accl_y_read() < -ACCLKEEPALIVETHRESH ||
23          gyro_z_read() > GYROKEEPALIVETHRESH || gyro_z_read() < -GYROKEEPALIVETHRESH ||
24          knee_vel() > ENCVELKEEPALIVETHRESH || knee_vel() < -ENCVELKEEPALIVETHRESH)
25          dead_man_switch_push();
26  }
27
28
29  //The Lead Out is executed immediately after the state machine
30  //advances
31  //Its execution counts against the user space timeout.
32  //
33  //Lead out is intended as a home for output updates which must occur
34  //every cycle regardless of state
35
36  void lead_out(void)
37  {
38      led_off_all();
39      led_set(0, state_get()==EARLYSWING || state_get()==ON ? 255 : 0);
40      led_set(1, state_get()==MIDSWING ? 255 : 0);
41      led_set(2, state_get()==SWING ? 255 : 0);
42      led_set(3, state_get()==TERMINALSWING ? 255 : 0);
43      led_set(4, state_get()==EARLYSTANCE ? 255 : 0);
44
45      led_set(8,breakbeam_closed() ? 255 : 0);
46      led_set(9,breakbeam_closed() ? 255 : 0);
47      led_set(10,breakbeam_closed() ? 255 : 0);
48      led_set(11,breakbeam_closed() ? 255 : 0);
49
50      breakbeam_led_on(); //ToDo: Save some power by turning off the breakbeam when it isn't needed
51      solenoid_power_set(solenoid_feedback(state_get()==ON || state_get()==TERMINALSWING || state_get()==
            EARLYSTANCE));
52  }
```

project/mydebugger.c

```
1   /*mydebugger.c
2   Contains definition for void debug_setup(void)
3
4
5   Fill in your variables to be debugged here.
6   You may use:
7   debug_insert_ubyte
8   debug_insert_sbyte
9   debug_insert_uint
10  debug_insert_sint
11  debug_insert_ulong
12  debug_insert_slong
13  Note that 4*debugsize total bytes are available
14  (ints require 2 bytes and must begin on a multiple of two)
15  (longs require 4 bytes and must begin on a multiple of four)
16  Ask your system designer how big debugsize is for your system
17  Functions passed as arguments to these must take no arguments
18  and return the appropriate type.
19  Make a wrapper (in myhelpers) if necessary.
20  Place no other functions in this file.
21  Example:
22  ***********************************
23  void debug_init(void) {
```

```
24        debug_insert_ulong(0,&enc_1_read);        //bytes 1-4
25        debug_insert_sint(4,&imu_zgyro_read);     //bytes 5-6
26        debug_insert_uint(6,&adc_aux1_read);      //bytes 7-8
27        debug_insert_ubyte(8,&state_to_byte);     //byte 9
28        debug_insert_ubyte(9,&bridge_1_get_speed); //byte 10
29   }
30   *********************************
31   */
32
33   void debug_setup(void) {
34        debug_insert_sint(0,&knee_read);
35        debug_insert_sint(2,&gyro_read);
36        debug_insert_sint(4,&accl_horiz_read);
37        debug_insert_uint(6,&breakbeam_read);
38        debug_insert_uint(8,&state_timer_read);
39        debug_insert_ubyte(10,&solenoid_power_get);
40        debug_insert_ubyte(11,&state_get_as_ubyte);
41        debug_insert_slong(12,&eta_get);
42   }
```

project/myconfig.h

```
1    //myconfig.h
2    //Sets constants needed for system level configuration
3    //Constants needed here vary with system
4    //This file should be setup by the system builder
5
6    //Each INVERSION channel may be set to:
7    //NORMAL - default directionality on all boards
8    //INVERT - inverted directionality on all boards
9    //RIGHTINVERT - inverted directionality on right boards only
10   //LEFTINVERT - inverted directionality on left boards only
11
12   //Encoder channels
13   //Inversion flips the sign
14        #define ENC_INVERSION        LEFTINVERT
15
16   //IMU channels
17   //inversion flips the sign
18   //Note that this makes it possible to create other than a right handed coordinate frame
19        #define IMUXACCL_INVERSION   NORMAL
20        #define IMUYACCL_INVERSION   LEFTINVERT
21        #define IMUZGYRO_INVERSION   LEFTINVERT
22
23   //LED channels
24   //Inversion mirrors the LEDs
25        #define LED_INVERSION        LEFTINVERT
26
27   //Dead Man Switch
28   //In periods, 0 to disable
29        #define DEADMANSWITCH_DELAY 0//time_s_to_periods(120)
```